

QATAR UNIVERSITY

COLLEGE OF ENGINEERING

MODELLING OF WHIPLASH TRAUMA; PARAMETRIC STUDY OF REAR-END

COLLISION AND DEVELOPMENT OF HEAD-RESTRAINT SYSTEM

BY

OTHMAN SHUKRI ABDELKARIM ABU LABAN

A Thesis Submitted to the Faculty of the

College of Engineering

in Partial Fulfillment of

the Requirements for the

Degree of

Masters of Science in Mechanical Engineering

January, 2017

©2017. Othman Abu Laban. All Rights Reserved.

COMMITTEE PAGE

The members of the Committee approve the Thesis of Othman Shukri Abu Laban
defended on December 26th, 2016

Prof. Elsadig Mahdi
Thesis Supervisor

Dr Homayoun Hadavinia
Committee Member

Dr. Abdel Magid Hamouda
Committee Member

Mohammad Roshun Paurobally
Committee Member

Approved:

Khalifa Al-Khalifa, Dean, College of Engineering

ABSTRACT

Abu Laban, Othman, Shukri, Masters: January: 2017, Master of Science in Mechanical Engineering

Title: Modelling of Whiplash Trauma; Parametric Study of Rear-End Collision and Development of Head-Restraint System

Supervisor of Thesis: Elsadig Mahdi Saad.

Whiplash is a common neck injury people usually suffer from after a rear car accident. Over the past decade, both engineers and physicians were trying to analyze the biomechanics of the injury to develop an effective prevention system design. Car Manufacturers and researchers developed various types of head-restraints, including re-active and pro-active systems, to protect the neck against whiplash. A few works have been done on developing a robust tracking head-restraint system to adjust its position automatically relative to the occupant's head position. The current study illustrates the effect of head-restraint position and material properties on whiplash injury using finite element modelling. Accordingly, a tracking head-restraint system was developed to maintain the optimum head-restraint position while driving to effectively protect the neck against whiplash.

DEDICATION

This Thesis is dedicated to the people without whom I would not be where I am,

*To my mother, Inaam, who raised me, filled me with love, and have always inspired me to do
what I love.*

*To my father, Shukri, who have worked the days and nights to support my education and give
me all what I've needed to succeed.*

*To my dear wife, Farah, for encouraging me to achieve better throughout my studies, carrier,
and personal life.*

*To my brothers and sister, for motivating me to continue pursue my post-graduate degree and
never doubting my abilities to do so.*

*I am also very grateful to my supervisor, Elsadig, for being so supportive from day 1 and
treating me like one of his sons.*

ACKNOWLEDGMENTS

This project was carried out in the Mechanical and Industrial Department of Qatar University. The author is grateful to the university and all faculty member who supported the project by their great ideas.

The author would like to acknowledge the financial support of the Qatar National Research Fund (a member of Qatar Foundation) through the National Priorities Research Program NPRP # 6-292- 2-127.

TABLE OF CONTENTS

DEDICATION	iii
ACKNOWLEDGMENTS	iv
LIST OF TABLES	ix
LIST OF FIGURES	xi
NOMENCLATURE	xvi
ABBREVIATIONS	xviii
CHAPTER 1 INTRODUCTION	1
1.1 Background	1
1.2 Objectives.....	3
1.3 Significance of the study	3
1.4 Thesis layout	4
CHAPTER 2 LITERATURE REVIEW	5
2.1 Introduction	5
2.2 Anatomy of the Human Vertebral Column	5
2.3 Occupant Kinematics	7
2.4 Whiplash Injury Mechanisms.....	9

2.4.1	Hyperextension Mechanism.....	10
2.4.2	Hydrodynamic Mechanism.....	10
2.5	Neck Injury Criteria	12
2.5.1	Neck Injury Criterion (NIC)	12
2.5.2	Normalized Neck Injury Criterion (Nij)	13
2.5.3	Neck Protection Criterion (Nkm).....	14
2.5.4	Intervertebral Neck Injury Criterion (IV-NIC).....	16
2.5.5	Neck Displacement Criterion (NDC).....	16
2.5.6	Lower Neck Load (LNL) Criterion.....	18
2.6	Head-Restraint (HR) Systems	19
2.6.1	Re-AHRs.....	21
2.6.2	Pro-AHRs.....	23
2.6.3	Material Properties of Head-Restraints.....	24
2.6.4	Effect of Airbags and Seatbelts on Whiplash	25
2.7	Discussion	26
CHAPTER 3 METHODOLOGY		29
3.1	Introduction	29

3.2	Experimental Program.....	29
3.2.1	HR Material Density Measurements.....	32
3.2.2	HR Material Tensile Test.....	32
3.2.3	Indentation Force Deflection (IFD) Test	32
3.2.4	Development of Tracking Head-Restraint (T-HR) System	34
3.3	Finite Element Modelling Program.....	34
3.3.1	Development of Finite Element Model (FEM).....	34
3.3.2	Effect of Head-Restraint Position on Whiplash.....	49
3.3.3	Effect of Head-Restraint Material Properties on Whiplash	49
3.4	Discussion	51
CHAPTER 4 RESULTS & DISCUSSION		53
4.1	Introduction	53
4.2	Experimental Program.....	53
4.2.1	Sample Preparation	53
4.2.2	Head-Restraints (HR) Material Density Measurements	54
4.2.3	Head-Restraints (HR) Material Tensile Behavior.....	54
4.2.4	Indentation Force Deflection (IFD) Test of Flexible HR Materials	59

4.3	Finite Element Modelling (FEM) Program	62
4.3.1	Development of Finite Element Model.....	62
4.3.2	Effect of Head-Restraint Position	67
4.3.3	Effect of Head-Restraint Material Properties	80
4.4	Development of Tracking Head-Restraint (T-HR) System.....	87
4.4.1	Tracking Head-Restraint (T-HR) Mechanism Development.....	88
4.4.2	Sensory System.....	90
4.4.3	1 st Tracking Head-Restraint (T-HR) Prototype.....	92
4.4.4	2 nd Tracking Head-Restraint (T-HR) Prototype.....	94
4.4.5	3 rd Tracking Head-Restraint (T-HR) Prototype	95
4.5	Overall Discussion	100
CHAPTER 5 CONCLUSIONS		102
CHAPTER 6 FURTHER RECOMMENDATIONS		104
REFERENCES		106
APPENDIX A FINITE ELEMENT RESULTS DATA		114
APPENDIX B T-HR PROTOTYPE VIEWS		132
APPENDIX C ARDUINO PROGRAM CODE		135

LIST OF TABLES

Table 1. Intact physiological motion limit for each intervertebral level in extension and flexion along with injury threshold.	17
Table 2. NDC injury classification according to natural range of motion [53].	17
Table 3. Acceleration pulse specifications according to IIHS (RCAR-IIWPG V3) standard.	48
Table 4. Vehicles dimensions, weights, and the measured densities for their HR materials.	55
Table 5. Material properties for the selected head-restraints (\pm standard deviation).	57
Table 6. IFD test results for the selected head-restraints and their typical dimensions.	60
Table 7. CPU times, maximum internal energy and Von Mises stress.	64
Table 8. Developed FEM head retraction results compared with work of Stemper et al. [17]. ...	66
Table 9. NDC injury rating thresholds according to natural range of motion [50].	73
Table 10. NDC classification of HR effectiveness in whiplash protection.	73
Table 11. Summary of whiplash injury assessments at different backset gap distances.	77
Table 12. Maximum IV-NIC values at intervertebral levels for all HR positions from FEM.	80
Table 13. Mechanical properties of head-restraint cushion materials.	83
Table 14. Summary of neck injury assessments at different HR materials.	85
Table 15. Advantages and drawbacks of servo, brushed and stepper motors.	89

Table 16. Performance of ultrasonic sensor in detecting target distance. 98

Table 17. The initial and corrected T-HR system vertical (V) and horizontal (H) positions for the three occupants..... 99

LIST OF FIGURES

Figure 1. Human spinal column (left) and cervical spine (right) [22].	6
Figure 2. Structure of atlas (C1) and axis (C2) vertebrae [23].	7
Figure 3. Cervical spine ligaments anatomy [30].	8
Figure 4. Head-neck kinematics and phases of whiplash injury due to rear-end impact; (A) initial posture, (B) S-shape curvature phase, (C) neck extension phase, and (D) head rebound (neck flexion) phase [36].	9
Figure 5. Cross-section of the cervical spine [33].	11
Figure 6. Nij combination of axial forces and bending moments acting on the neck.	15
Figure 7. IIHS static rating standard for head-restraints geometry (RCAR-IIWPG V3).	20
Figure 8. Examples of Re-AHRs with different approach; (A) Volvo WHIPS tilting backwards, (B) Saab SAHR adjusting backset gap, and (C) Toyota WIL adjusting height [55, 56, 58].	22
Figure 9. Example of Pro-AHR with a stationary part and moving cushion [10].	23
Figure 10. Schematic of occupant's head-neck response to rear-end impact with respect to pulse time. The response is divided into three different stages; (I) S-curve phase, (II) maximum extension phase, and (III) head rebound phase [22].	28
Figure 11. Flow chart summarizes experimental program.	30

Figure 12. The front, side, and top views of the selected commercially available head-restraints for experimental testing; (A) Toyota Land Cruiser, (B) Toyota Prado, (C) Toyota Camry, (E) Mazda M3, (F) Kia Cerato, and (G) Nissan Tida.	31
Figure 13. Dimensions of flat tensile HR specimens as per ASTM D3574-E standard.	33
Figure 14. Flow chart of numerical modelling investigation on head-restraints.	35
Figure 15. Academic version 4.0 of THUMS AM50 model; (A) occupant view and (B) side view showing the seven cervical vertebra [84].	38
Figure 16. The geometry model for (A) Toyota Land Cruiser seat, (B) CAD seat model, (C) front view, and (D) side view.	39
Figure 17. Sphere striking a pad used to perform mesh size study on driver’s seat.	42
Figure 18. Mesh element volumes used in mesh size study; (A) 15×15×15 mm ³ , (B) 10×10×10 mm ³ , (C) 8×8×8 mm ³ , (D) 5×5×5 mm ³ , (E) 4×4×4 mm ³ , and (F) 3×3×3 mm ³	43
Figure 19. Passenger head position at 20 mm gap from the cubic head-restraint.	45
Figure 20. Behavior of foam (left) hysteretic factor is unity or (right) less [85].	45
Figure 21. Upper and lower bounds for acceleration pulse variations according to IIHS (RCAR-IIWPG V3).	48
Figure 22. Human head-neck model developed by Stamper et al. [17] to study the effect of backset gap on whiplash injury.	50
Figure 23. HRs tensile samples following an ASTM D3574-E standard.	54

Figure 24. Scanning electron microscope at 50x for the HR materials.	56
Figure 25. Tensile stress-strain curve for the selected HR materials.....	58
Figure 26. 3D-graph comparing the material properties for the HR materials.	58
Figure 27. Toyota Land Cruiser head-restraint during IFD test; (A) depth (T) measure at 4.5 N preload, (B) indentation up to 0.25T where the load $F_{25\%}$ was recorded after 60 ± 3 seconds, and (C) indentation up to 0.65T where the load $F_{65\%}$ was recorded after 60 ± 3 seconds.	60
Figure 28. IFD indentation force vs. deflection for the HR materials.	61
Figure 29. Energy absorption versus compressive extension of the six HRs during IFD test.....	61
Figure 30. Internal energy and Von Mises stress versus mesh size. Mesh convergence began at element volume of $4 \times 4 \times 4 \text{ mm}^3$	63
Figure 31. A Rigid sphere impacting soft HR until 40% of its depth.....	64
Figure 32. Von Mises stress distribution (MPa) corresponding to element volumes (mm^3) (A) $15 \times 15 \times 15$, (B) $10 \times 10 \times 10$, (C) $8 \times 8 \times 8$, (D) $5 \times 5 \times 5$, (E) $4 \times 4 \times 4$, and (F) $3 \times 3 \times 3$	65
Figure 33. Comparison between (A) Stemper et al. [17] and (B) developed FEM in head-neck kinematics of whiplash injury during rear-end impact.	67
Figure 34. Whiplash phases of the developed FEM (left) and the position of head-neck (right) during rear-end impact with HR position at 100 mm gap.	70
Figure 35. Neck kinematics and injury assessments at 100 mm HR position.	71

Figure 36. Curves of maximum head extension angle and maximum shear & vertical displacement relative to T1 at different HR positions.	75
Figure 37. NIC, Nij, Nkm, and LNL injury criteria assessment versus HR gap.	78
Figure 38. Maximum energy absorbed by the head-restraint position at different gaps during rear-end collision.	79
Figure 39. Back (left) and isometric (right) views of the cervical spine (C1-C7) linked with the occipital Condyle (OC) from the top and the first thoracic vertebrae (T1).	79
Figure 40. Head-restraint made of FGCM with 33.5% soft JC80 foam and 66.5% stiff Mazda or FVLD foam, positioned at 20 mm gap.	82
Figure 41. Comparison of HR energy absorption, maximum head retraction, NIC, Nkm, and LNL injury criteria assessments at different HR foam materials.	85
Figure 42. Comparison of HR deflection for different foam materials at maximum head indentation.	86
Figure 43. Rack-and-pinion mechanism (left) and pin-and-slot mechanism (right).	90
Figure 44. The response of (A) infrared sensor and (B) ultrasonic sensor to four different occupant hair colors [63].	91
Figure 45. Effects of interference sources on the distance detection performance of (A) infrared sensor and (B) ultrasonic sensor. [63].	92
Figure 46. First T-HR prototype built entirely using 3D-printing ABS material.	93

Figure 47. Second T-HR prototype built with 3D-printing ABS material and aluminum rods.... 94

Figure 48. The electrical wiring diagram for controlling the T-HR system using Arduino UNO board and H-bridge. 96

Figure 49. Evaluating the functionality of the T-HR system by the third volunteer; (A) initial HR height position, (B) corrected HR height position, (C) initial HR backset gap, and (D) corrected HR backset gap. 100

NOMENCLATURE

a	Acceleration
a_{rel}	Relative acceleration
v	Velocity
v_{rel}	Relative velocity
F	Force
F_x	Neck shear force
F_y	Neck bending force
F_z	Neck axial force
F_{int}	Intercept force
M	Moment
M_x	Neck bending moment
M_y	Neck extension moment
M_{int}	Intercept Moment
C_{moment}	Moment constant
C_{shear}	Shear constant
$C_{tension}$	Tension constant
C_{length}	Length constant
θ	Angle
θ_{OC}	Head's extension angle
ρ	Density
m	Mass
V	Volume
ρ_D	Density of Mazda M3 material
ρ_E	Density of Johnson Controls 80 material

ρ_F	Density of Flexible Very Low Density material
$\rho_{FGCM-EF}$	Equivalent density for FGCM-EF material
$\rho_{FGCM-DE}$	Equivalent density for FGCM-DE material
C	Constant
g	Gravitational coefficient (9.81 m/s ²)
E_n	Absorbed Energy
E	Young's Modulus
E_D	Young's Modulus for Mazda M3 material
E_E	Young's Modulus for Johnson Controls 80 material
E_F	Young's Modulus for Flexible Very Low Density material
$L^0\%$	Ultimate elongation percentage
X_{OC-T1}	Shear Neck displacement
Z_{OC-T1}	Axial neck displacement
N_{fa}	Flexion-anterior load case
N_{ea}	Extension-anterior load case
N_{fp}	Flexion-posterior load case
N_{ep}	Extension-posterior load case
f_s	Normal reaction force
l	Penetration depth
k_i	Contact stiffness
A_i	Element's area
V_i	Element's volume
K_i	Bulk modulus
f_{si}	Scale factor
σ_f	Tearing stress
R^2	Correlation coefficient

ABBREVIATIONS

ABS	Acrylonitrile Butadiene Styrene material
AHR	Active Head-Restraint
C1-C7	Cervical vertebrae
CAD	Computational Aided Design
Class	Classification
FEM	Finite Element Model
FGCM	Functionally Graded Cellular Material
FVLD	Flexible Very Low Density material
G	Gap
HR	Head-Restraint
IFD	Indentation Force Deflection
IFD	Indentation Force Deflection
IIHS	Insurance Institute for Highway Safety
IV-NIC	Intervertebral Neck Injury Criterion
JC80	Johnson Controls 80 material
LNL	Lower Neck Load Criterion
NDC	Neck Displacement Criterion
NHTSA	National Highway Traffic Safety Administration
NIC	Neck Injury Criterion
Nij	Normalized Neck Injury Criterion
Nkm	Neck Protection Criterion
OC	Occipital Condyle
PU	Polyurethane foam
Ref	Reference

Retr	Retraction
Rev	Relative
ROM	Range of Motion
SAHR	Saab Active Head Restraint
T	Depth
T1	First thoracic vertebrae
T-HR	Tracking Head-Restraint
THUMS	Total Human Model for Safety
UTS	Ultimate Tensile Strength
WAD	Whiplash Associated Disorder
WHIPS	Whiplash Protection System
WIC	Whiplash Injury Criterion
WIL	Whiplash Lessening

CHAPTER 1

INTRODUCTION

1.1 Background

Automobiles have been the number one transportation option since the discovery of gasoline fueled heat engines. This is due to the transportation need that differs from everyone to another and the freedom associated with it. As the population grows, the use of private automobiles increases. Hence, automotive industries recorded a massive increase in their production and accordingly the number of vehicles is expected to double up to billions by 2035 [1-4]. Nowadays, the development in automotive industry and roads quality yielded to faster cars [5]. Accordingly, number of vehicle accident has increased rapidly as well over the past years which led to higher rate of casualties. Around one million deaths recorded annually from automobile accidents and two thousand million victims suffer from non-fatal injuries [1, 4]. Vehicle crashes is considered the major cause of death worldwide for the age group between 5 to 44 years old [5, 6]. Hence, engineers and scientists must enhance vehicle's design to maximize the occupant's safety levels.

Based on a study done by the National Center for Biotechnology Information (NCBI); head and neck injuries following the road traffic crashes are the most common cause of temporary or permanent disability and may even result in fatal injury [7]. Ivancic et al. [8] reported that rear-end collisions are the most common type of traffic collision and neck injury is the most common type of injuries of those whom complaining physical issues. In addition, Berglund et al. [9] stated that the most frequent cause of neck injury is rear impact (38% of cases) while 23% of neck injury cases occur in frontal impacts. The increase in accidents rate yielded to an increase in Whiplash Associated Disorders (WADs) over the past decades [4, 10]. Neck injuries and strain are commonly known as whiplash trauma which is caused by sudden distortion of the neck. WADs

are very likely to occur in motor vehicle accidents, especially during rear-end collisions due to unsupported head [11]. During the acceleration impact pulse, occupant's head lags behind the torso forcing the neck to deflect suddenly causing tear in muscles, ligaments, nerves and fracture in bones in severe cases [12, 13]. This study is designed to bridge the gap in literature related to whiplash injury resulted from rear-end collision.

Since whiplash injury has been highlighted in the early 90s, vehicle seats have been equipped with passive head restraints. Head restraints are the primary prevention system used to protect the cervical spine from whiplash [14]. It limits the backward motion of the occupant's head during collision; relative to the torso during rear-end collisions [15]. However, the effectiveness of head restraints in reducing WADs is highly dependent of its location relative to the head [16]. Stemper et al. [17] observed from their study that there is a lack of proper adjustments of head restraint position by the passengers due to low public awareness of its significances. Hence, Active Head Restraints (AHRs) have been developed and designed to automatically adjust their position during impact. However, to date effect of HR gap and using of an active HR have not received enough attention from researchers. These have been the motivations behind this study.

As well-known, experimental program using volunteers are restricted to a very low impact pulses to avoid causing long-term neck injuries [18, 19]. In addition to the risk, it is very challenging to measure loading forces and moment on the neck, especially between segmental levels [20]. By using cadavers, on the other hand, most of these challenges are not an issue. However, passive muscles can lead to big deviations in replicating the real impact case [21]. Crash Test Dummies (CTDs) are widely being used in automotive collisions field. Several CTDs have been developed, each with specific test purpose. Based on author's knowledge, there is no CTD which can replicate the human neck due to the absence of many details, such as active muscles,

ligaments, intervertebral discs, and spinal cord fluid. On the other hand, numerical modelling offers more accurate approach, compared to others, for simulating human biomechanics during vehicle collisions. By using Finite Element Modelling (FEM), the crash environment and data collection can be easily controlled and optimized.

1.2 Objectives

The present study focuses on the investigation into the effect of head restraints on whiplash injury. In general, the main aims of the current study are:

- To study the effect of head-restraint position (gap) on whiplash injury during rear-end collision,
- To determine the optimum head-restraint material properties and investigate their effects on whiplash injury, and
- To develop an effective tracking head-restraint system to protect the neck against whiplash.

1.3 Significance of the study

Current development is mainly focused on whiplash kinematics and injury prevention mechanisms which are embedded in occupant's seat. However, insufficient investigation has been made to study head-restraint material independently from the seat design itself. Each component has its function and hence must have specific material properties for that purpose. In addition, head-restraint materials greatly influence the severity of whiplash injury due to their energy-absorption capability. The current study investigates the effect of head restraint material at various backset gaps. Furthermore, the optimum head-restraint material in reducing neck injuries is investigated. Moreover, a new whiplash injury prevention system is developed based on the obtained results to maximize occupant safety.

1.4 Thesis layout

The thesis is divided into five chapters. Following this chapter, Chapter 2 contains a comprehensive literature review on the fundamentals of whiplash biomechanics, current development in whiplash injury prevention systems, occupant's seat characteristics and WADs injury criteria. Chapter 3 explains the two approaches implemented to carry out this study; experimental program and finite element simulation program. Chapter 4 includes the detailed analysis of results and discussion. Chapter 5 summarizes the main conclusions of this study. Finally, Chapter 6 presents recommendations for future consideration.

CHAPTER 2 LITERATURE REVIEW

2.1 Introduction

Prior to develop an effective whiplash prevention system in vehicles, it is crucial to understand the anatomy of human neck to locate and identify possible injury spots and sources of pain. In addition, studying the behavior of head-neck-torso under different vehicle collision scenarios helps in further improving passenger safety protection systems. Currently, available literature is concentrating on developing accurate human models and whiplash evaluating criteria to investigate in depth the consequences of aggressive vehicle crashes on the neck. Therefore, in this chapter, human neck anatomy, occupant kinematics during impact, and various whiplash injury evaluating criteria used in practice are discussed.

2.2 Anatomy of the Human Vertebral Column

In human anatomy; the spinal column is the axis that supports the head, neck, and torso. As illustrated in Figure 1, the spinal column consists of 33 articulating vertebrae, which are divided into cervical (C1-C7), thoracic (T1-T12) and lumbar vertebrae (L1-L5). The cervical vertebrae form the neck region; which are placed immediately below the skull. The spinal cord and nervous systems are parts of the spinal canal which runs within every single vertebra. The spine serves three main purposes; protect the spinal cord, transfer the load and moments of upper body to the pelvis, and support the motion of the whole body [14]. Occipital Condyle (OC) bone is located at the bottom-end of the skull, in contact with the superior facets of the first cervical vertebra (atlas vertebra). The first cervical vertebra (C1) or “atlas” is the most superior cervical vertebra of the spinal column. The name atlas came from a Greek mythology; which means supporting the globe of the head [22]. The second vertebra (C2) or “axis”; it is the second – uppermost of the cervical vertebrae. The axis vertebra name was derived from its function in allowing the head to rotate from

its support atop the atlas. C1 and C2 are different from the other cervical vertebrae; they create the joint connecting between the head and the spinal column as shown in Figure 2 [23]. C1 and C2 allow a great range of lateral motion than the other cervical vertebrae. They are also responsible for nodding and rotation movements of the head [24].

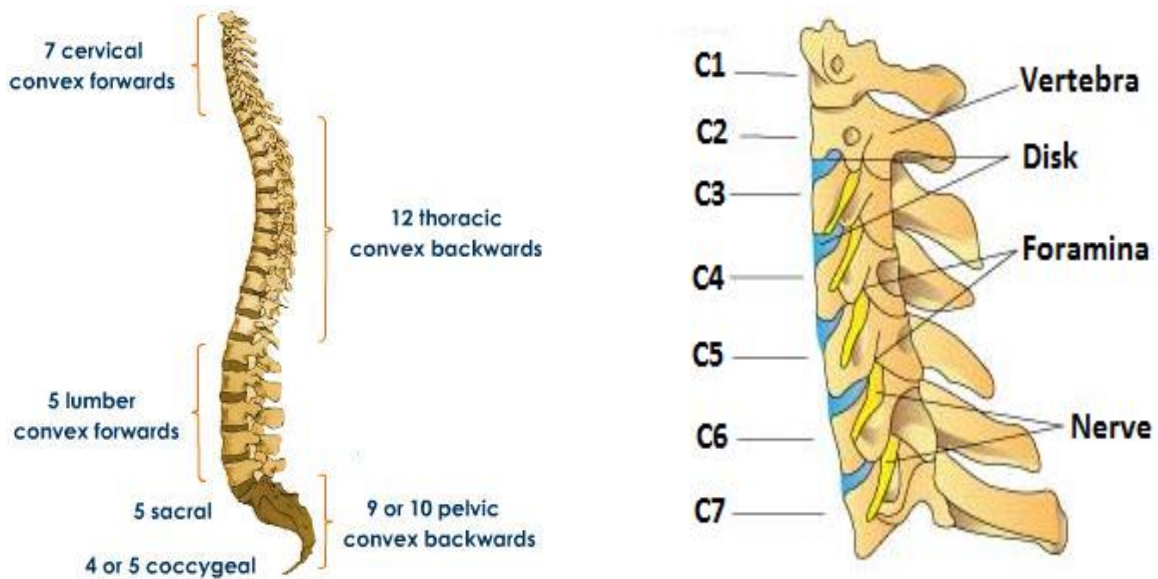


Figure 1. Human spinal column (left) and cervical spine (right) [22].

Intervertebral discs links between each two adjacent vertebrae and carries the loads from one vertebra to the inferior one [13]. It consists of three parts; the nucleus pulposus (core gel fluid), annulus fibrosis (outer shell), and cartilaginous end-plate (hyaline cartilage). Ligaments connect bones together and transfers tensile loads across the whole skeletal structure. Longitudinal ligaments are attached to the posterior and anterior surface of the whole spine (Figure 3). Capsular ligaments located at facet joints provides stability to the spine flexion movement. Ligamentum

flavum ligament has the highest elasticity to allow high deformation, while the weakest ligament is the Interspinous ligament which connect adjacent spinous processes [25].

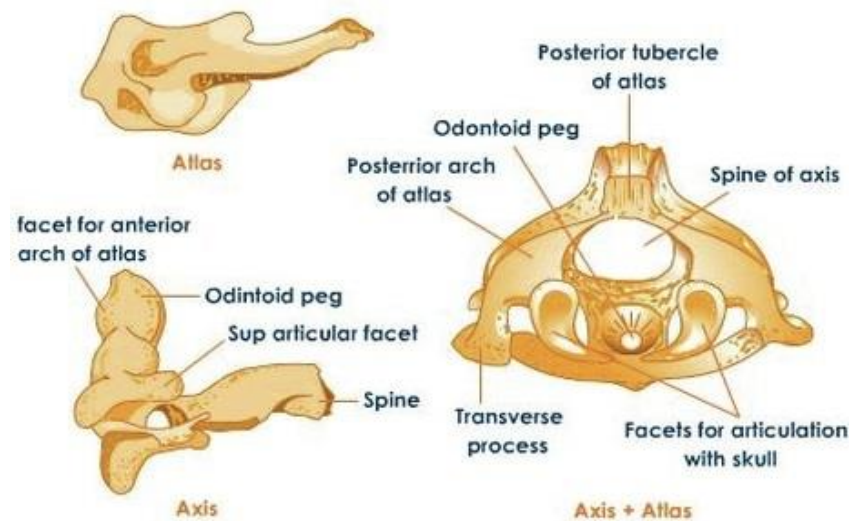


Figure 2. Structure of atlas (C1) and axis (C2) vertebrae [23].

2.3 Occupant Kinematics

Whiplash injuries are the most common symptom in vehicle collisions at low speeds [26]. During the impact, the occupant is subjected to loading due to posterior to anterior acceleration. This load is transmitted through the seat and experienced by the torso and the neck-head complex [27]. Specifically, the load is first felt by the upper back and shoulders, then the head arches rearward and comes into contact with the head restraint of the seat [28]. As a result, the neck undergoes severe sudden back and forth transitions between extension moment (rearward bending of the neck) and flexion moment (forward bending of the neck) [29].

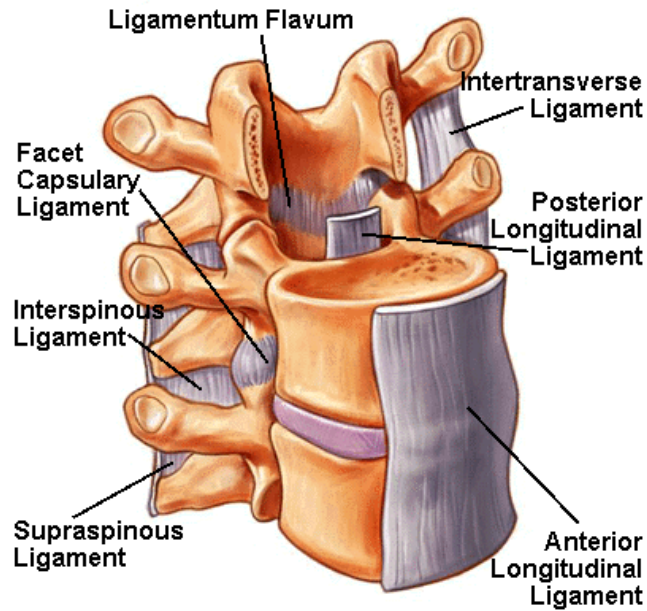


Figure 3. Cervical spine ligaments anatomy [30].

The overall movement of the head-neck-torso complex during rear-end impact of an occupant with a typical seatbelt and headrest is divided into four stages as can be seen in Figure 4. In the first stage, impact forces are applied to the shoulders and the upper torso by the seat back while the head is still stationary. While, the shoulders and upper torso move forward, the head moves rearward. On other hand, the head does not undergo any significant angular displacement at this stage [25]. Following this the lower cervical spine forcefully extends while the upper cervical becomes fully flexed. Consequently, the cervical spine forms an S-curve shape caused by flexion at C2–C3 and C3–C4 levels and extension at C4–C5 through C6–C7 levels [31, 32]. The continued anterior motion of the torso with respect to the head combined with the motion of the cervical spine results in the head striking the seat head restraint. Here the force applied will depend on the design of the seat and the head restraint. This force causes the head to rebound forwards and at the same time the cervical spine straightens [33].

2.4 Whiplash Injury Mechanisms

Up to date, the exact cause of whiplash injury is not fully understood due to the complexity of the neck anatomy and highly dependency on many factors, such as crash pulse shape and vehicle seat characteristics [34, 35]. The occurrence of vertebral fractures is rare as there is normally insufficient axial force applied to the osteoligamentous cervical spinal column [28]. However, the soft tissues of the body, namely the muscles, ligaments, joints in the spine and annulus fibrosus can be significantly damaged [28]. Furthermore, diagnosis of the damage may be difficult even when magnetic resonance imaging and computed tomography are employed. The treatment of the long term consequences of these types of injuries worldwide amounts to billions of dollars [24]. Various mechanisms explaining how whiplash injury occurs have been suggested over the past two decades [28, 31].

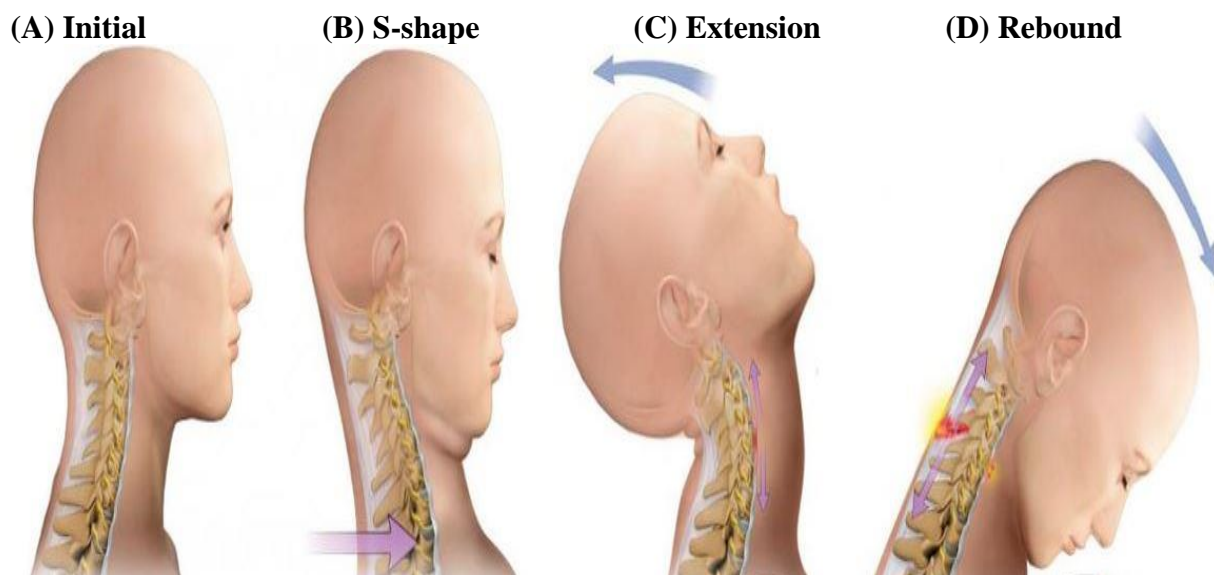


Figure 4. Head-neck kinematics and phases of whiplash injury due to rear-end impact; (A) initial posture, (B) S-shape curvature phase, (C) neck extension phase, and (D) head rebound (neck flexion) phase [36].

2.4.1 Hyperextension Mechanism

One of the proposed mechanisms of whiplash injury is the hyperextension mechanism [22, 28]. This mechanism focuses on the second stage of the motion of the head-neck complex (Figure 4) where extension of the lower cervical spine occurs [22]. This extension in turn stretches the anterior longitudinal ligament and anterior annulus of the intervertebral disk. Therefore, according to Munoz et al. [31], injuries are mostly limited to, or originate from the anterior column of the spine. The degree of injury and symptom chronicity depends on the amount of extension that occurs. The anterior longitudinal ligament may slacken or tear, meaning that the annular fibers would have decreased stiffness [28]. This could lead to chronic changes in the invertebrate disk. As stated by Yoganandan et al. [33], added range of movement due to this type of injury can eventually cause long term segmental spinal instability and spine degeneration. Patients that have experienced rear end collision often sustain anterior longitudinal ligament ruptures and disk separation, which lends weight to the hyperextension mechanism [34]. Various experiments carried out using primates and human cadavers have demonstrated the occurrence of outer annulus damage and anterior longitudinal ligament tears [28].

2.4.2 Hydrodynamic Mechanism

Hydrodynamic mechanism is another proposed theory explains the cause of whiplash injury based on pressure gradients variations in spinal canal [23, 37]. This mechanism concentrates on the change in size of the cervical spinal canal that occurs as a result of the load applied due to posterior to anterior acceleration. The canal elongates shortens due to flexion and extension which consequently means that its volume changes [23]. In the initial stages of posterior to anterior acceleration, extension of the spine reduces the area of the canal and decreases the inter-laminar space. This in turn may result in inward buckling or protrusion of the spine ligaments which

reduces the space available to the spinal nerves shown in Figure 5. As the volume of the canal further reduces there is a corresponding increase in hydrodynamic pressure gradients. Since spinal fluid is incompressible this causes an outward displacement of the spinal canal's contents [28]. Blood within the anterior internal venous plexus moves through the foramen to the anterior external venous plexus [28]. At the same time, cerebrospinal fluid enters through the nerve root sleeves. The increased amount of blood and cerebrospinal fluid leads to compressive loads being applied to nerve roots. If the compressive load exceeds tolerance levels, this can result in chronic dysfunction of the nerve roots involved [28]. The fact that occupants of vehicles involved in rear end collisions often experience neck and shoulder pain gives some credit to this theory [23].

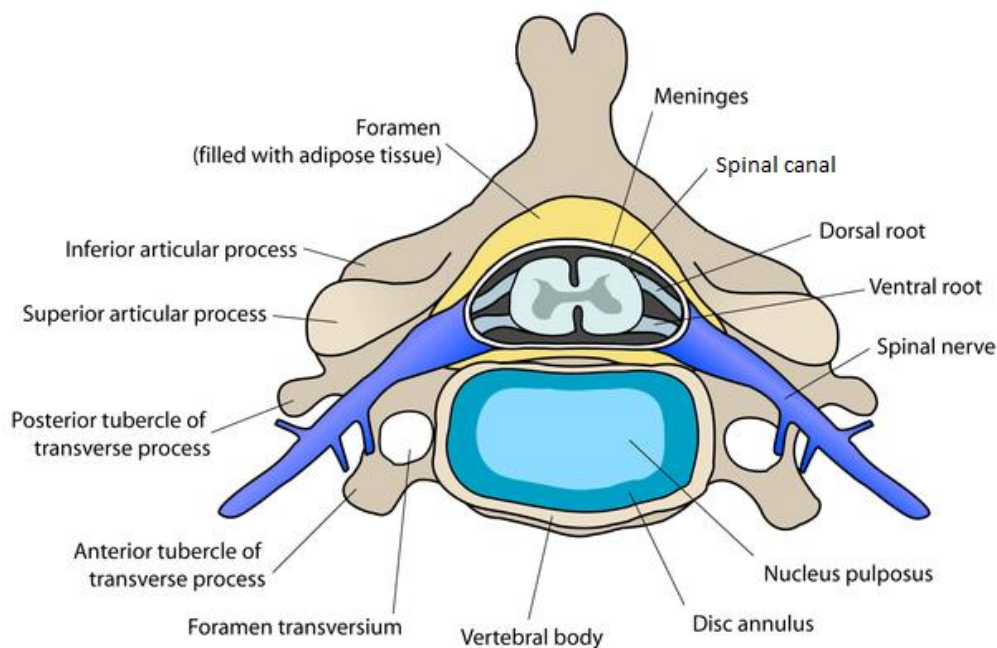


Figure 5. Cross-section of the cervical spine [33].

2.5 Neck Injury Criteria

Neck injury criteria is a tool used to estimate injury probability and severity based on specific parameters, such as displacements, accelerations, velocities, and loads. In the current study, five injury criteria were selected; NIC, Nij, Nkm, IV-NIC, and NDC. Many other neck injury criteria were proposed by several authors with different assessment approach, such as Lower Neck Load (LNL) [38] and Whiplash Injury Criterion (WIC) [31]. Each injury criterion has its pros and cons. However, the selection criterial of whiplash injury criteria are based on injury assessment accuracy and their common use in practice.

2.5.1 Neck Injury Criterion (NIC)

Neck Injury Criterion (NIC) was proposed by Boström et al. [39] in 1996 to predict neck injuries in low impact pulse rear-end collisions. They developed the criteria by conducting several experiments using pigs. The mathematical modelling was developed based on Navier-Stokes equations. They noticed that pressure transients inside the spinal cord is correlated to the S-shape curvature, when the neck shift phase at maximum retraction during rearward movement of the head. NIC criterion is expressed in terms of the horizontal (X-axis direction) relative acceleration (a_{rel}) and velocity (v_{rel}) of the atlas vertebrae (C1) to the first thoracic vertebrae (T1) as follows:

$$NIC = C_{length} a_{rel} + v_{rel}^2 \quad (1)$$

$$a_{rel} = a_x^{T1} - a_x^{C1} \quad (2)$$

$$v_{rel} = \int a_{rel} dt \quad (3)$$

where, C_{length} is a constant representing the maximum change in length of the spinal canal relative to horizontal displacement. The estimated value of L is 0.2 m for both pigs and human beings [39].

Boström et al. [39] experiments yielded a threshold value of $15 \text{ m}^2/\text{s}^2$ for NIC criterion. However, later studies [40, 41] suggested that the proposed threshold of $15 \text{ m}^2/\text{s}^2$ is not appropriate level for neck injuries because soft neck tissues were damaged at lower thresholds. A recent study by Ivancic et al. [42] recommended a threshold of $14.4 \text{ m}^2/\text{s}^2$ which may cause extension injury at C7/T1. Panjabi et al. [43] recommended injury threshold of $8.7 \text{ m}^2/\text{s}^2$, which is considerably less than Bostrom et al. [39] proposal.

2.5.2 Normalized Neck Injury Criterion (Nij)

The Normalized Neck Injury Criterion (Nij) was developed by National Highway Traffic Safety Administration (NHTSA) in 1999 to assess whiplash trauma in frontal car collisions [44]. The Nij criterion considers five injury tolerance limits; axial compression of the neck, axial tension stretching the neck, shear perpendicular to the neck axes, flexion moment rotating the neck forward, and extension moment rotating the neck rearward. Tolerance values were obtained from cadavers, volunteer, and dummy tests [45-50]. It is worth to mention that “ij” indices in the criterion term Nij represent the four main injury mechanisms; tension-extension (N_{TE}), compression-extension (N_{CE}), tension-flexion (N_{TF}), and compression flexion (N_{CF}). However, “i” index represents the axial load type while “j” represents the bending moment. In reality, neck injuries are produced by tension-extension mechanism where a tensile load stretch both the anterior and posterior soft tissues of the neck [44]. When a superimposed extension moment (rearward bending moment) acts upon the tensile load, the posterior soft tissues will be less stretched while the anterior tissues become further stretched. Hence, the value of N_{TE} is expected to have the highest value compared to the other three mechanisms.

The Nij criterion states that if the axial loads and bending moments are plotted on a single graph, then the dummy response must fall within the area enclosed by the critical intercept values for each load (Figure 6). The critical intercept values differ depending on the dummy size and type. For a medium sized (50th percentile) male dummy, the intercept values are 6806 N for tension, 6160 N for compression, and 125 N.m for extension moment [44]. Axial tension/compression loads and extension/flexion bending moments are measured at the occipital condyles. At each instance, these loads and moments are normalized with the critical intercept values. Thus, Nij can be expressed as:

$$N_{ij}(t) = \frac{F_z(t)}{F_{int}} + \frac{M_y(t)}{M_{int}} \quad (4)$$

where, F_z , F_{int} , M_y , and M_{int} represent axial tension/compression load, critical intercept value corresponding to the load, extension/flexion bending moment, and critical intercept value corresponding to bending moment, respectively. Ivancic et al. [42] suggested that neck injury might occur at Nij threshold of 0.09.

2.5.3 Neck Protection Criterion (Nkm)

In 2002, Schmitt et al [51] proposed the Neck Protection Criterion (Nkm) to evaluate neck injuries. The proposed criterion has similar derivation concept as the Nij criterion and thus it can be considered as a modification to be suited for rear-end collisions. In rear-end impacts, sagittal shear forces dominate the injury mechanism rather than axial forces in frontal impacts situation. Excessive shear forces can cause a damage to the facet joints, especially in the upper vertebrae of the neck. The shear forces are only used to calculate the bending moment in Nij criterion while these are regarded as the critical load case in Nkm criterion.

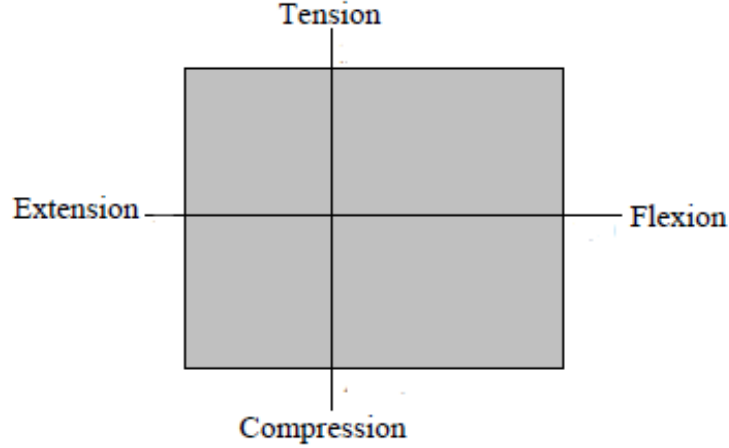


Figure 6. Nij combination of axial forces and bending moments acting on the neck.

The first index “k” in the criterion term Nkm indicates extension/flexion bending moment while the second index “m” represents anterior/posterior shear force. Four injury load cases are represented by Nkm criterion; flexion-anterior N_{fa} , extension-anterior N_{ea} , flexion-posterior N_{fp} , and extension-posterior N_{ep} . Shear forces F_x and extension/flexion bending moments M_y are measured at the occipital condyles. At each instance, these loads and moments are normalized with the critical intercept values. Thus, Nkm can be expressed as:

$$N_{km}(t) = \frac{F_x(t)}{F_{int}} + \frac{M_y(t)}{M_{int}} \quad (5)$$

where, F_{int} and M_{int} constants are the critical intercept value corresponding to the shear force, and critical intercept value corresponding to bending moment, respectively. Both anterior (positive x-direction) and posterior (negative x-direction) shear forces have intercept value of 845 N [51]. the intercept values used to calculate extension and bending moments are 47.5 Nm and 88.1 Nm, respectively [51]. The value of N_{ep} in extension-posterior load case is usually the highest in rear-

end collisions. The Swedish Road Administration recommended a threshold of $N_{km} < 0.3$ based on experiments conducted to assess the performance of seats and head-restraints [52]. Ivancic et al. [42] suggested that neck injury might occur at N_{km} threshold of 0.33.

2.5.4 Intervertebral Neck Injury Criterion (IV-NIC)

Intervertebral Neck Injury Criterion (IV-NIC) hypothesis was proposed by Panjabi et al. [43]. During whiplash impact, IV-NIC criterion compares intervertebral motion to the rotational physiological limit of each cervical vertebra. Any rotational movement beyond this limit can potentially cause injury to annulus fibers, ligaments, and facet joints.

$$IV - NIC_i(t) = \frac{\theta_{dynamic,i}(t)}{\theta_{physiological,i}} \quad (6)$$

where, t represents time, $\theta_{dynamic,i}$ is the dynamic intervertebral rotational displacement, and $\theta_{physiological,i}$ is the corresponding physiological range of motion (ROM) limit. The physiological intervertebral ROM limit was obtained from intact flexibility test of six human cervical spine samples [43]. Table 1 lists the computed physiological limit for each intervertebral level in extension and flexion.

2.5.5 Neck Displacement Criterion (NDC)

Neck Displacement Criterion (NDC) was proposed by Viano and Davidsson [53] in 2002. NDC criterion assess neck injury based on relative horizontal (x_{OC-T1}) and axial (z_{OC-T1}) displacements of the occipital condyle (OC) to T1 vertebrae. Moreover, it also considers maximum head extension angle (θ_{OC}) after the early S-shape curvature. These parameters are related to hyperextension at the point where the facet joints are mostly damaged [53]. NDC classifies neck injury likelihood, based on natural range of motion of both volunteers and dummies, into four

zones; excellent, good, acceptable, and poor as given in Table 2. A poor rating indicates high probability of neck injury when the neck motion response is beyond the natural range of motion.

Table 1. Intact physiological motion limit for each intervertebral level in extension and flexion along with injury threshold.

Intervertebral level	Physiological limit [deg.]		Injury threshold
	Extension	Flexion	
Head/C1	13.7	13.7	< 1.6
C1/C2	6.4	8.8	No injury
C2/C3	3.6	5.4	No injury
C3/C4	4.2	5.7	< 2.0
C4/C5	6.7	7.6	< 2.1
C5/C6	6.5	7.7	< 1.5
C6/C7	7.1	8.0	< 1.8
C7/T1	3.1	3.7	< 3.4

Table 2. NDC injury classification according to natural range of motion [53].

Classification	Head Extension	Posterior Shear	Axial Compression
	Angle	Displacement	Displacement
Excellent	$\theta_{OC} < 25^\circ$	$x_{OC-T1} < 35$ mm	$z_{OC-T1} < -15$ mm
Good	$\theta_{OC} < 40^\circ$	$x_{OC-T1} < 55$ mm	$z_{OC-T1} < -25$ mm
Acceptable	$\theta_{OC} < 55^\circ$	$x_{OC-T1} < 75$ mm	$z_{OC-T1} < -35$ mm
Poor	$\theta_{OC} > 55^\circ$	$x_{OC-T1} > 75$ mm	$z_{OC-T1} > -35$ mm

2.5.6 Lower Neck Load (LNL) Criterion

Lower Neck Load (LNL) criterion was proposed in 2003 by Heitplatz et al. [38] to assess whiplash injury due to rear-end collision. The authors considered not only the initial phase, when the neck shows S-shape deformation, they correlated LNL to maximum retraction and head rebound phases of neck distortions as well.

LNL injury criterion incorporates forces acting in three different directions and moments about two perpendicular axes. LNL index is calculated using force and moments measurements at the lower neck (T1) during the impact pulse. LNL can be expressed as:

$$LNL - index(t) = \left| \frac{\sqrt{M_y(t)^2 + M_x(t)^2}}{C_{moment}} \right| + \left| \frac{\sqrt{F_y(t)^2 + F_x(t)^2}}{C_{shear}} \right| + \left| \frac{F_z(t)}{C_{tension}} \right| \quad (7)$$

where, M_y and M_x are the moments about the lateral and anterior-posterior axes, respectively. F_x and F_y are the shear forces acting in the anterior-posterior and lateral directions, respectively. F_z represent the axial force causing tension or compression loading. The constants C_{moment} , C_{shear} , and $C_{tension}$ are the critical intercept values.

The critical intercept values depend on human tolerance in real world collisions. In case of experimental work, the crash test dummy affects intercept values. Heitplatz et al. [38] conducted experiments on three most widely used crash test dummies; Hybrid III, RID2, and BioRID II. Based on their results, intercept values of 15, 250, and 900 were proposed for moment, shear, and tension, respectively.

2.6 Head-Restraint (HR) Systems

Head restraint are considered as the main prevention system in limiting neck injuries in rear-end vehicle collisions [4, 16]. Therefore, recent biomechanical studies have illustrated the crucial point of developing effective HRs [6, 11, 14]. The effectiveness of the system is highly dependent of the relative head position to the system [17, 54]. Moreover, the geometry and material properties of the HR play a major role in reducing the neck injury [10, 12]. Various types of HR have been proposed by the researchers and automobile companies (e.g. Saab, Volvo, Toyota and Mercedes-Benz) [10, 55-59].

One of the main factors which has a direct effect on whiplash is the HR position relative to the head. Insurance Institute for Highway Safety (IIHS) standard considers properly positioned head restraint as the first crucial step towards whiplash prevention system. IIHS published a rating scheme for HRs based on the backset gap and distance from top of head as illustrated in Figure 7. A static evaluation can lead to four classifications are present; good (zone 1), acceptable (zone 2), marginal (zone 3), and poor (zone 4). The top of the head restraint should be higher than the occupant's head's center of gravity and the backset gap is less than 9 cm to be efficient in protecting the neck (good or acceptable). Otherwise, marginal or poor rated head restrains are rejected and cannot undergo dynamic evaluation. Stemper et al. [17] studied whiplash in various backset gaps and showed that as the gap increases, maximum head retraction (relative horizontal distance between head and torso) increases as well. In addition, they also stated that S-shaped curvature prior to head restraint contact also increases leading to more sever neck injury. Based on Maher [60] findings, arresting head movement before hyperextension occurs will prevent serious neck injury such as posterior wall misalignment and tear drop fractures of the vertebrae.

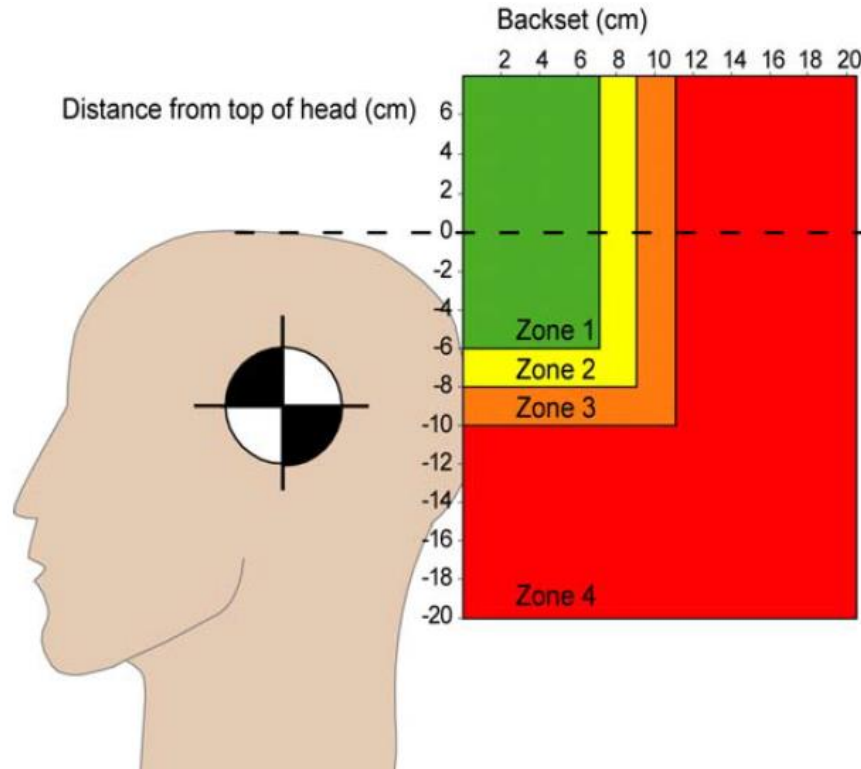


Figure 7. IIHS static rating standard for head-restraints geometry (RCAR-IIWPG V3).

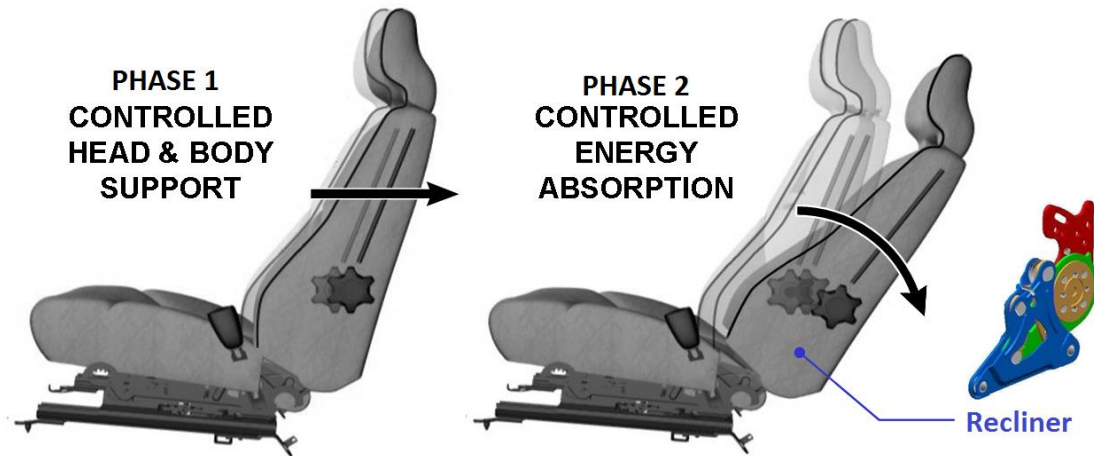
According to Kai et al. [25], whiplash injuries can be prevented if the relative motion between the head and torso is eliminated which can be achieved by simply having a backset of zero. Based on this concept, head restraint systems have been modified to be active rather than passive [61]. Active Head Restraints (AHRs) can automatically adjust their relative position to occupant's head to minimize the gap. Most developed AHR systems available in the market are designed to be triggered during the collision and therefore called Re-AHRs [62]. Recent studies are focusing on developing Pro-AHRs which deploys prior to an impact. This can be achieved by measuring relative distance and speed of nearby vehicles which can lead to potential collisions [63].

2.6.1 Re-AHRs

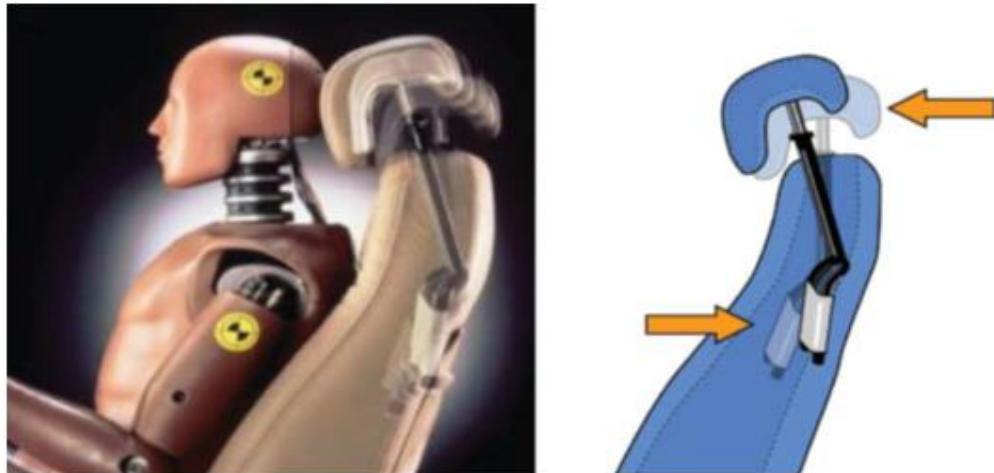
Re-AHRs will usually be deployed by the occupant's torso rearward momentum. One of the most well-known neck injury prevention seat is Whiplash Protection System (WHIPS) developed by Volvo Car Corporation [56, 57]. At the beginning of impact, WHIPS seat supports passenger's head-neck-torso to minimize relative accelerations (Figure 8-A). After that, the torso is allowed to move backward together with the head to allow further absorption of energy [56]. This is achieved by using a recliner to attach the backrest to the seat base. Saab Active Head Restraint (SAHR) is also considered as a re-active head restraint system. When the occupant's rearward inertial sticks the seatback, it engages a mechanism embedded inside the seat-back [55]. Consequently, the head-restraint will immediately move toward the head to minimize the backset gap (Figure 8-B).

Toyota Whiplash Lessening (WIL) system, developed by Toyota Motor Corporation, uses a unique seat design and geometry to reduce relative head-torso motion [58]. WIL seat consists of thick seat-back cushion with rigid side frame to secure the passenger in case of an impact. Moreover, the head restraint quickly moves toward the occupant's head and upward while the upper portion of the seat moves rearward and downward (Figure 8-C). Similar to most AHR designs, the previous examples of Re-AHRs can refunction and return to their initial state after deployment by simply replacing a sacrificial pin [24]. Other head-restraint designs however must be replaced totally after impact. For example, Latchford and Chirwa [64] developed an airbag head restraint system which cannot be used again once deployed. Their approach showed better protection against whiplash injury due to lower rebound velocity, lower impact forces and better energy-absorption.

(A) Whiplash Protection System (WHIPS)



(B) Saab Active Head Restraint (SAHR)



(C) Toyota Whiplash Lessening (WIL)

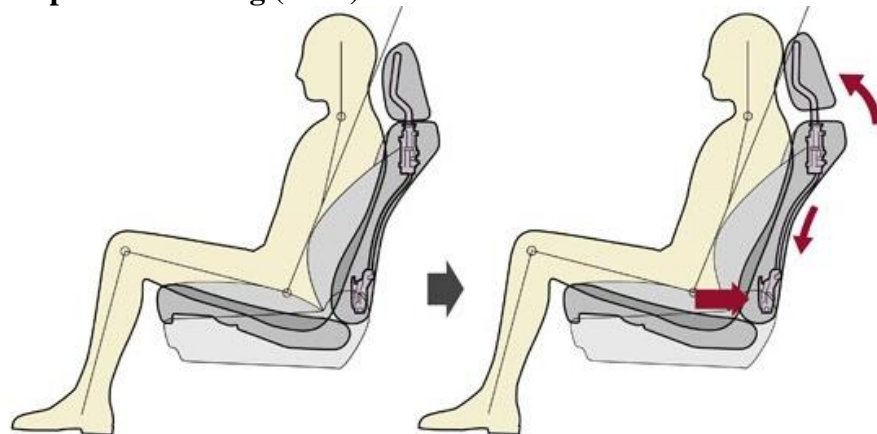


Figure 8. Examples of Re-AHRs with different approach; (A) Volvo WHIPS tilting backwards, (B) Saab SAHR adjusting backset gap, and (C) Toyota WIL adjusting height [55, 56, 58].

2.6.2 Pro-AHRs

Various concepts of deployment have been proposed utilizing sensors to trigger mechanical, airbag, magnetic or another device to activate the head restraint. These devices do not require occupant physical interaction and they are usually re-usable after the collision [24]. Mercedes-Benz (Neck-Pro) and BMW Head Restraint are the most common examples of Pro-AHRs [10]. Both systems consist of two parts as illustrated in Figure 9; a stationary part fixed to the seat containing movement actuators and electronics, and moving cushion to close the backset gap. These systems are actuated by crash sensors on either the bumper or inside the vehicle [65]. Neck-Pro seat releases its energy stored in loaded springs to create forward and upward motion of the head restraint [59]. BMW Head Restraint, on the other hand, uses a gas filled cartridge to propel the head restraint [66].



Figure 9. Example of Pro-AHR with a stationary part and moving cushion [10].

2.6.3 Material Properties of Head-Restraints

Many of early studies investigated the effect of seat-back constitutive properties on whiplash injury. Nilson et al. [67] reported that reducing the stiffness of the seat-back reduces some whiplash injury criteria and kinematics parameters, while Boström et al. [68] reported the exact opposite. On another level, Ono et al. [19] stated that little or no effect of the back-seat stiffness on whiplash injury. Similarly, Morris et al. [69] found that whiplash potential can be minimized by increasing the plastic yielding of the seat-back material, while Olsson [70] reported the opposite. The contradictions in research findings can be related to the different properties of the head-restraints of the seats tested as well as the test conditions. Therefore, researchers have started studying a variation of seat-back properties accompanied with head restraint adjustments to understand the effect of these properties on whiplash potential.

Recent developments in the head restraint materials prospective have been done to enhance its energy-absorption while arresting the head [12]. Schmitt et al. [71] investigated the influence of using various types of foam as padding material in seats. They reported that the maximum head acceleration is reduced by using viscoelastic foam material which consequently reduced whiplash injury. Özdemir et al. [72] concluded from their investigation of various seat designs that lower backseat stiffness, especially the upper part of the seat-back, decreases the risk of whiplash injury. This is because lower stiffness will allow the torso of the occupants to move backward easier which yields reduction in the relative displacement between the head and neck [72]. Similarly, Kitagawa et al. [73] pointed out that increasing the depth of the seat-back frame would give the torso more degree to move backwards which significantly reduces the joint capsules strain value and thus decreasing the whiplash injury potential.

2.6.4 Effect of Airbags and Seatbelts on Whiplash

Seatbelts and airbags are systems that complement each other's functions in protecting vehicles passengers. The major function of the airbag is to protect the occupant from impacting the interior vehicle's components by absorbing the occupant's energy. Similarly, the main aim of the seatbelt system is to prevent the ejection of occupant in case of a crash by using the lap belt, as well as protecting the occupant from the internal components of the vehicle such as the steering wheel and the dashboard by using the shoulder belt [74].

Seatbelt actions during vehicle accidents does not influence whiplash associated disorder or whiplash injury potential. Kumar et al. [75] compared the effect of using 3-point versus 5-point seatbelts on the cervical muscles electromyogram reaction during a rear-end impact. The seatbelt was installed on a rigid seat where 17 healthy volunteers were seated and subjected to different impacts of varying acceleration from 4.4 to 16.8 m/s². They concluded that 5-point seatbelt and 3-point restrains seatbelt has no adverse effect on the cervical muscles at low impact speeds. Seatbelts are mainly effective in protecting the face, chest, and pelvic areas, but they are not as much effective in protecting the neck against whiplash. However, when the seatbelt is accompanied with a functioning airbag, protection against cervical/neck injury is significantly increased in frontal impacts only [76].

Whiplash injuries risk was reported to increase in cases where the occupant's head rebounding off the inflated airbag in motor crashed, especially occupants who are not restrained by seatbelts [74]. Therefore, many airbags restraint systems have been developed recently and mainly to reduce whiplash injury. Ford has released a new airbag system in its 2012 Ford Focus [77]. The system is designed specifically to protect the head and neck of the occupant by recognizing the occupant's weight and height, and inducing the airbag-inflation pressure

accordingly so the occupant's head does not move backwards aggressively. General Motors has also released a dual-depth side airbags system that inflates the airbag in different sizes [78]. Volvo has released a similar system to general motors, however the inflation speed is measured instead [79]. The speed of inflation in Volvo's system depends on the severity of the crash as well as the seat-belt usage. These systems were designed to provide an inflation rate/pressure based on the occupant's characteristics, so no sudden rebound of the neck/torso is obtained, and thus they protect the occupants from WAD.

2.7 Discussion

Recent research focuses mainly on the design of head restraint of the seat with lack of concentration on studying the effect of seat-back properties such as energy absorption, stiffness and yielding of the supporting frames [80]. Similarly, car manufacturer's focus was on head-restraints systems developments and enhancement rather than enhancing the seat-back constitutive properties and parameters [72]. Researchers reported that seatbelts and airbags are not effective in protecting the neck against whiplash in rear-end collisions. This is very reasonable in case of numerical simulations because the data is being recorded until the head rebounds from the headrest which limits the forward motion of the body. Therefore, seatbelt system was not added to the model nor airbag system. These injury prevention systems are effective only in frontal-collision scenarios where the headrest becomes ineffective.

Figure 10 shows schematic of occupant's head-neck response to rear-end impact with respect to pulse time. NIC criterion has been widely used as one of the main indicators of whiplash injury. It evaluates the most essential risk factor for neck injury; head retraction during the first 75 milliseconds of the impact pulse. However, incorrect results occur the head is no longer parallel to T1, particularly when the head rotates 20-30°, at approximately the first 50-100 milliseconds of

the crash [51]. In addition, whiplash injury assessment must not rely on NIC criterion alone because it does not consider hyperextension injury mechanism in its assessment [31]. Moreover, NIC requires additional parameters to involve the forward rebound motion of the neck [41].

Nij and Nkm criteria are more stable throughout the crash time interval than the others. This is an advantage of using forces and moments which are not influenced by effects such as rotational angles. Nij criterion was developed to assess neck injuries in frontal car impacts. Applying Nij criterion to rear-end impacts will produce difficulties in the interpretation of the results [51]. Nkm criterion seems to assess the S-shape formation well due to the combination of shear forces and bending moment [31]. However, both Nij and Nkm criteria depend on the forces and moments measured at occipital condyle only, while neck injury is more common to occur between the vertebrae C5/C7 [31]. Moreover, involving head-restraint contact will influence the dynamics of the neck response and further complicate the loading phases.

One of the main advantages of IV-NIC criterion is it correlated to soft tissue injury and can identify the intervertebral injury site. In addition, it can predict the mode, severity, and exact time of the injury. The main drawback of IV-NIC criterion is it does not consider the influence of compression and shear displacement on neck injury, it only assesses extensions of individual vertebrae. Using IV-NIC criteria will give accurate evaluation in the S-curve and maximum extension phases. NDC criterion provides a meaningful assessment because it represents real kinematics of the head-neck-torso. NDC are most suitable to be used to evaluate whiplash injury during S-shape formation and maximum extension phases where the cervical vertebrae experience excessive relative translational and rotational displacements beyond their physiological limit. LNL injury criterion assess whiplash using combined loading measurements whereas others use either axial or horizontal loading measurements only. This gives LNL added versatility, especially when

the loads are acting on oblique neck elements. Thus, it is very effective in predicting whiplash injury in the maximum extension and rebound phases where forces and moments are very complex. NIC and IV-NIC have more precise injury evaluation at the S-curve phase due to the involvement of relative neck kinematics more than forces and moments. It is worth mentioning that the proposed LNL critical intercept values are very sensitive on the human tolerance or crash test dummies. The proposed values are based on old crash test dummies which have number of limitations, especially when measuring the lower neck extension moment (M_y) due to the absence of lower neck load-cell. Moreover, Heitplatz et al. [38] did not propose neck injury threshold value for LNL criterion.

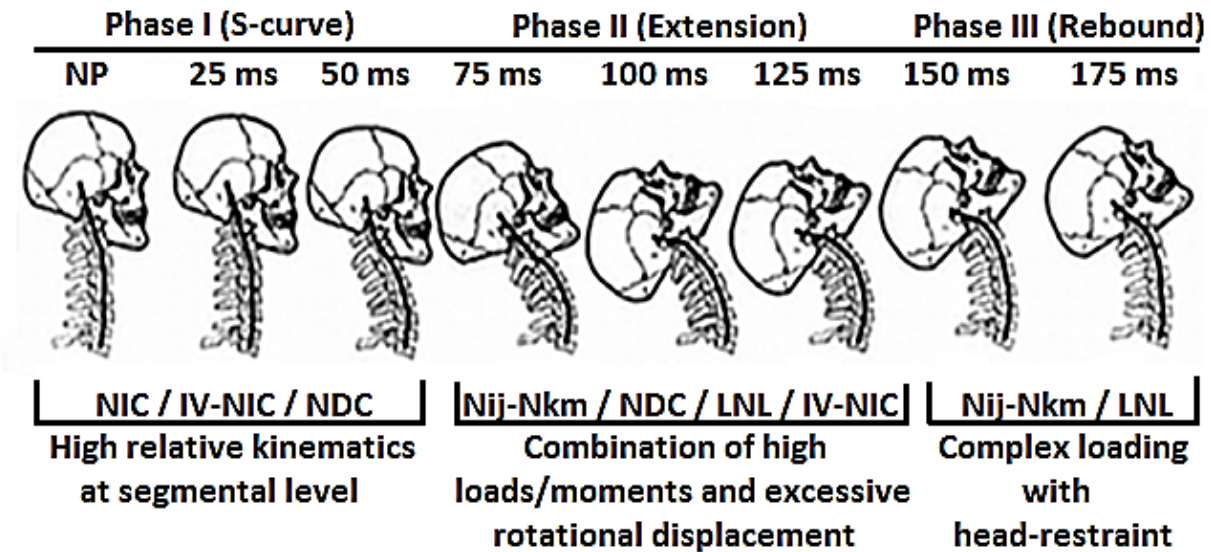


Figure 10. Schematic of occupant's head-neck response to rear-end impact with respect to pulse time. The response is divided into three different stages; (I) S-curve phase, (II) maximum extension phase, and (III) head rebound phase [22].

CHAPTER 3 METHODOLOGY

3.1 Introduction

In this chapter methods that were implemented to carry out the study are described. Experimental and finite element modelling (FEM) techniques have been used to achieve the objectives of this study. Firstly, experimental tests were performed to characterize head-restraints (HRs) materials. Secondly, a FEM is developed for simulating rear-end impacts and to investigate the effect of HR position and material on neck injury. Finally, HR prototypes are presented to effectively reduce neck injuries.

3.2 Experimental Program

Experimental program initially aims to assess the diversity of geometrical and material properties of Head Restraints (HRs) available in the market today. As shown in Figure 11, indentation force deflection and tensile tests were carried out to assess the mechanical properties of HR material namely; density, Young's modulus (stiffness), tearing stress, ultimate elongation percentage, and energy absorption capability. In this study, six commercial HRs were selected from different car manufacturers as listed Figure 12.

In addition, three tracking HR prototypes were developed to eliminate the gap between the passenger's head and head restraint while driving. Consequently, the best tracking mechanism will be combined with the optimum HR cushion material properties to produce effective anti-whiplash protection system.

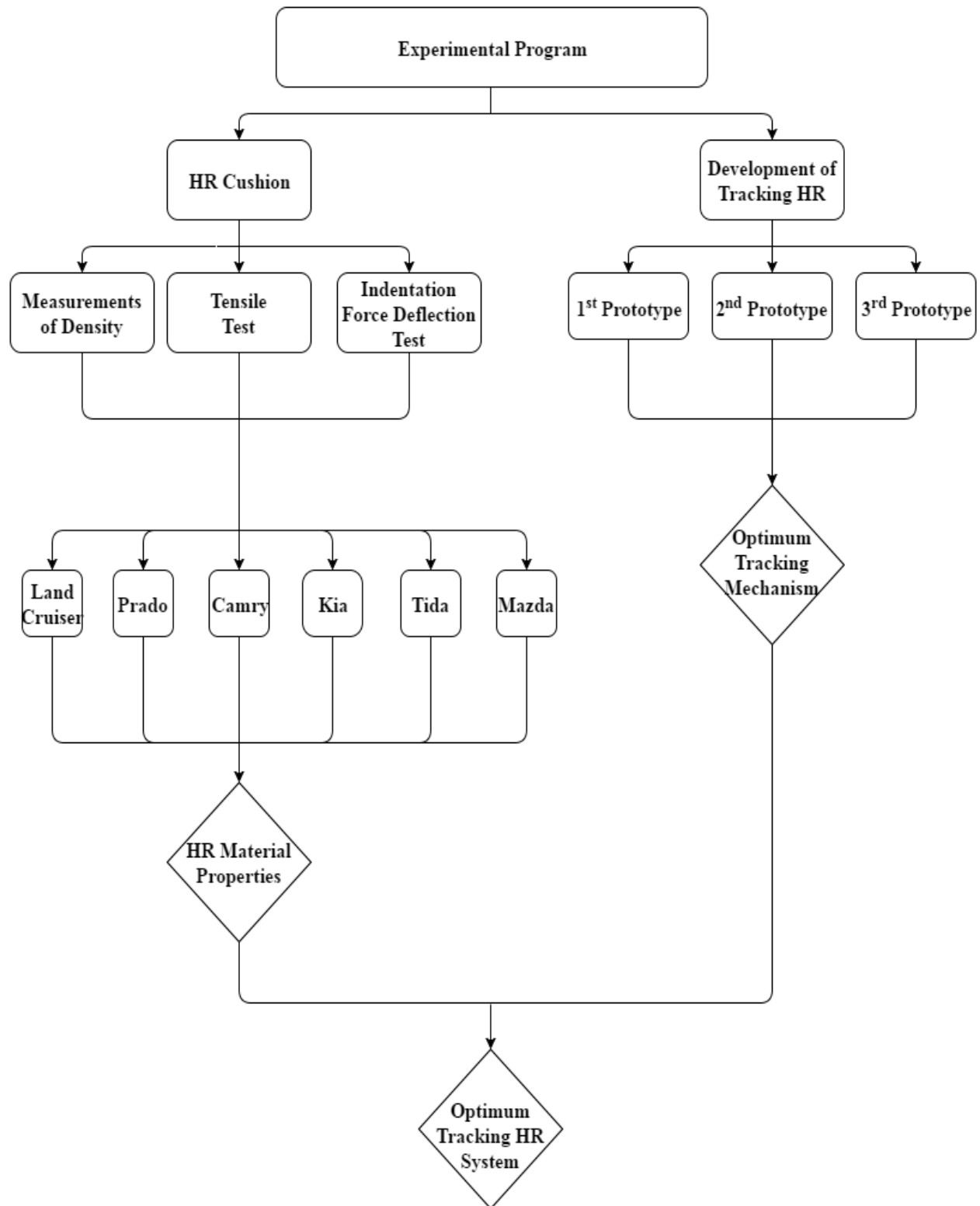


Figure 11. Flow chart summarizes experimental program.












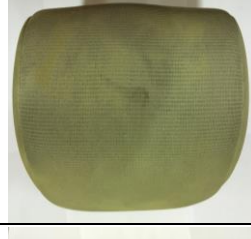






	Front View	Side View	Top View
(A) Toyota Land Cruiser			
(B) Toyota Prado			
(C) Toyota Camry			
(E) Mazda M3			
(F) Kia Cerato			
(G) Nissan Tida			

Figure 12. The front, side, and top views of the selected commercially available head-restraints for experimental testing; (A) Toyota Land Cruiser, (B) Toyota Prado, (C) Toyota Camry, (E) Mazda M3, (F) Kia Cerato, and (G) Nissan Tida.

3.2.1 HR Material Density Measurements

The core densities of the six HRs were determined by calculating the mass and the volume of the specimen based on ASTM D3574-A standard. Three cubic specimens were prepared from each HR material. A weight balance with an accuracy of 0.001 g were used to measure the weight of the specimens. A digital measuring machine was used to accurately measure the dimensions of the specimens. The following equation was used to obtain the density in kg/m³:

$$\text{Density } (\rho) = \frac{m}{V} * 10^6 \quad (8)$$

where, m and V are the mass (g) and volume (mm³) of specimen, respectively.

3.2.2 HR Material Tensile Test

Tensile testing includes pulling the cushion specimen from one end while the other end is fixed until it tears apart within the gauge length. Consequently, the Young's modulus (E), ultimate elongation ($L\%$), and stress-strain diagram are obtained. Three tensile samples were prepared from each HR as per ASTM D3574-E standard. The dimensions of the tensile specimen are shown in Figure 13. Because HR cushion material is very soft, a laser cutting machine (Universal Laser machine VLS 6.60) was used to produce accurate cuts and free of sharp edges. The test was carried out on 250 kN INSTRON universal machine at crosshead speed of 15 mm/min.

3.2.3 Indentation Force Deflection (IFD) Test

Six commercially used head-restraint models were tested experimentally using INSTRON universal testing machine. Indentation Force Deflection (IFD) test was carried out based on ASTM D5672 standard to measure IFD of various types of flexible foam materials. IFD is the force required to indent a flexible foam material up to a defined depth. Lower IFD values corresponds

to less firmness foam material, while high values represent stiff foams. Based on ASTM standards, the diameter of the circular indenting plate should remain constant at 203 mm. However, the width of almost all commercially available head-restraints does not exceed 200 mm. If the standard plate size is followed, then a compression test will be performed on head restraints rather than IFD test. Therefore, the standard was violated on only this point and the chosen flat indenter was 120 mm in diameter.

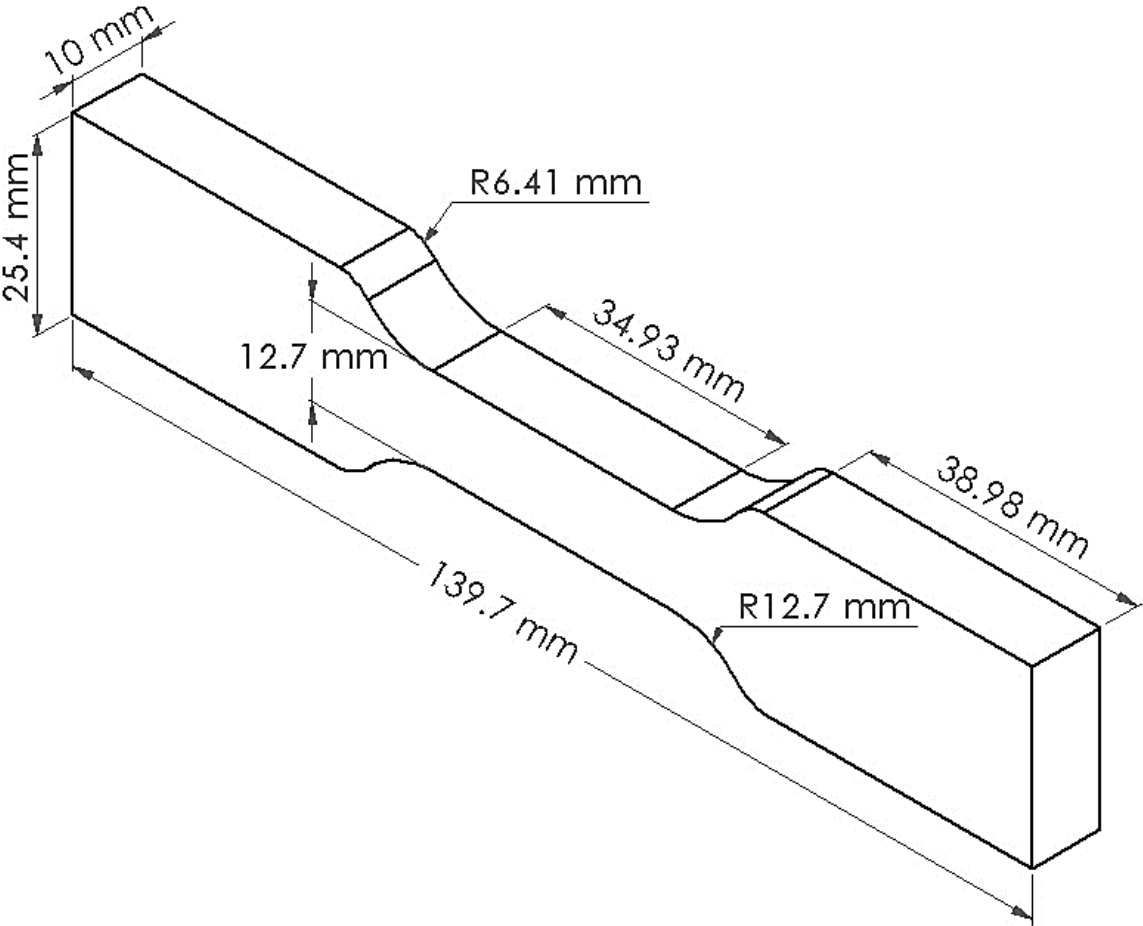


Figure 13. Dimensions of flat tensile HR specimens as per ASTM D3574-E standard.

3.2.4 Development of Tracking Head-Restraint (T-HR) System

The T-HR system will track the occupant's head and maintain its position with the safe backset gap range to protect the neck from whiplash at the incident of rear impact during driving. In addition, it will adjust its altitude until it reached the top of the head, as per the recommendations of the Insurance Institute for Highway Safety (IIHS), demonstrated in Figure 7. Therefore, the system requires at least two motors to control the two degrees of freedom. Moreover, distance detection sensors must be used to detect and track the passenger's head during driving the vehicle.

3.3 Finite Element Modelling Program

The flow chart of finite element modeling program is illustrated in Figure 14. The simulations were carried out using the developed FEM of 50-percentile human model seated on a 2012 Toyota Land Cruiser seat. This program will investigate firstly the effect of backset gap between the occupant's head and HR on whiplash injury. Once the optimum HR position is known, the influence of HR material properties on whiplash will be evaluated at this specific HR position. Consequently, the optimum material properties at the best HR position is concluded. After that, the performance of those material properties at different HR positions is tested. This will indicate whether these material properties are inclusive of HR position or not.

3.3.1 Development of Finite Element Model (FEM)

3.3.1.1 FEM Tool

Finite Element Modelling is one of numerical techniques widely employed in simulating engineering case studies. FEM method lays on splitting the objects into much smaller parts called

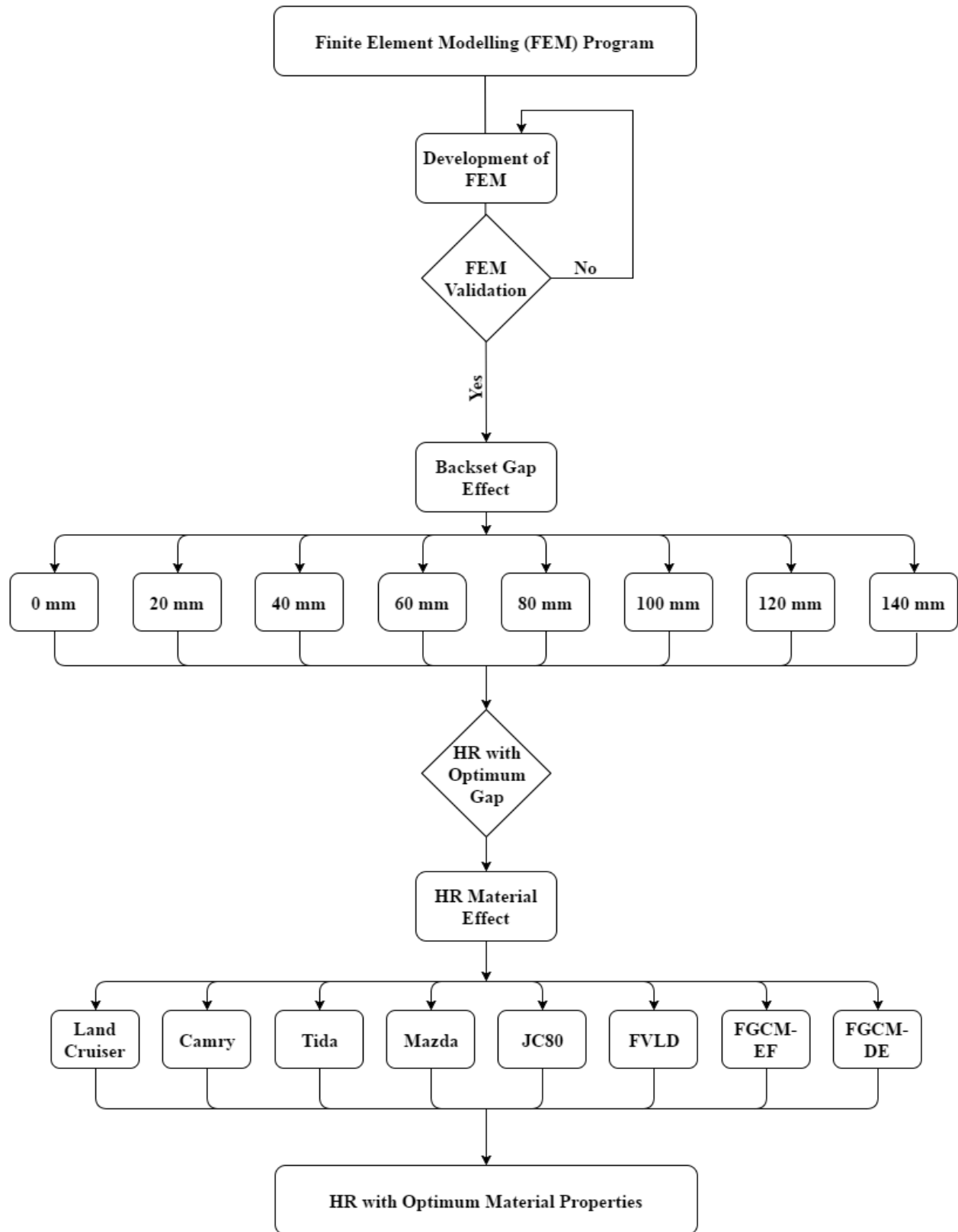


Figure 14. Flow chart of numerical modelling investigation on head-restraints.

finite elements. Thus, simpler equations are used to simulate the overall model. Finally, all the equations are combined to provide a solution for the entire problem. The accuracy of the numerical solution is dependent on many factors including; mesh size (elements count), type of elements (quadratic, tetrahedron, etc.), numerical solution method (explicit or implicit), boundary and initial conditions.

LS-DYNA solver is a FEM tool capable of simulating complex real world cases. It is commonly used by the aerospace, automobile, manufacturing, military and bioengineering industries [24]. LS-DYNA simulates highly nonlinear physical problems which uses explicit and implicit time integration. Usually these problems are subjected to high speed and large deformations in short time duration where inertial forces are very important, and that what is meant by transient dynamics, e.g. automotive crashing (deformation of chassis, airbag inflation, seatbelt tensioning), explosions, bullet impact, drop testing, sheet metal forming.

LS-DYNA offers many options that makes it very useful tool for solving complex problems. One of the main important options that is provided by the software is creating an automatic definition of the contact type between geometries in the structure. The software also provides a huge library of material types with different failure modes and behaviors. In this study, the FE model was created and built using LS-PREPOST pre-processor and solved by LS-DYNA solver. The first step was creating the geometry of the structure and assigning its dimensions, then meshing it with the suitable mesh type and size, as the solution of the meshed geometry will be affected by the type and size of the mesh, all was done using the pre-processor LS-PREPOST. The defined materials, contact type, boundary, and initial conditions were specified in the pre-processor.

3.3.1.2 Geometry of Human Model and Car Seat

In this study, Total Human Model for Safety (THUMS) has been used to model the human body. THUMS is a FEM developed by Toyota Central R&D Labs (TCRDL) and Toyota Motor Corporation. Up to date, THUMS is the most detailed CAD model compared to humans; it consists of skeletal structure, muscular structure, organs, tendons, ligaments, and nerve system. All of these structures were modelled based on ultra-resolution CT-scans of humans. THUMS model is used mainly in automotive crash simulation application, either in pedestrian or occupant scenarios. Many type of THUMS are available including; average size male adult (AM50), small size female adult (AF05), and large size male adult (AM95). A clinical study about obesity in Qatar, collected from 1,552 citizens, reported that the average Qatari population height and weight are 162.84 ± 9.65 cm and 77.51 ± 15.97 kg, respectively [81]. Therefore, THUMS AM50 model (Figure 15) was selected to represent the majority Qatari citizens. The model height and weight are 175 cm and 77 kg, respectively. Over the past decade, great efforts were made to improve the accuracy of THUMS model. To date, there are five available versions of THUMS. The fourth version (4.0) is used in this investigation which contains around two million elements. This version was developed in 2010 and aims to simulate internal injuries and bone fractures.

The Car seat model was developed based on a Toyota land cruiser 2012 GXR seat as illustrated in Figure 16-A. Toyota Land Cruiser is one of the most driven vehicles in the middle east [82, 83]. The driver's seat-base and seatback had an inclination of 10 degrees from its base. Figure 16-B shows the Computer Aided Design (CAD) for the seat. The overall dimensions of the seat are mentioned in Figure 16-C&D. It is worth to mention that the seatback and base padding contains thicker sections. This allows the passenger's torso to be positioned in the center rather than shifting aside which may prevent the head from touching the HR during an impact.

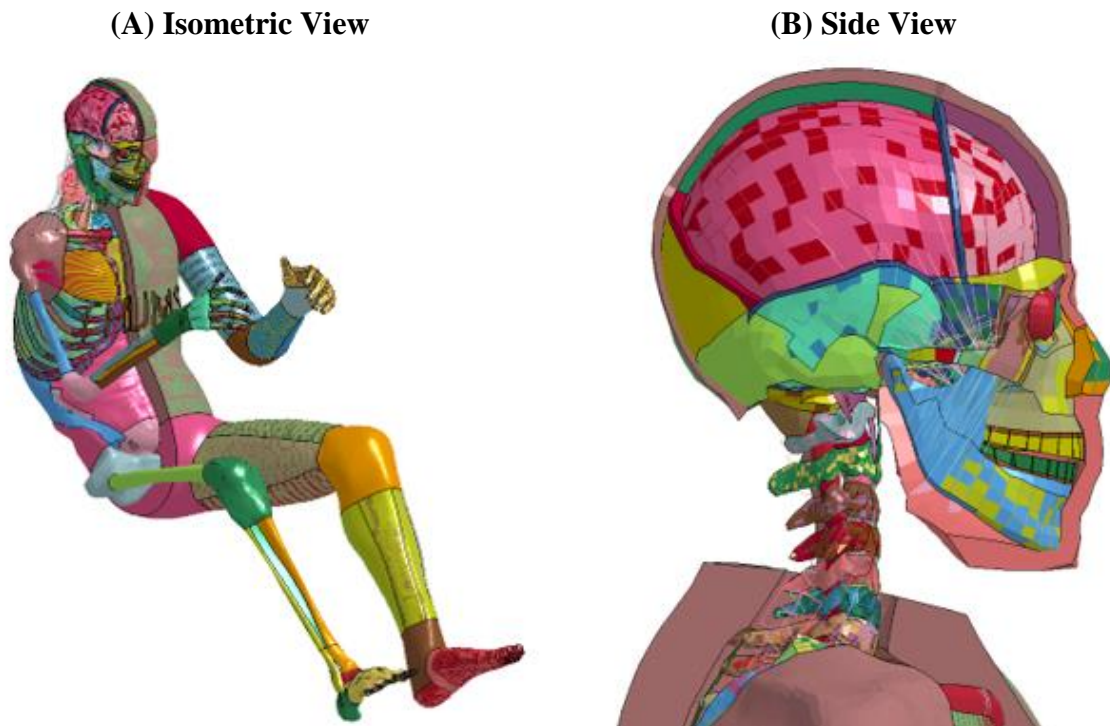


Figure 15. Academic version 4.0 of THUMS AM50 model; (A) occupant view and (B) side view showing the seven cervical vertebra [84].

3.3.1.3 Optimization of Element Type and Mesh Size

Finite elements can be either shell element (two-dimensional elements) or solid elements (three-dimensional elements). Computational time for shell elements more efficient because they are a mathematical simplification of solid elements. Furthermore, unlike shell elements, solid elements account for the stresses perpendicular to any of its surfaces. Consequently; solid elements were used in this study for three reasons compared to shell elements; no need for geometric or loading assumptions, boundary conditions are applied more realistically, and better physical visualization of the model.

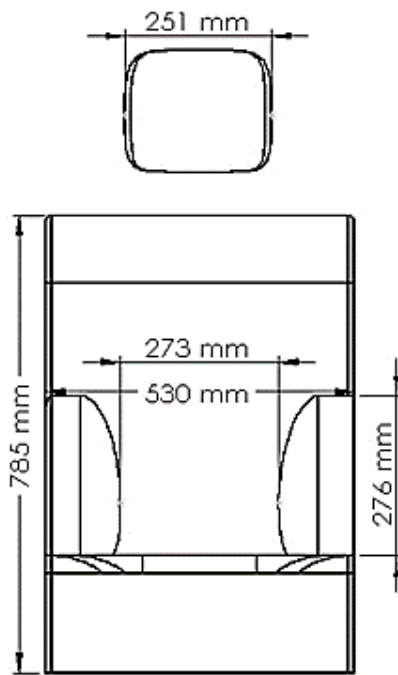
(A) Land Cruiser Seat



(B) CAD Seat



(C) Front View



(D) Side View

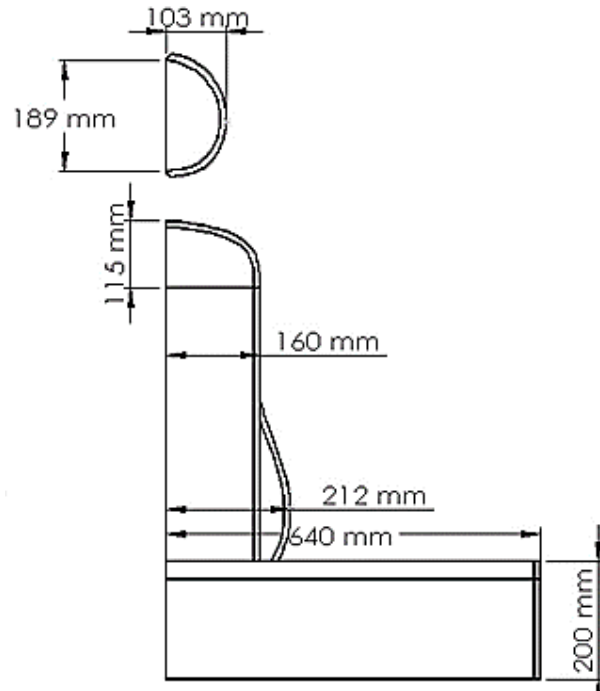


Figure 16. The geometry model for (A) Toyota Land Cruiser seat, (B) CAD seat model, (C) front view, and (D) side view.

There are many theories on how to formulate solid elements in FEM. Finite element type must be selected based on its shape (hexahedron, tetrahedron, etc.), material (solid, viscoelastic, fluid, etc.), loading case (tensile, bending, torsion, etc.) and boundary conditions. Based on this study scenario, three element types can be used; One point integrated solid elements (type 1), fully integrated solid elements (type 2), and fully integrated quadratic 8-node element with nodal rotations (type 3). Type 1 solid elements are frequently used in application containing large deformations. This type has a constant stress section properties with one integration point. Therefore, bending and torsion modes in a single solid element are not accounted for. Moreover, in type 1 solid elements, hourglassing modes are zero energy modes which become present due to having only one integration point. These modes have shorter periods compared to structural response periods [85]. Therefore, hourglass control may be required if excessive element deformations are present. This control may lead to energy dissipated because hourglass forces are interfering with hourglass modes. The fully integrated selective reduced (S/R) solid element (type 2) assumes constant pressure rather than constant stress. Type 2 elements do not require hourglass stabilization because it uses eight integration points. However, type 2 elements exhibit a very stiff behavior due to the formation of excessive transverse shear locks, especially when the elements have poor aspect ratio. This phenomenon occurs because type 2 elements must introduce shear strains to develop pure bending modes. Consequently, this may lead to excessive shear locking and restrict the element from deforming. Type 3 solid element has full integration (12 point) with nodal rotations (6 DOF per node). By using this type, accurate results are obtained especially for small strains [86]. However, it is not stable for high deformations due to shear locking similar to type 2 solid element type. In addition, type 3 requires much more computational time compared to others due to its complexity. As a conclusion, for high strain explicit numerical

problems, type 1 solid elements are more efficient than type 2 and type 3 elements. Therefore, this study will be carried out using type 1 solid elements without hourglass control, unless needed when the elements fail to converge due to negative volume errors.

The accuracy of the model solution improves by increasing the mesh density. However, the required computational time will increase correspondingly. Thus, a mesh convergence study is performed to find the suitable mesh density to provide satisfying accuracy with efficient utilization of computer resources. Mesh convergence study will not consider for THUMS human model because several researchers and institutes have validated it [87-91]. THUMS 4.0 AM50 model consists of 395,000 shell elements and 1,325,820 solid elements with total of 630,000 nodes. As for the driver seat, a simpler mesh convergence study has been carried out as illustrated in Figure 17. The model consists of a rigid sphere indenting a 260 x 260 x 100 mm³ padding at a constant speed 50 mm/s until it reaches almost half of the depth. The rigid sphere represents a 50 percentile occupant's head with average diameter of 200 mm [92]. The gravitational acceleration is defined to be parallel to sphere's initial velocity direction. The padding is made of type 1 cubic hexahedron solid elements with aspect ratio of 1 without defining hourglass control. The padding will have similar material properties as the driver seat cushion used in the main model. The padding will be fully fixed from its bottom nodes and the falling sphere has one translational freedom. At the beginning of the study, mesh size will be coarse (20×20×20 mm³ elements). After that, the mesh will become denser, as shown in Figure 18, until a convergence is reach. The maximum internal energy of the pad and maximum Von Mises stress will be plotted against number of elements. Moreover, computational CPU time will be listed for each mesh size.

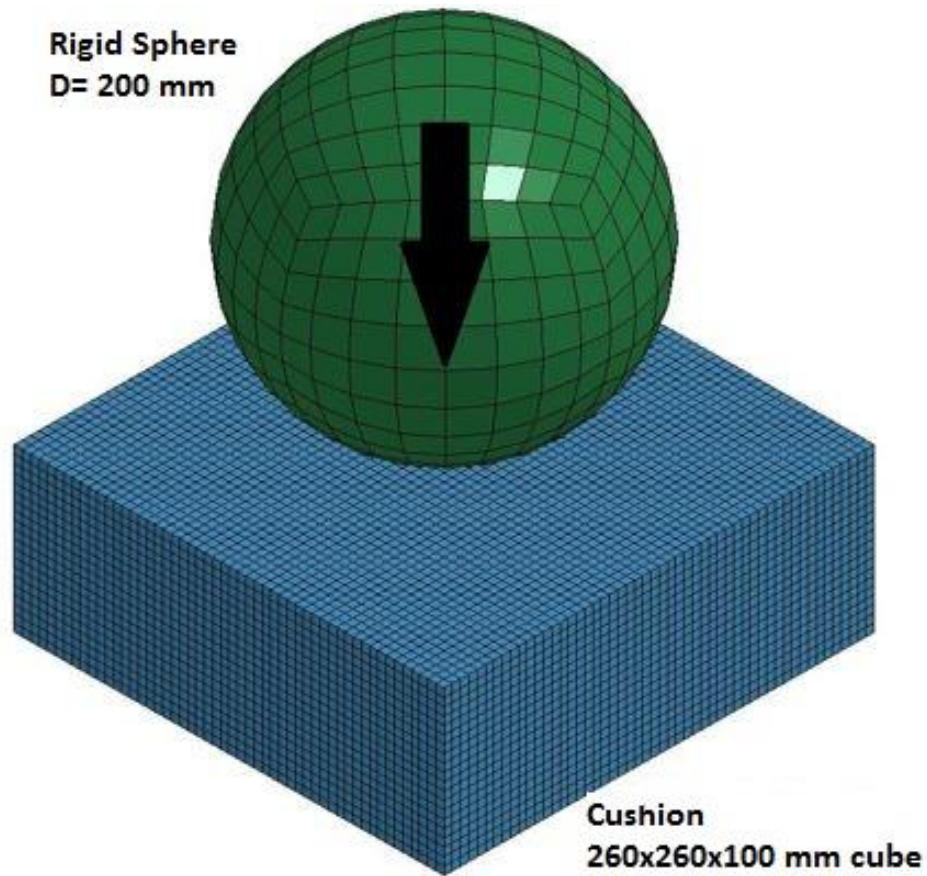


Figure 17. Sphere striking a pad used to perform mesh size study on driver's seat.

3.3.1.4 Material Modelling

(THUMS) Elasto-plastic material properties were defined for the skeletal structure while the soft tissues, such as skin and flesh, were assumed to have hyper-elastic material behavior. Ligaments and tendons showed low stiffness and high stiffness response to short elongation and large elongation percentages, respectively. Incompressible material properties were defined to model solid organs, for example kidney and liver. Hollow organs, such as lungs, were defined with compressible properties. Although the heart is considered a hollow organ, it was defined with incompressible material because it has thick muscular walls and filled with blood.

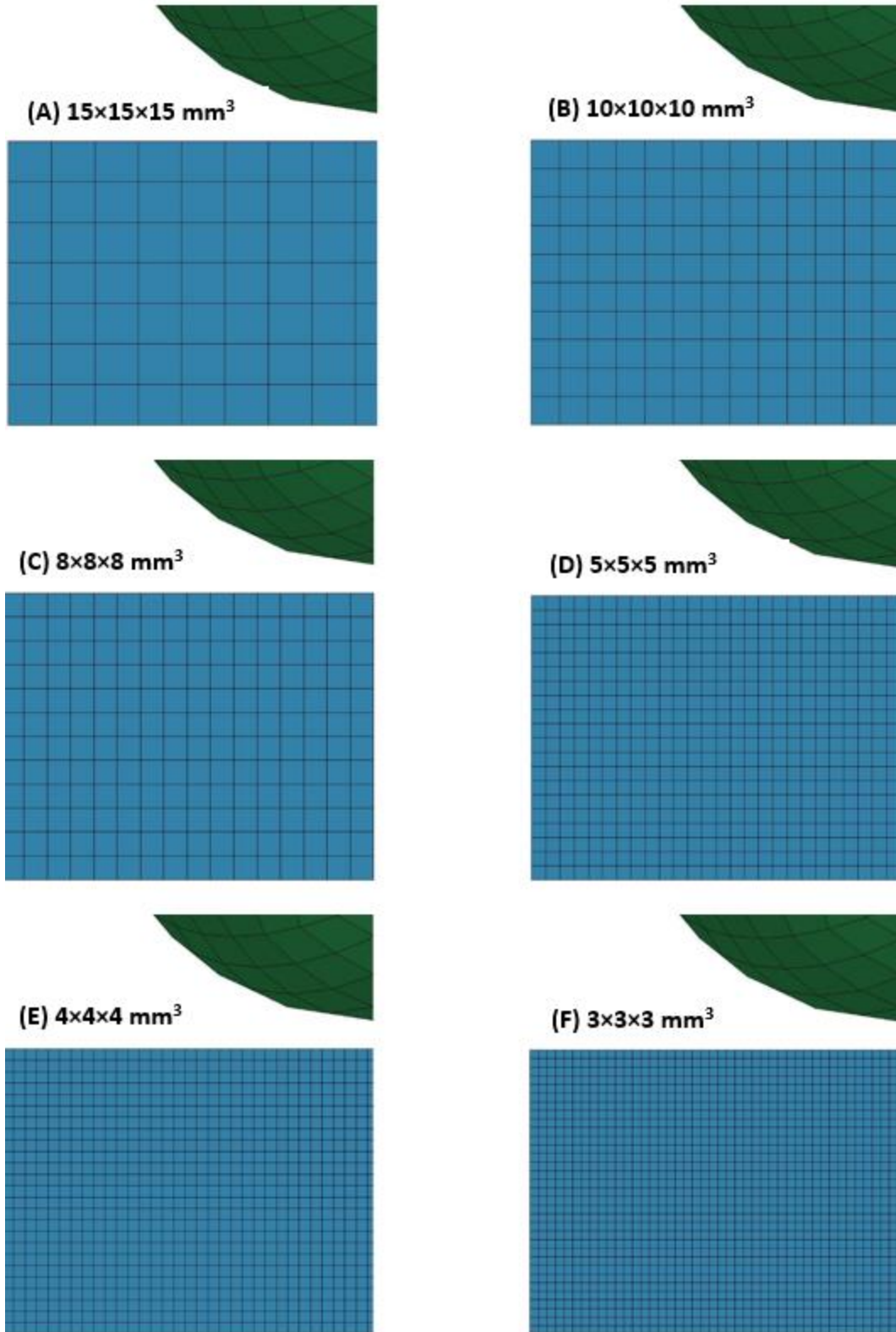


Figure 18. Mesh element volumes used in mesh size study; (A) $15 \times 15 \times 15 \text{ mm}^3$, (B) $10 \times 10 \times 10 \text{ mm}^3$, (C) $8 \times 8 \times 8 \text{ mm}^3$, (D) $5 \times 5 \times 5 \text{ mm}^3$, (E) $4 \times 4 \times 4 \text{ mm}^3$, and (F) $3 \times 3 \times 3 \text{ mm}^3$.

The driver's seat consists of two materials; rigid frame and flexible cushion, as shown in Figure 19. The blue portion (frame) is defined as a rigid material to provide structural support during excessive deformation. Rigid part elements do not experience any deformation process which consequently simplifies the model and save calculation time. The red portion, on the other hand, represents the energy-absorbing cushion of foam material. Head-restraint material model was defined as MAT-LOW-DENSITY-FOAM (057) in LS-PrePost keyword. This material is used to model highly compressible urethane foams which are widely being used in vehicle seat padding. Material model 57 is defined by the density (ρ), effective stiffness (E), stress-strain diagram, hysteretic unloading factor, and decay factor (β) measured in the experimental tensile and IFD tests carried on the six HRs. Hysteresis behavior allows foam materials to store some of the absorbed energy while unloading rather than releasing it back immediately. Figure 20 demonstrates the response of low density urethane foam during loading/unloading compression test [85]. When the hysteretic unloading factor is equal to unity, almost no energy is being dissipated by the foam. However, as the hysteretic factor magnitude decreases, the foam absorbs more energy. Decay factor (β) causes the foam material to become softer when the loading/unloading process is repeated. For example, if the decay factor is equal zero, then the reloading curve will exactly track the unloading path.

3.3.1.5 Boundary and Loading Conditions

Crash acceleration or impact pulse is the sudden change of the vehicles acceleration when it is impacted by another vehicle in case of an accident. The nature of the acceleration pulse generated from the impact has a direct effect on the severity of neck injuries [18]. Many researchers studied the influence of acceleration pulse shape (jerk) on neck response [18, 20, 27]. The common conclusion was that with higher acceleration jerks, a longer-term neck injury is developed. The

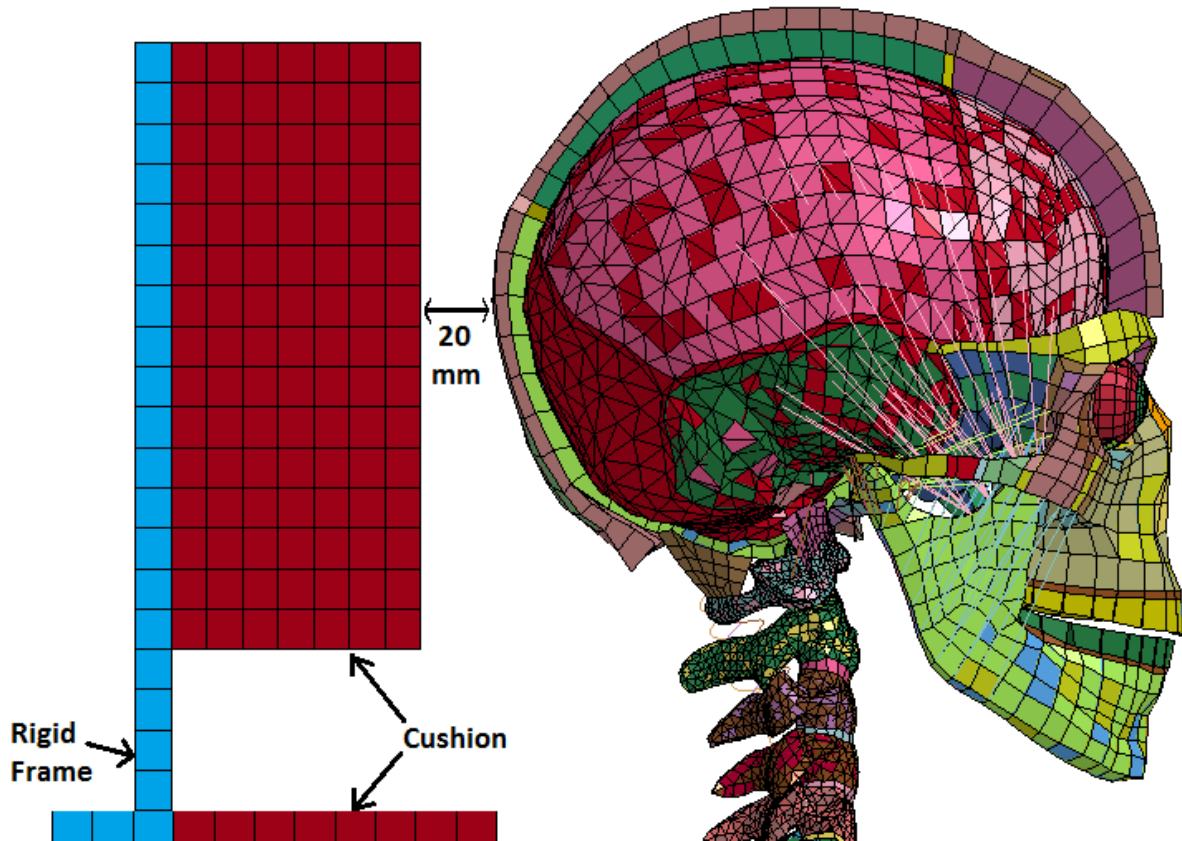


Figure 19. Passenger head position at 20 mm gap from the cubic head-restraint.

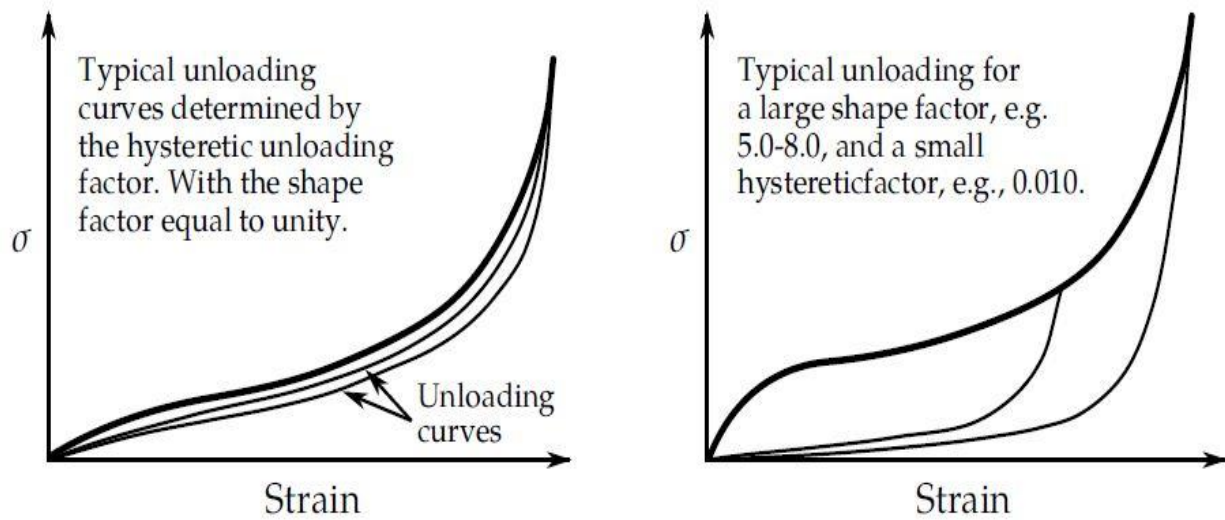


Figure 20. Behavior of foam (left) hysteretic factor is unity or (right) less [85].

Insurance Institute for Highway Safety (IIHS) proposed a standard acceleration pulse for rear-end collisions (Figure 21). Crash pulse specifications are given in Table 3, where the pulse curve must lay within the lower and upper bounds. The current study applies IIHS acceleration pulse in every simulation case. According to IIHS standard, the crash results must be recorded until the occupant's head rebounds from the HR or after a period of 300 ms from the beginning of acceleration pulse, whichever comes first.

Rigid seat frame elements and both ends of the seatbelt were given the prescribed acceleration pulse in positive x-axis direction. Gravitational acceleration (9.8 m/s^2) is included in the model to obtain more realistic results. It is defined in negative z-axis direction perpendicular to the motion direction. the human model (THUMS) is not constrained in translation nor rotational movements (6 DOF). However, the defined gravitational acceleration and seatbelt will arrest it and limit its upward or frontal movements.

3.3.1.6 Contact Algorithm

Due to the severity of the impact and large deformations between the human model and the seat, automatic surface-to-surface contact option was selected. Automatic contacts are non-oriented to allow the detection of contact penetration coming from all side of the elements. In case initial penetrations are detected; the slave nodes will be moved to the master's part surface to eliminate penetrations. During the crash, contact penetrations are commonly being eliminated by a Penalty-Based interface algorithm (SOFT=0). This algorithm checks at every time step for potential penetration of slave nodes through the master surface. If the model finds a node (n_i) penetrating through a master segment, a force (f_s) is generated normal to penetration depth to resist it.

$$f_s = -lk_i n_i \quad \text{if } l < 0 \quad (9)$$

As illustrated in Equation (9), the normal reaction force (f_s) is dependent on the penetration depth (l). Moreover, it is influenced by the contact stiffness (k_i) which is given in Equation (10) in terms of the element's area (A_i), volume (V_i), bulk modulus (K_i), and scale factor (f_{si}).

$$k_i = \frac{f_{si} K_i A_i^2}{V_i} \quad (10)$$

Due to the presence of soft foam material in the driver's seat, the calculated contact stiffness is very low which caused excessive penetration. This issue can be solved by increasing the scale factor (f_{si}) to raise the contact stiffness (k_i). However, this technique may cause instabilities, especially for values larger than 0.1. These instabilities can be eliminated by modifying the time step size. Another alternative to increase the contact stiffness factor (k_i) without causing instabilities is to use Soft Constraint Penalty Formulation (SOFT=1). This formulation adds an additional stiffness to the previous contact stiffness factor. The additional stiffness is calculated based on the stability of the local system contains slave nodes mass and master nodes mass connected by a spring. Therefore, SOFT=1 penalty contact type was introduced in this model with a friction coefficient of 0.1.

3.3.1.7 Validation of Developed FEA Model

To validate the developed overall model, the obtained results were compared against published studies with similar impact scenario. It is worth mentioning that the boundary condition may not match, especially the impact pulse shape, which will create more variations. The obtained head retraction results at various backset gaps were compared to Stamper et al. [17] numerical

Table 3. Acceleration pulse specifications according to IIHS (RCAR-IIWPG V3) standard.

Acceleration Pulse Characteristics	Upper Bound	Lower Bound
Acceleration at time = 0 ms	-0.25 g	0.50 g
Acceleration at time = 27 ms	9.5 g	10.5 g
Time that sled acceleration returns to 0 g	88 msec	94 msec
Velocity change (delta v)	14.8 km/h	16.2 km/h

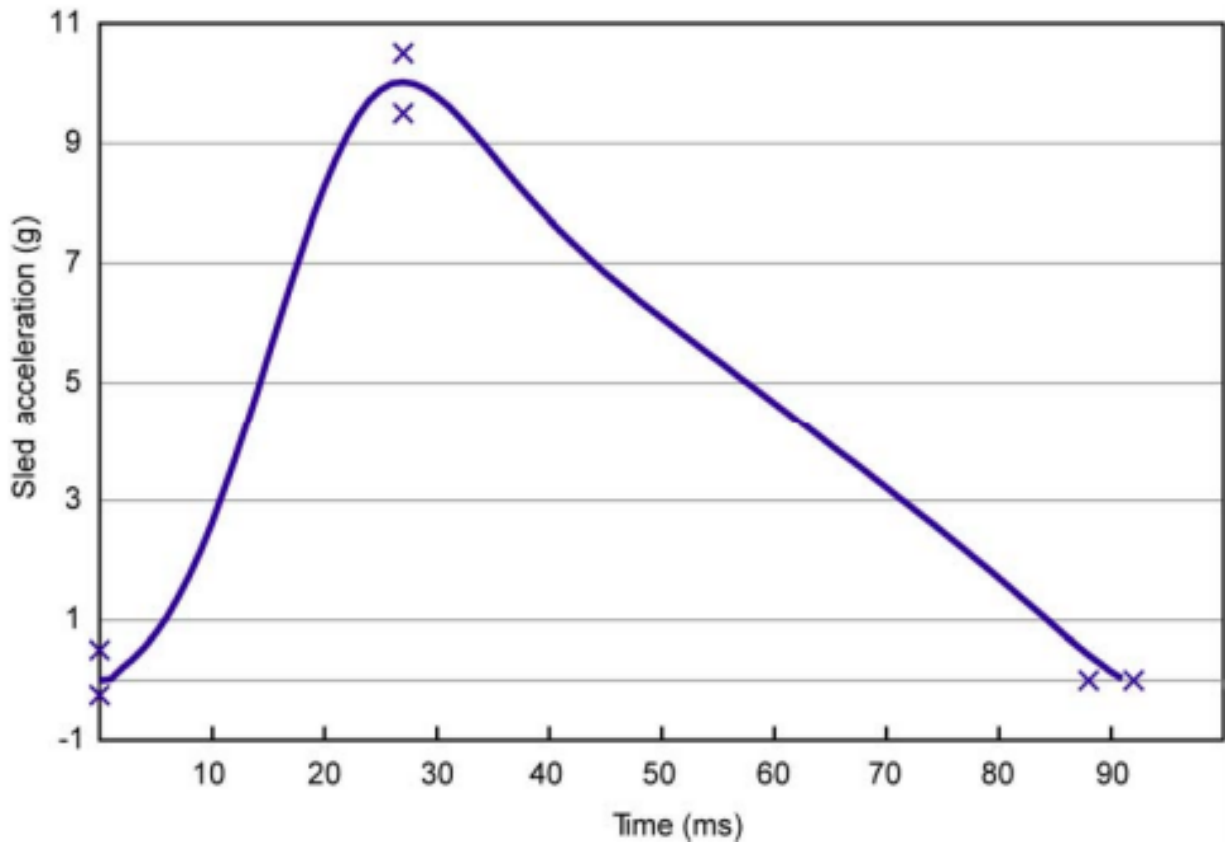


Figure 21. Upper and lower bounds for acceleration pulse variations according to IIHS (RCAR-IIWPG V3).

results. They have used a finite element head-neck complex, shown in Figure 22, to simulate rear-end impact. The HR were made of a thin shell rigid material. HR backset gap was varied in their study from 0 mm to 140 mm. Their study was performed by having a 4.1 m/s rear-end impact, with maximum acceleration of 10 g and 92 ms pulse width. The acceleration pulse was applied to the first thoracic vertebrae (T1) and the HR.

3.3.2 Effect of Head-Restraint Position on Whiplash

To investigate the influence of head position relative to the head-restraint on whiplash injury, the backset gap was gradually increased from 0 mm to 140 mm with a constant increment of 20 mm. The HR had a consistent cubic shape throughout all the cases and positioned at the same level of the passenger head to eliminate the influence of geometry and its variation in height on the results. To compare the obtained results from each case, the assessment of six injury criteria are used; NIC, Nij, Nkm, IV-NIC, NDC, and LNL. Furthermore, the type of whiplash mechanism will be observed and injury sites will be located (bones, ligaments, soft tissue, etc.). Based on the thresholds of the six injury criteria, HR positions which will effectively prevent whiplash will be listed, and the best position will be used throughout the next section. Moreover, the developed HR tracking mechanism will maintain this optimum HR position while driving.

3.3.3 Effect of Head-Restraint Material Properties on Whiplash

Aside from experimental testing, finite element modelling investigation using LS-Dyna tool has been carried out to study the effect of head-restraint (HR) material properties on whiplash injury. HR foam material properties were varied in the finite element simulations. The chosen material properties were obtained from the experimental test carried out on the selected HRs shown in Figure 12. In addition, two materials were included from the works of De Vries [93] and Ouellet et al. [94] to increase the range of material properties. This will allow the effect of very soft and

stiff material properties to be more obvious. In addition, two combinations of material properties were formed to produce a Functionally graded cellular material (FGCM).

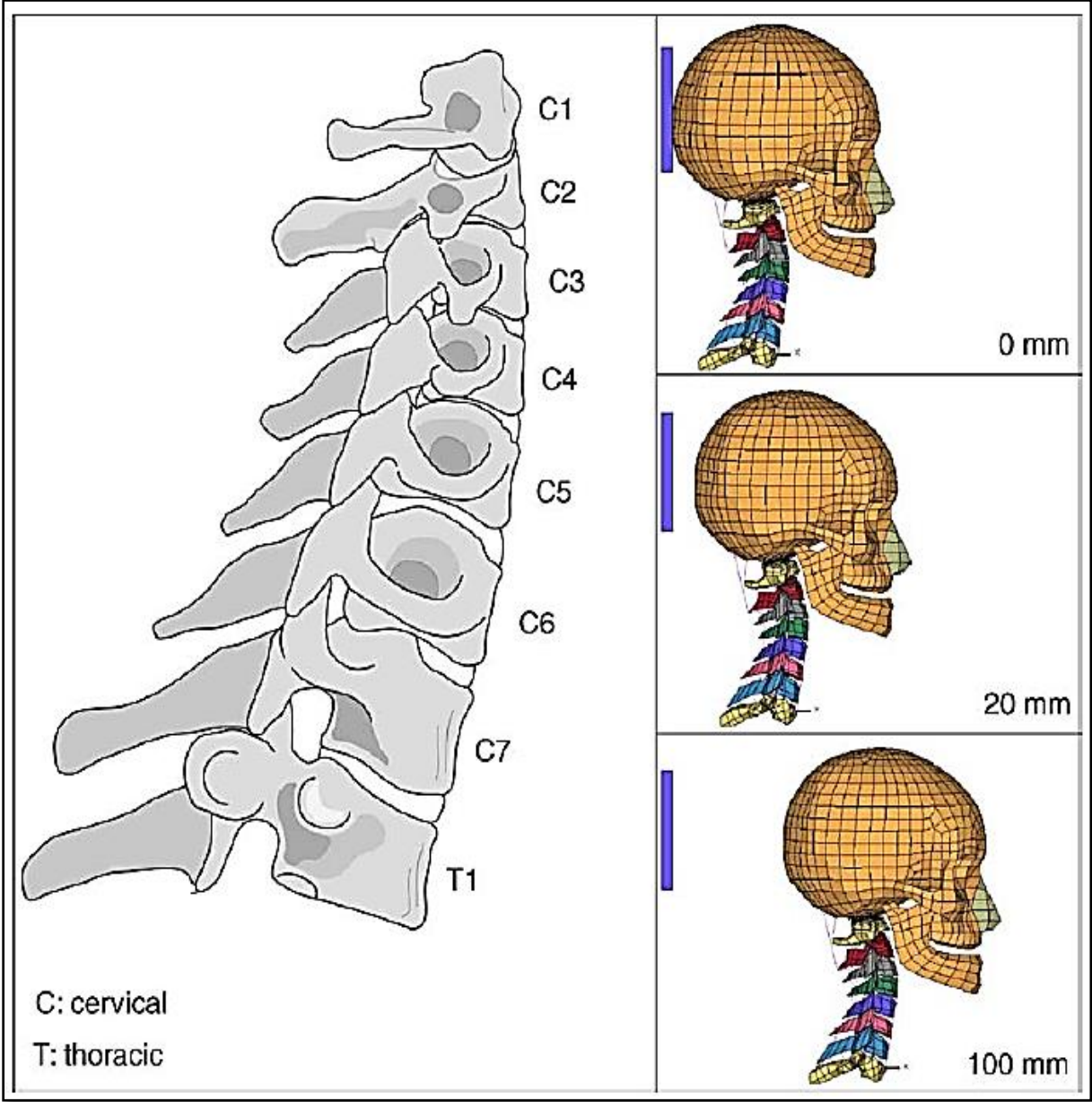


Figure 22. Human head-neck model developed by Stamper et al. [17] to study the effect of backset gap on whiplash injury.

3.4 Discussion

To achieve the objectives of this study, both experimental and numerical investigations are conducted. Initially, Indentation Force Deflection (IFD) and tensile tests are carried out experimentally on six commercially available head restraints. These tests will provide a range of material properties which will be used in the numerical models. Finite Element Modelling (FEM) of seated human model using THUMS is developed using LS-DYNA FE tool. The geometry of the seat was based on Toyota Land Cruiser GX 2012 driver seat. Vehicles seat back characteristics, for example increment angle and cushion depth, greatly influence occupant kinematics and neck injuries. Therefore, the seat base was set to an upward angle of 10 degrees in each case so that it cannot alter the results when studying purely the effect of head-restraint backset gap. Element type was properly selected and the mesh size was determined based on mesh conversions study. The seat was developed based on low density urethane foam material model with parameters obtained from the experimental tests. Boundary and loading conditions were defined properly based on the Insurance Institute for Highway Safety (IIHS). The developed numerical model will be validated by comparing its results to published numerical and experimental data. Once it is validated, then the effect of backset gap on whiplash will be evaluated by running the model at various backset gaps. Then the influence of head restraint material properties on whiplash is investigated at the optimum backset gap.

Finally, a head tracking mechanism is developed and installed in a vehicle to test its effectiveness and robustness in preventing whiplash injury. The system consists of actuating motors, two ultrasonic sensors to detect the head, and one Arduino electrical board to control the system. The main drawback of using ultrasonic sensors to detect the head is their sensitivity to hair styles and hats. Capacitance-based sensors and 3D- imagery cameras can be used instead to

overcome this issue. However, these systems are less compact in size, much more expensive and complex in terms of operation and sensitivity to other factors, such as visibility [95]. Ultrasonic sensors offer more feasible cost-effectiveness solution to track the head and ideal way for detecting incoming rear-end collisions. Other sensing devices have been used by others for head detection task, for example radar, sonar and magneto-resistive sensors [54, 95]. However, they can lead to side-effects on passenger's health.

CHAPTER 4 RESULTS & DISCUSSION

4.1 Introduction

This chapter presents and discusses in details the findings of this study. Accordingly, material characterization results of the six Head-Restraints (HRs) will be presented. Then the developed Finite Element Model (FEM) have been optimized and validated. After validating the FEM, the effect of HR position was evaluated by varying the backset head-to-HR gap. Moreover, the effect of HR material properties on whiplash was investigated using the material properties tested experimentally. Finally, a tracking HR system is developed, based on the optimum HR position and high performance material, to protect the neck against injury.

4.2 Experimental Program

4.2.1 Sample Preparation

A total of 42 specimens and 6 Head Restraints (HRs) were used to carry out the experimental program. Indentation force deflection test was performed on the 6 HRs as received from the manufacturer, as shown in Figure 12. Three cubic ($2 \times 2 \times 2 \text{ cm}^3$) foam specimens were prepared from each HR for density measurement test based on ASTM D3574-A standard. Three tensile samples were prepared from each HR as per ASTM D3574-E standard, as shown in Figure 23. The gauge length, thickness, and width were the same for all the tensile specimens. All the tensile specimens had a uniform distribution on air vacancies and the existence of any defect lead to discarding the specimen avoid stress concentration areas. The mean and standard deviation were calculated and reported for all the tests.

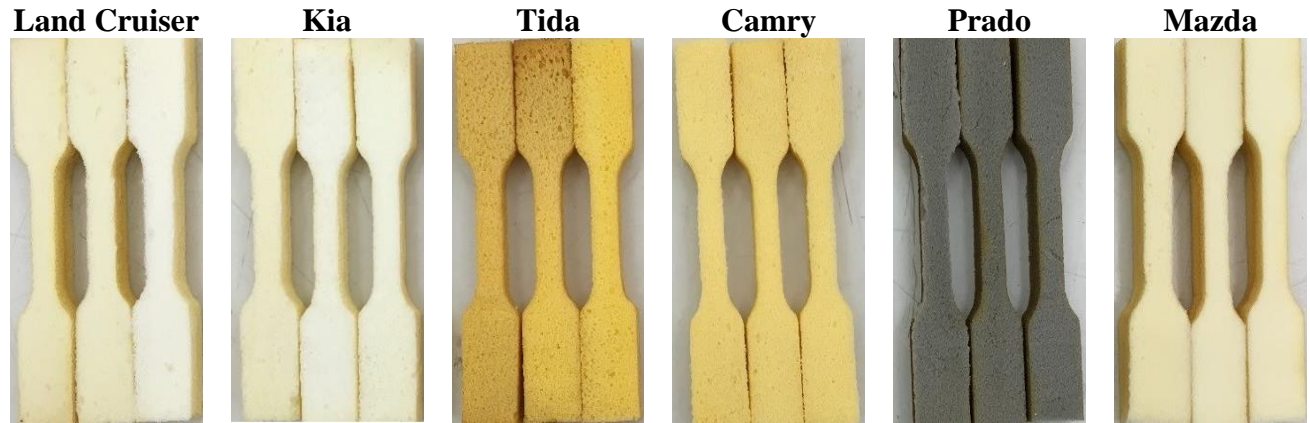


Figure 23. HRs tensile samples following an ASTM D3574-E standard.

4.2.2 Head-Restraints (HR) Material Density Measurements

The core densities of the six HRs were determined by calculating the mass and the volume of the specimen based on ASTM D3574-A standard. The dimensions, weights, and measured HR densities for the selected vehicle models are presented in Table 4. Among measured materials, Toyota Land Cruiser HR material exhibited the highest density while Toyota Prado had the least. This concludes that even within the same car manufacturers, HR material properties may have wide variations. Scanning Electron Microscope (SEM) images at 50x magnification for the HR materials are presented in Figure 24. The images show that Toyota Land Cruiser, Kia Cerato, and Mazda M3 have a denser foam structure with smaller vacancies among the other materials which indicates that their densities are the highest.

4.2.3 Head-Restraints (HR) Material Tensile Behavior

As is well-known that tensile test is a very important tool to characterize HR material properties and evaluate their failure modes. Tensile test was performed to the six HRs materials to measure their materials properties to use them as an input for the developed FEM.

Table 4. Vehicles dimensions, weights, and the measured densities for their HR materials.

Car Model	Length	Width	Height	Curb Weight	HR Density	S.D.
	[mm]	[mm]	[mm]	[kg]	[kg/m³]	
Land Cruiser	4950	1970	1880	2725	386.54	13.28
Prado	4750	1885	1845	2330	154.58	7.07
Toyota Camry	4850	1825	1470	2100	170.15	3.29
Kia	4560	1780	1445	1330	250.81	9.26
Tida	4295	1760	1520	1257	189.78	3.70
Mazda	4595	1755	1470	1295	287.63	3.81

Table 5 presents the measured Young's modulus (stiffness), failure stress, and ultimate elongation percentage of HR materials. Figure 25 shows that engineering stress versus engineering strain curves for the six HRs. The stress-strain curves keep increasing linearly up to the material tearing point during tensile testing. Uniform reduction along the gauge length has been observed during the test. This is in contrast with the behavior of metallic material where necking occurs in the middle of the gage length. It is also observed that all HR materials behave as hyper-elastic materials where no plastic deformation occurs. With regards to the stiffness and strength, Land Cruiser recorded the highest values. HR materials that show increase in the strength and stiffness can be attributed to the strong bonding energy between their atoms compared to other tested HR materials. This can be obviously seen from the SEM images which are shown in Figure 24. Figure 26 compares the tested HR materials in terms of their densities, Young's modulus (stiffness), tearing strength, and elongation. The comparison shows that tearing stress exhibited

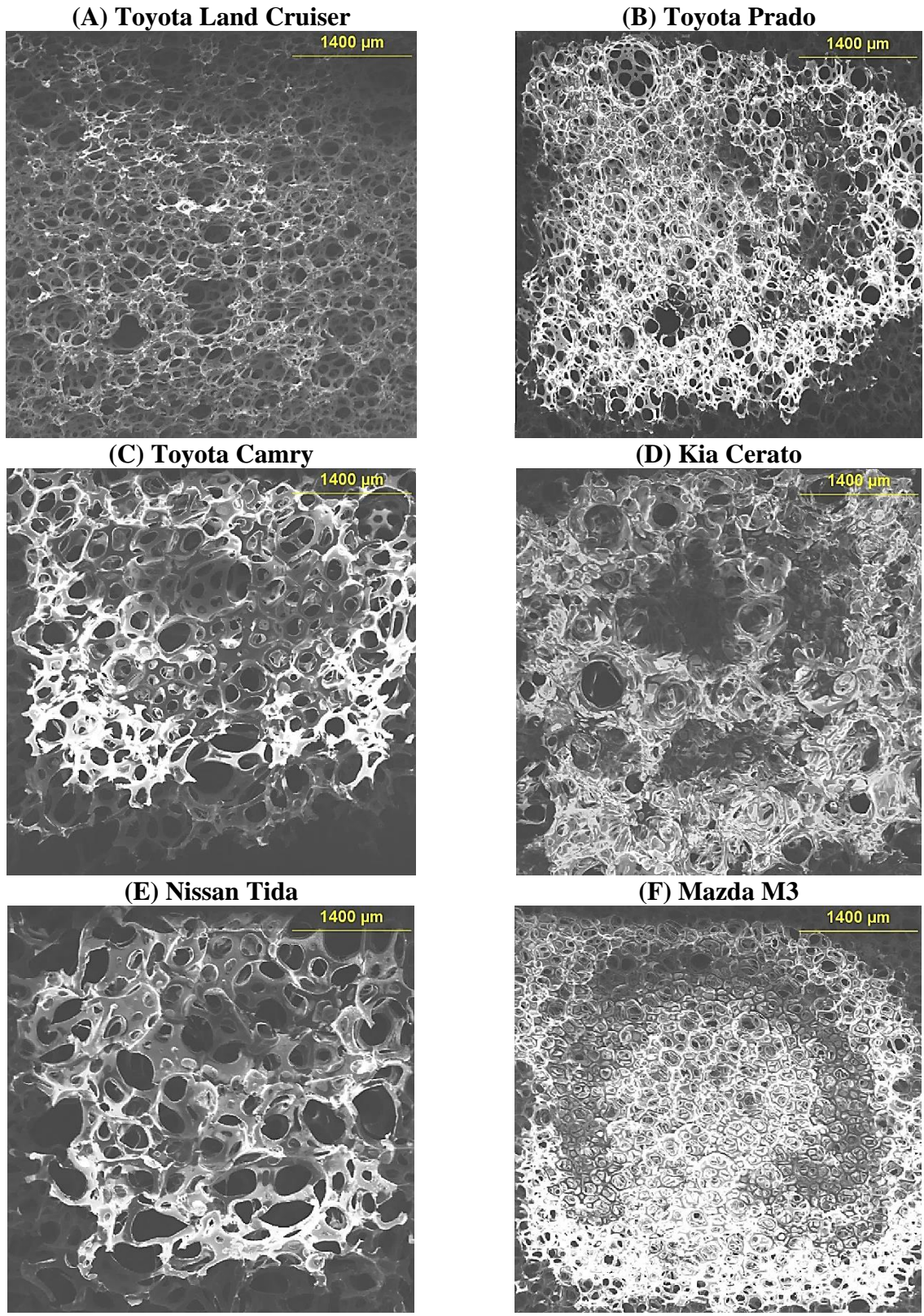


Figure 24. Scanning electron microscope at 50x for the HR materials.

similar behavior as the Young's modulus. In addition, Among HR from same manufacture (Toyota), the density influences the stiffness, strength, and elongation. As the density increases the strength increases sharply. Similar relationship was observed for the stiffness. However, no significant effect was observed with regards to their elongation. Among SUV cars (Land cruiser and Prado), the effect of density is very significant and as it increases, the other mechanical properties increase. Among sedan cars, there is no obvious trend with regards to the increase in density. For instance, Kia Cerato HR material has higher density than Toyota Camry, but exhibited almost half the stiffness and tearing stress. It is worth mentioning that although Camry HR material has low density compared to others, its mechanical properties is the second highest and thus it has the highest specific material properties among the rest.

Table 5. Material properties for the selected head-restraints (\pm standard deviation).

Car Model	Young's Modulus (E)	Tearing Stress (σ_f)	Elongation
	[kPa]	[kPa]	(L%)
Land Cruiser	216.3 (11)	240.3 (12)	107.1
Prado	137.5 (9)	101.6 (15)	76.9
Camry	186.7 (7)	216.1 (10)	105.8
Kia	104.9 (18)	103.2 (13)	94.5
Tida	105.4 (11)	114.5 (10)	116.0
Mazda	158.9 (13)	162.3 (10)	98.5

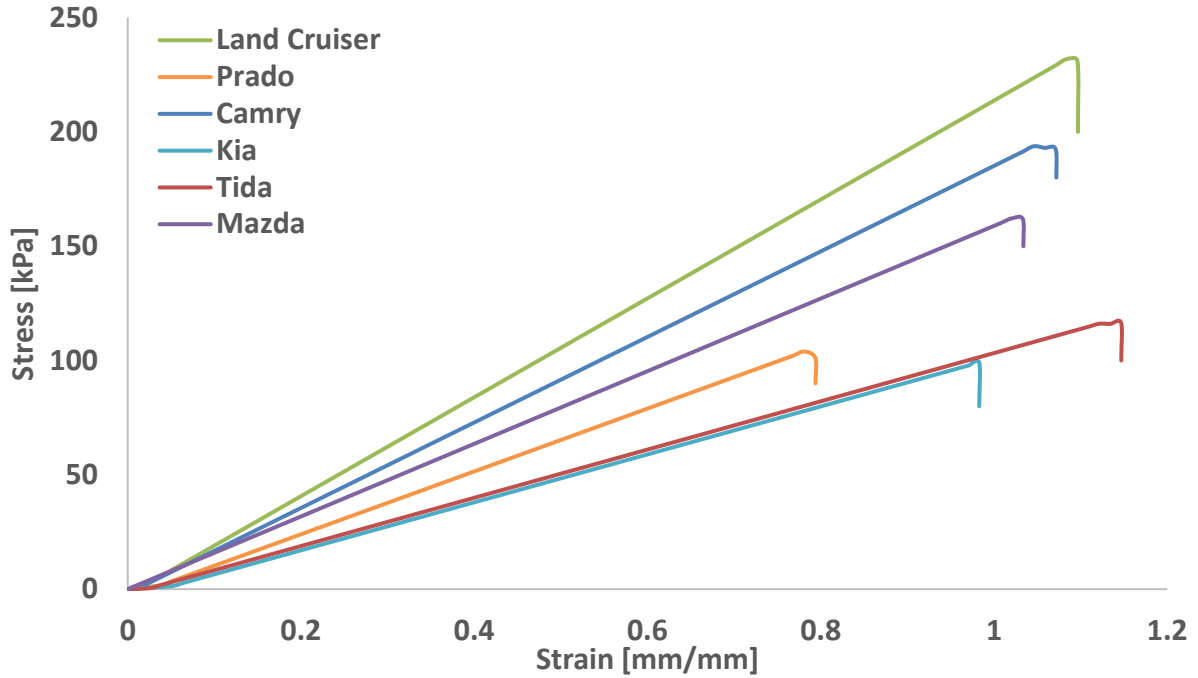


Figure 25. Tensile stress-strain curve for the selected HR materials.

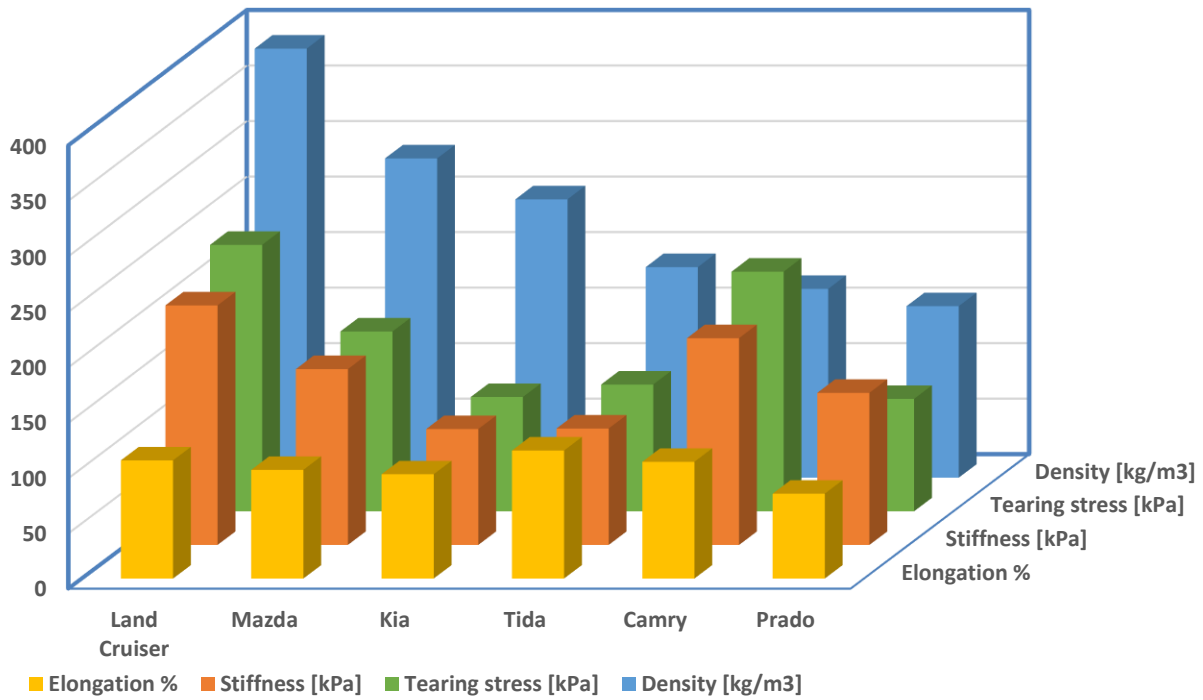


Figure 26. 3D-graph comparing the material properties for the HR materials.

4.2.4 Indentation Force Deflection (IFD) Test of Flexible HR Materials

Indentation Force Deflection (IFD) test have been carried out on the selected HRs to determine their firmness and energy absorption capability based on ASTM D5672 standard. The depth of the HR was measured at a preload of 4.5 N. The compression crosshead speed was set to 50 ± 5 mm/min as per standard. Firstly, the test progressed until the indenter reached 25% of the HR depth (T) and the load was recorded after drifting for 60 ± 3 seconds, as illustrated in Figure 27. Then the test proceeded until indenter reached 65% of the HR depth and the load was recorded after drifting for 60 ± 3 seconds. Table 6 presents the typical dimensions of the tested HRs along with their total energy absorption capability, indentation force magnitudes at 0.25T and 0.65T of their original depth (T). The indentation force versus indentation deflection IFD curves are illustrated in Figure 28. The drift in the load caused stress relaxation is obvious at 0.25T and 0.65T stages when the loading was paused for 60 ± 3 seconds. The ratio of instantaneous load to the drifted load varies among the six foams, especially at the 0.65T stage. The produced relaxation and hysteresis behaviors are very essential properties to control the rebound phase of whiplash [61]. The difference in the force level at 0.25T among the tested HR materials is small compared to the force level at 0.65T as clearly shown in Table 6. This can be attributed to the initial compression stage where the vacancies within the foam are being decreased. There is a huge difference in the load carrying capacity between the Toyota Land Cruiser HR material and other HR tested materials. Figure 29 shows that Land Cruiser HR material have absorbed significant energy between the deflection range of 55 mm and 85 mm. It is worth to mention that since the foam materials used in HRs has very small Poisson's ratio, therefore no shape expansion was observed in both transverse x and y directions, as shown in Figure 27.

Table 6. IFD test results for the selected head-restraints and their typical dimensions

Vehicle	Depth	Width	Height	F _{25%}	F _{65%}	Absorbed Energy
	[mm]	[mm]	[mm]	[N]	[N]	[J]
Land Cruiser	130	250	200	100.2 (11)	1712.1 (24)	51.1 (9)
Prado	108	175	235	93.8 (8)	271.4 (13)	11.0 (2)
Camry	158	295	200	108.9 (8)	517.4 (18)	18.3 (3)
Kia	150	215	220	189.8 (14)	595.2 (18)	27.9 (3)
Tida	112	180	260	143.1 (10)	633.0 (19)	19.3 (2)
Mazda	155	255	200	144.8 (10)	429.4 (14)	18.7 (4)

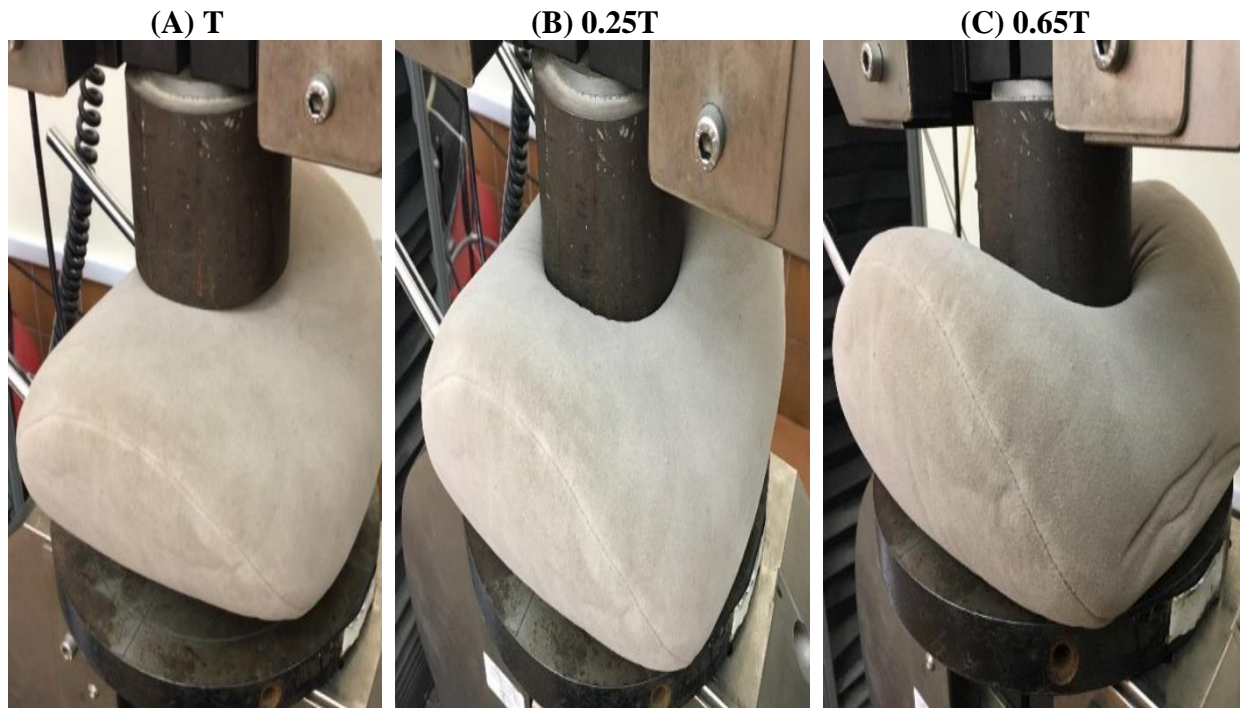


Figure 27. Toyota Land Cruiser head-restraint during IFD test; (A) depth (T) measure at 4.5 N preload, (B) indentation up to 0.25T where the load F_{25%} was recorded after 60 ± 3 seconds, and (C) indentation up to 0.65T where the load F_{65%} was recorded after 60 ± 3 seconds.

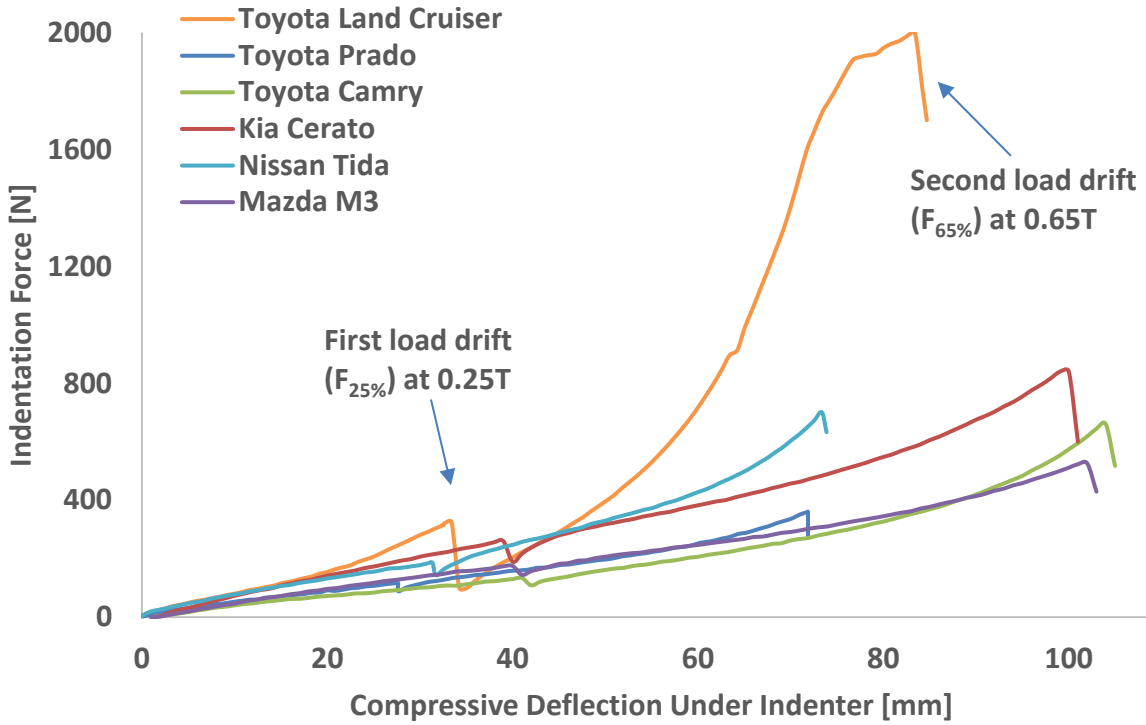


Figure 28. IFD indentation force vs. deflection for the HR materials.

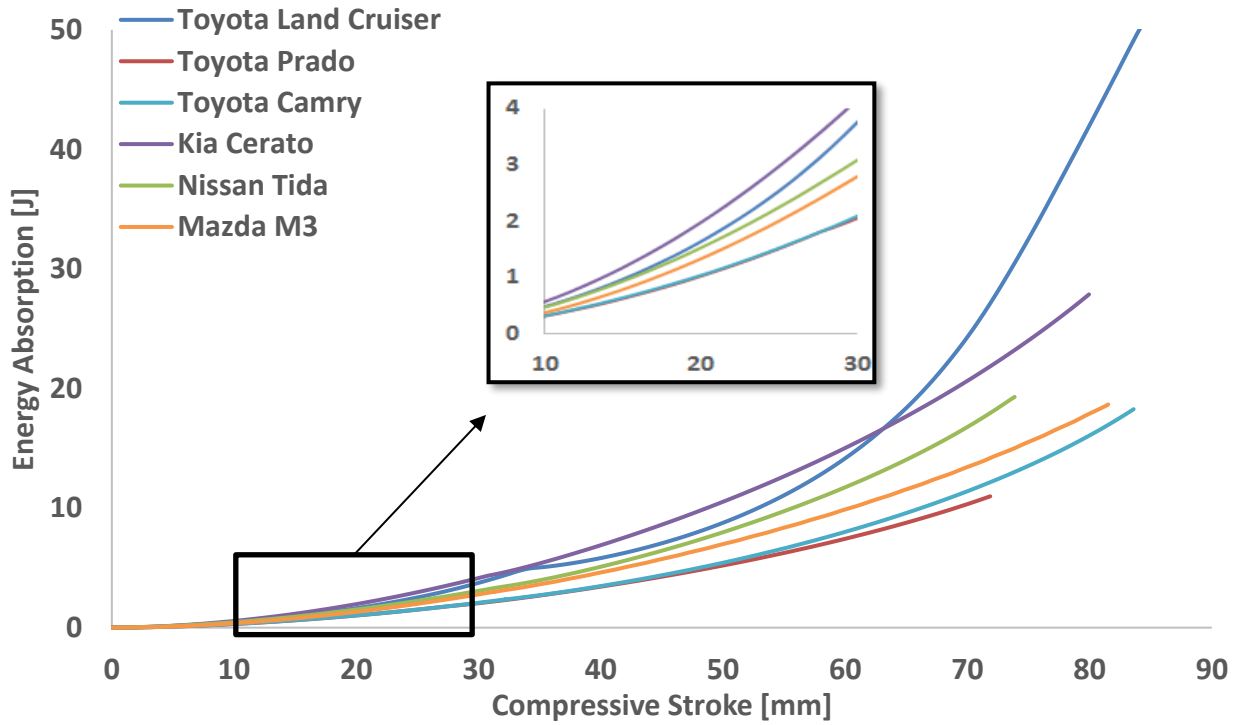


Figure 29. Energy absorption versus compressive extension of the six HRs during IFD test.

4.3 Finite Element Modelling (FEM) Program

4.3.1 Development of Finite Element Model

4.3.1.1 Mesh Size Optimization

Mesh size optimization study was performed to determine the suitable mesh size for the driver seat. The model used in this study, shown in Figure 31, which simulates the impact between the occupant's head and HR. This causes an indentation in HR up to 40% of its original depth. To study the effect of mesh size, mesh element volume was varied from $20 \times 20 \times 20 \text{ mm}^3$ to $3 \times 3 \times 3 \text{ mm}^3$. The mesh size optimization results are listed in Table 7. The mesh size and computational time started to increase exponentially at element volumes smaller than $8 \times 8 \times 8 \text{ mm}^3$. The maximum internal energy and maximum Von Mises stress were plotted against mesh size in Figure 30. Both curves started to converge at element volume of $4 \times 4 \times 4 \text{ mm}^3$. Figure 32 shows the accuracy of stress distribution in the HR material and is found to be highly dependent on element volume. For all the cases with different mesh sizes, the HR sides did not absorb any impact energy. Therefore, the mesh of the driver's seat was optimized by having an element size of $10 \times 10 \times 10 \text{ mm}^3$ at non-critical areas, such as seat sides and base, and $4 \times 4 \times 4 \text{ mm}^3$ at the seat-to-human contact areas. Consequently, the passenger's seat structure consisted of 140997 hexahedron solid elements with total of 160151 nodes.

4.3.1.2 Finite Element Model (FEM) Validation

The developed FEM was validated by comparing it against the published work of Stemper et al. [17]. Their study was performed by having a 4.1 m/s rear-end impact, with maximum acceleration of 10 g and 92 ms pulse width. This acceleration shape was adopted from the Insurance Institute for Highway Safety (IIHS) and used in this study. For comparison purpose, the driver's seat was removed and the impact pulse was applied at T1 vertebrae, HR, and the

occupant's back. The HR contact time and maximum head retraction are presented and compared to the reference in Table 8. Stemper et al. [17] limited the maximum retraction to head rotation of 5 degrees to avoid combining it with extension phase. The developed FEM results are in good agreement with the reference, especially at HR gaps less than 80 mm. Discrepancies in modelling may have caused small variations in the results, such as; vertebrae and HR material properties, the magnitude of the defined springs which act as the muscles, and Stemper's model has consisted

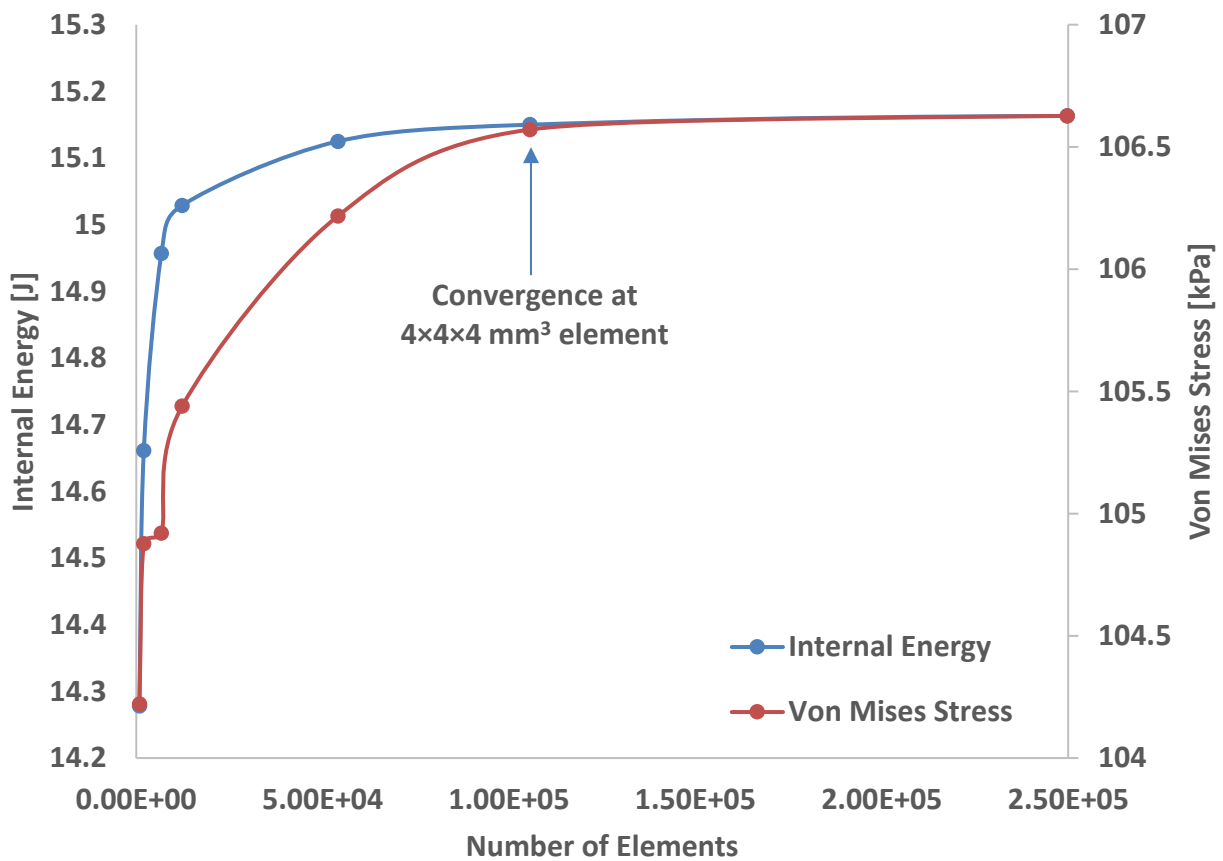


Figure 30. Internal energy and Von Mises stress versus mesh size. Mesh convergence began at element volume of $4 \times 4 \times 4 \text{ mm}^3$.

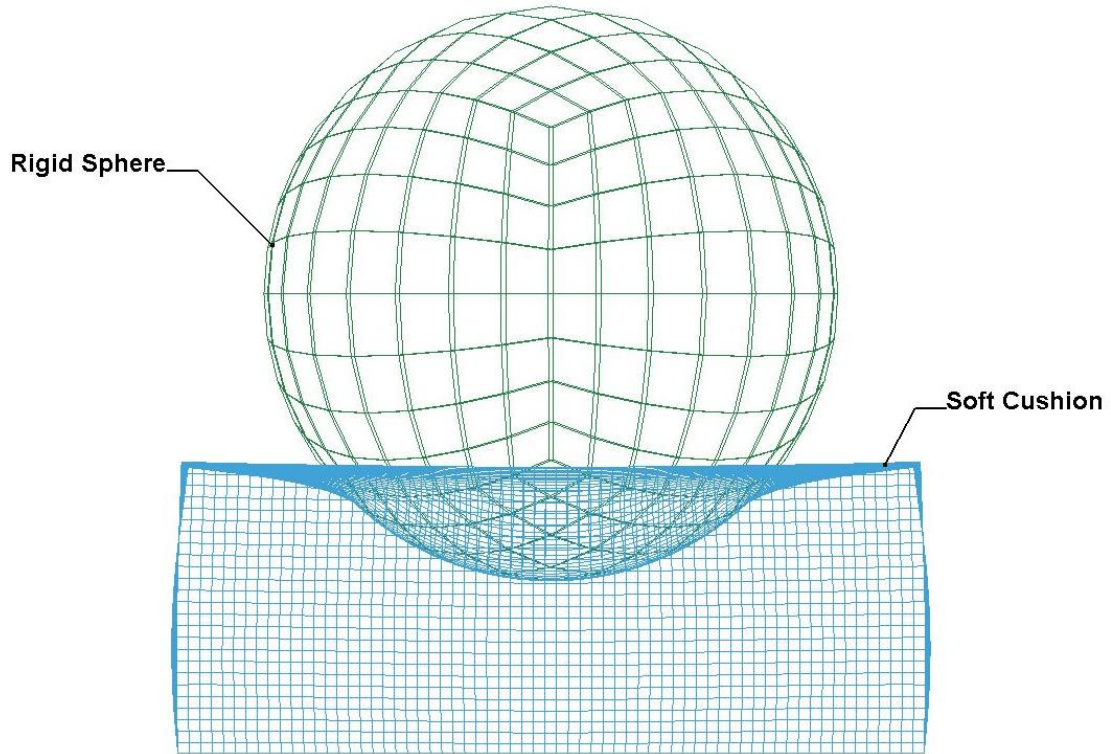


Figure 31. A Rigid sphere impacting soft HR until 40% of its depth.

Table 7. CPU times, maximum internal energy and Von Mises stress.

Element Size	Number of	CPU Time	Internal Energy	Von Mises Stress
[mm ³]	Elements	[sec]	[kJ]	[kPa]
20×20×20	8.45E+02	1	14.278	104.221
15×15×15	2.02E+03	2	14.661	104.877
10×10×10	6.76E+03	4	14.957	104.920
8×8×8	1.23E+04	8	15.029	105.439
5×5×5	5.41E+04	48	15.125	106.217
4×4×4	1.06E+05	118	15.150	106.571
3×3×3	2.50E+05	381	15.163	106.627
2×2×2	8.45E+05	1817	15.155	106.686

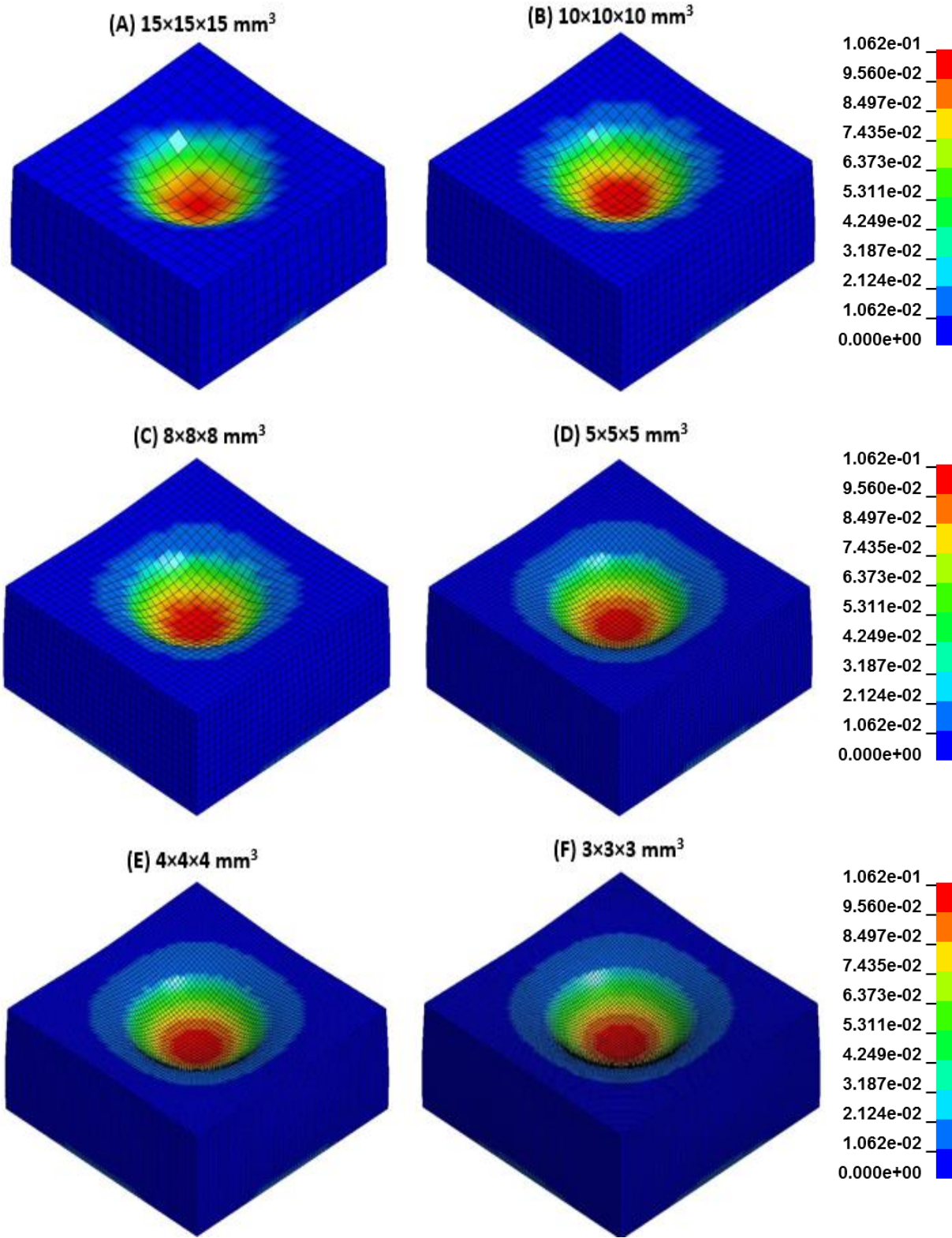


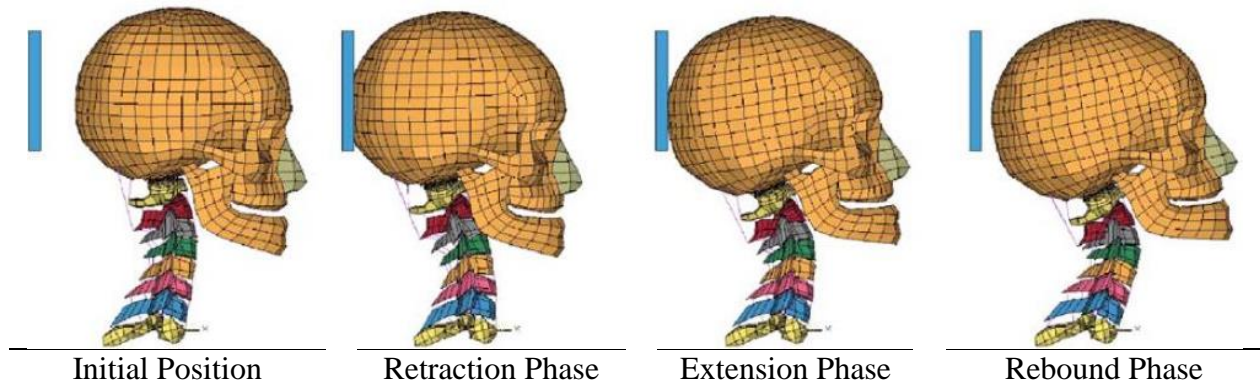
Figure 32. Von Mises stress distribution (MPa) corresponding to element volumes (mm³) (A) 15×15×15, (B) 10×10×10, (C) 8×8×8, (D) 5×5×5, (E) 4×4×4, and (F) 3×3×3.

of only head-neck skeletal system whereas the developed FEM contained head-neck-torso skeletal system with muscular and organs systems. The influence of including muscular system is obvious when comparing head/vertebrae rotation illustrated in Figure 33. Moreover, the initial rotational positions of the lower vertebrae are different, especially T1. This is because unlike Stemper's model, the developed FEM has T1 connected to the rest of thoracic spine which will result in a more realistic head-neck response. In addition, the initial flexion angle of T1 has limited the maximum head extension range which caused the variations in results after 80 mm gap and no head-to-HR contact at 120 mm and 140 mm gaps.

Table 8. Developed FEM head retraction results compared with work of Stemper et al. [17].

Gap	Contact	Ref.	Diff.	Retr.	Ref.	Diff.	Retr. ($\theta_{\text{head}} < 5^\circ$)	Ref.	Diff.
[mm]	[ms]	[ms]	%	[mm]	[mm]	%	[mm]	[mm]	%
0	0.0	0.0	0.0	17.6	18.4	4.6	17.6	18.4	4.6
20	36.0	33.0	9.1	28.8	26.3	9.7	28.8	26.3	9.7
40	45.0	42.0	7.1	41.0	37.9	8.2	39.0	37.9	3.0
60	55.0	49.0	12.2	51.3	51.3	0.0	39.1	51.3	23.9
80	65.0	56.0	16.1	52.1	61.6	15.4	39.5	53.5	26.3
100	75.0	63.0	19.0	59.8	69.5	14.0	39.6	53.5	26.0
120	NA	70.0	NA	64.6	75.9	14.9	38.7	53.5	27.6
140	NA	77.0	NA	64.6	81.2	20.4	38.7	53.5	27.6

(A) Stemper et al. Model



(B) Developed FEM

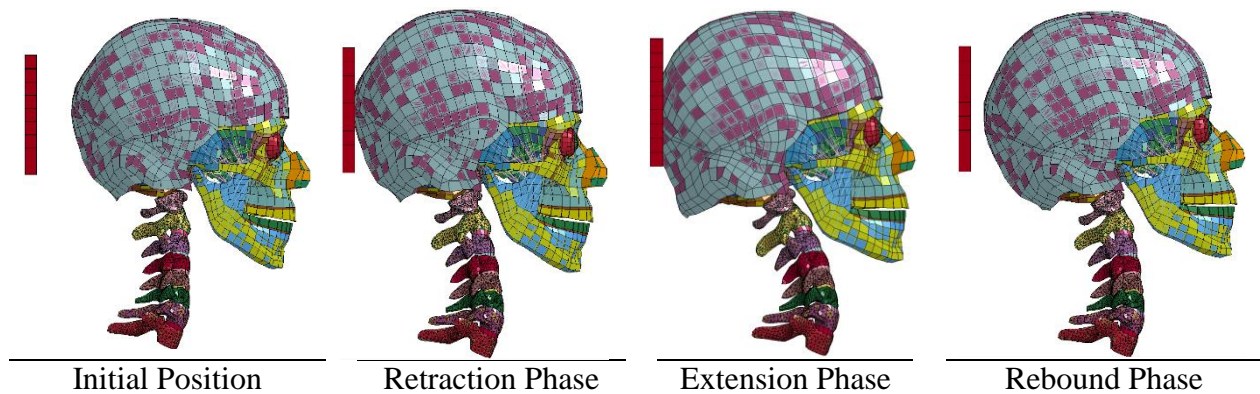


Figure 33. Comparison between (A) Stemper et al. [17] and (B) developed FEM in head-neck kinematics of whiplash injury during rear-end impact.

4.3.2 Effect of Head-Restraint Position

4.3.2.1 Head-Neck-Torso Kinematics

Sign conventions in studying human kinematics is essential to be established before analyzing and presenting the FEM results. Based on Society of Automotive Engineers sign convention (SAE J1733 & J211/2), cervical extension is represented with a negative sign, whereas cervical flexion is given a positive sign. In addition, X-, Y- and Z-axes represent the forward, rightward and downward motions, respectively. Furthermore, anterior shear (positive x-direction)

indicates that the head is moving rearward while posterior shear (negative x-direction) represent head rebound. Moreover, tensile load (positive z-direction) indicates stretching of the neck while compressive axial load (negative z-direction) is unlikely to occur in rear-end collisions [12].

To examine the kinematics of the neck during whiplash, the different phases along with their incident time were illustrated in Figure 34 for HR at 100 mm gap position. Neck displacements, loading & moments, and injury assessments versus impact time results are presented in Figure 35 for 100 mm HR position and APPENDIX A for all HR positions. At the beginning of rear impact (Figure 34-A), the occupant's back starts to indent into the seatback and the impact energy gets transferred to the torso. Thus, the neck does not experience any distortion during the first 30 ms of the impulse. This period gets longer when the stiffness of the seatback is softer. After that, the torso begins moving forward and upward (Figure 34-B) depending on the passenger's seatback angle with the vertical. Meanwhile, the head will not move accordingly due to its inertia and thus will begin retracting rearward. This retraction movement will force the lower vertebrae (T1-C7-C6) to experience extension moment while the top vertebrae (C1-C2-C3) experienced flexion rotational movement. Thus, the cervical spine will form an S-shape curvature, and it is most severe at maximum head retraction when the head gets into contact with HR at 65 ms, as shown in Figure 34-C. Then the HR provides support to the head by absorbing some of its kinetic energy and then lowering its relative acceleration with the torso. While doing so, the whole cervical spine become under extension moment when the head rotates backwards and the S-shape curvature disappears at 85 ms, as demonstrated in Figure 34-D. Excessive extension of the neck can cause very serious injury where the cervical vertebrae can come into contact with each other and might fracture [22]. In addition, the anterior longitudinal ligament and neck muscles will tear due to high tension strains. Furthermore, intervertebral discs will become excessively compressed

from posterior side and stretched from the anterior side which will cause it to slip from its location [96]. It is worth mentioning that damage to neck muscles can be healed within few months whereas tear in ligaments or intervertebral discs will require years to heal [32]. Once the impact acceleration smooths out, the seatback and the HR releases its stored energy and the passenger's head begin to rebound off the HR at 110 ms, as illustrated in Figure 34-E. While rebounding, the head experience a forward rotational movement which applies flexion moment on the cervical spine. This phase is greatly influenced by the passenger's seat design and its material properties. The flexion movement of the neck continues until it becomes very severe when the seatbelt restrains the occupant and limits its forward motion. The excessive flexion of the neck can damage the posterior ligaments such as supraspinous ligament, interspinous ligament, and ligamentum flavum [37].

4.3.2.2 Effect of HR Position on Relative Head Displacements

It is well known that excessive head movements relative to the torso will lead to neck injury. Neck Displacement Criteria (NDC) classifies the effectiveness of the head-restraint (HR) in preventing whiplash injury based on the range of head's motion. Three head movements were evaluated; the maximum head extension angle (θ_{OC}), relative maximum shear displacement (X_{OC-T1}), and relative vertical displacement (Z_{OC-T1}). Table 9 presents the NDC classification thresholds, while Table 10 gives the NDC rating for each HR position and highlights the rating with different colors. Figure 35-A shows an example of head extension angle, shear displacement, and vertical displacement curves versus time for HR positioned at 100 mm. Figure 36 shows the maximum values of head extension angle, shear displacement, and vertical displacement at different HR positions.

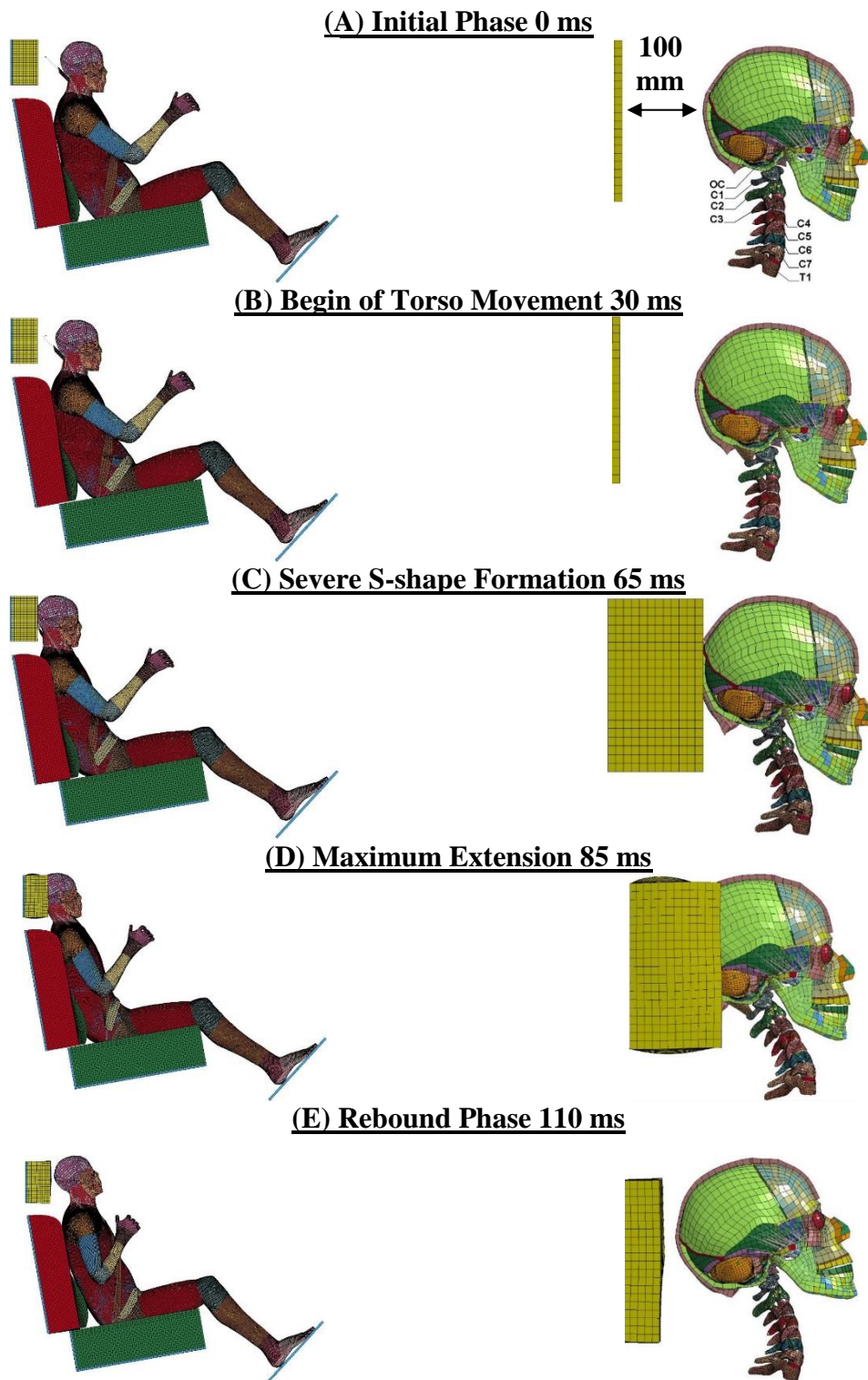


Figure 34. Whiplash phases of the developed FEM (left) and the position of head-neck (right) during rear-end impact with HR position at 100 mm gap.

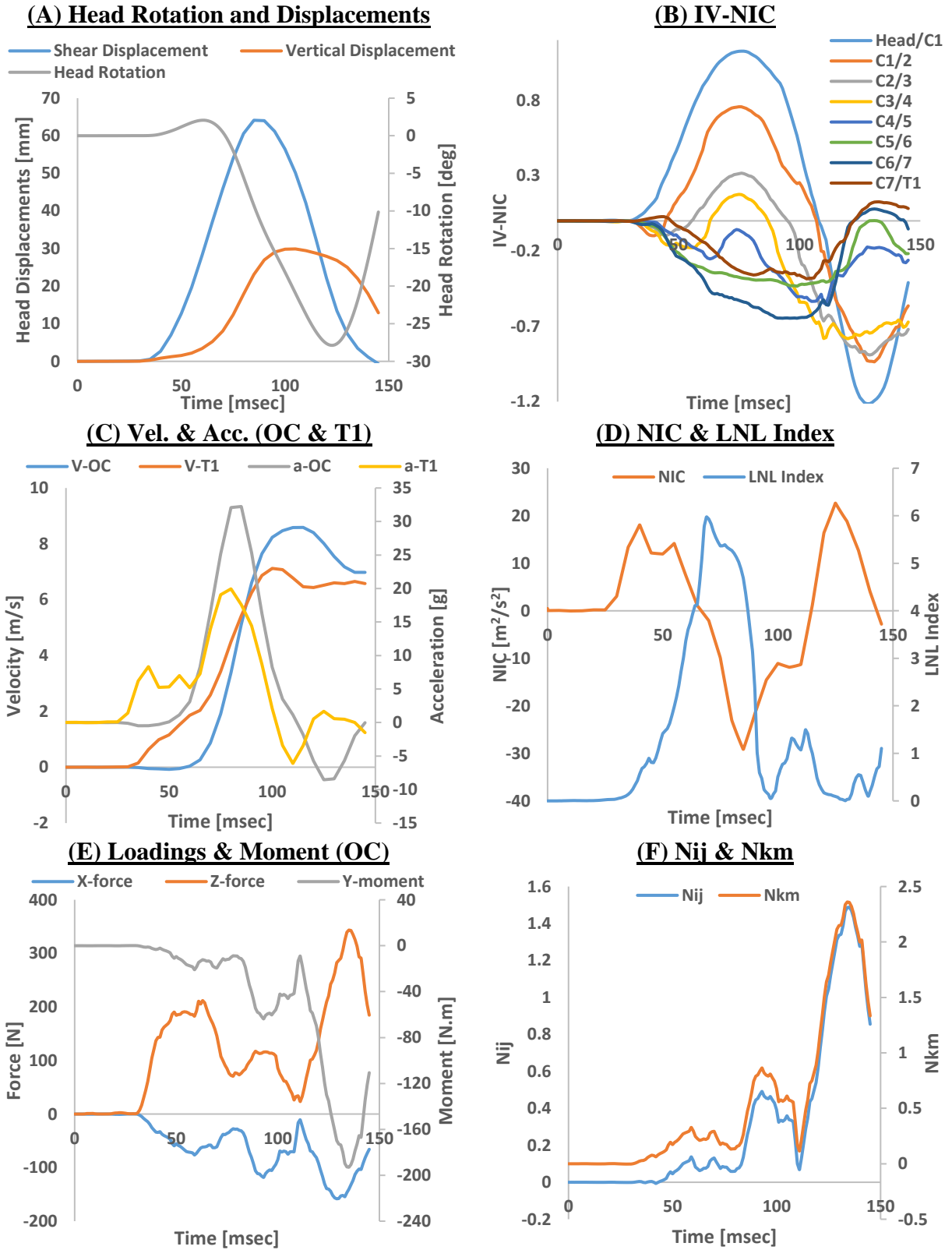


Figure 35. Neck kinematics and injury assessments at 100 mm HR position.

Head shear or retraction displacement and axial displacement increases with the HR gap. However, head extension begins at HR position further than 40 mm. This is because the seatback is fully deflected and the torso is moving forward while the head is not yet being in contact with the HR (i.e. gap $\neq 0$ mm). Vertical head displacement starts to increase rapidly only when the head extension occurs. NDC classification thresholds are listed in Table 9 and the overall rating will be based on the lowest rating given to either category. For example, 60 mm and 80 mm gaps were given an Excellent (Ex) NDC rating for the maximum head extension angle and relative axial displacement. However, the overall rating was Good (Gd) based on their Good rated performance in limiting head retraction range (X_{OC-T1}). HR support was not effective (i.e. Poor rating) in the last three cases (100 mm, 120 mm, and 140 mm) where the neck had experienced an excessive combined extension-tension loading causing high head retraction and vertical displacement. NDC classification does not consider the maximum head flexion angle during the rebound phase because it is limited by deploying an airbag system. Figure 36 indicates that the maximum head retraction (X_{OC-T1}) is a linearly related to the HR gap (G) as shown in Equation 11 as:

$$X_{OC-T1} = 0.6615G - 1.8987 \quad 0 \leq G \leq 140; (R^2 = 0.998) \quad (11)$$

where X_{OC-T1} is the head (occipital condyle OC) shear displacement relative to the first thoracic vertebrae (T1) and G is the gap distance in millimeters between the head to the head-restraint. The gap G must be greater or equal to zero where the HR is initially in contact with the head, and less than 140 mm where no head to HR contact occurs. Shear head displacement (X_{OC-T1}) will be constant at values of G greater than 140 mm. On the other hand, vertical displacement value gets amplified rapidly after 60 mm gap because it depends on the maximum neck extension.

Table 9. NDC injury rating thresholds according to natural range of motion [50].

Classification	Head extension angle	Shear Displacement	Axial Displacement
Excellent	$\theta_{OC} < 25^\circ$	$X_{OC-T1} < 35$ mm	$Z_{OC-T1} < -15$ mm
Good	$\theta_{OC} < 40^\circ$	$X_{OC-T1} < 55$ mm	$Z_{OC-T1} < -25$ mm
Acceptable	$\theta_{OC} < 55^\circ$	$X_{OC-T1} < 75$ mm	$Z_{OC-T1} < -35$ mm
Poor	$\theta_{OC} > 55^\circ$	$X_{OC-T1} > 75$ mm	$Z_{OC-T1} > -35$ mm

Table 10. NDC classification of HR effectiveness in whiplash protection.

Gap	θ_{oc}	Class.	X_{OC-T1}	Class.	Z_{OC-T1}	Class.	Overall
[mm]	[deg]	Rating	[mm]	Rating	[mm]	Rating	Rating
0	0.00	Ex	0.03	Ex	0.03	Ex	Excellent
20	0.00	Ex	11.27	Ex	0.99	Ex	Excellent
40	0.00	Ex	24.12	Ex	1.98	Ex	Excellent
60	7.14	Ex	36.01	Gd	8.53	Ex	Good
80	14.36	Ex	50.25	Gd	14.48	Ex	Good
100	27.87	Gd	64.12	Ac	29.90	Ac	Acceptable
120	42.54	Ac	76.31	P	53.70	P	Poor
140	82.14	P	93.15	p	152.52	p	Poor

4.3.2.3 Neck Injury Criteria Assessments

As stated in section 2.5, scientists and researchers in this field proposed neck injury criteria to predict neck injuries and evaluate the effectiveness of the prevention system. Table 11 presents the initial/end head-to-HR contact times along with the total impact energy dissipated in the HR for each HR position. In addition, it lists the values of the Neck Injury Criterion (NIC), Normalized Neck Injury Criterion (Nij), Neck Protection Criterion (Nkm), and Lower Neck Load criterion (LNL) for predicting neck injuries. Figure 37 plots the maximum values of NIC, Nij, Nkm, and LNL injury assessments against different HR positions. NIC evaluates neck injury probability based on the relative velocity and acceleration between the head (measured at the occipital condyle) and the first thoracic vertebrae (T1). On the other hand, Nij, Nkm, and LNL are given in terms of the applied bending moments combined with axial forces and shear forces. Nij and Nkm were measured at the occipital condyle (OC) whereas LNL was measured at the first thoracic vertebrae (T1). NIC assessment indicated that no neck injury will occur while the HR is positioned at 20 mm gap or below, as shown in Figure 37. Figure 35-C shows the velocity and acceleration curves for both the head (at OC) and T1. The NIC was measured until the relative head to T1 rotation is greater than 10° because the velocity and acceleration will no longer be parallel to X-axis direction. Therefore, its assessment ends within the early 40 ms of the impact and becomes constant after 40 mm gap HR position. Figure 35-D shows an example of NIC curve versus time for HR positioned at 100 mm. Hence, the first peak in NIC curve found to be at 39.91 ms and is considered the true value of NIC assessment.

As per Nij and Nkm injury criteria, all the HR positions seems to cause harmful tension and shear loadings to the neck because, as illustrated in Figure 37, the values are greater than 0.09 and 0.3 thresholds for Nij and Nkm, respectively. This is reasonable because the crash pulse is 10 g

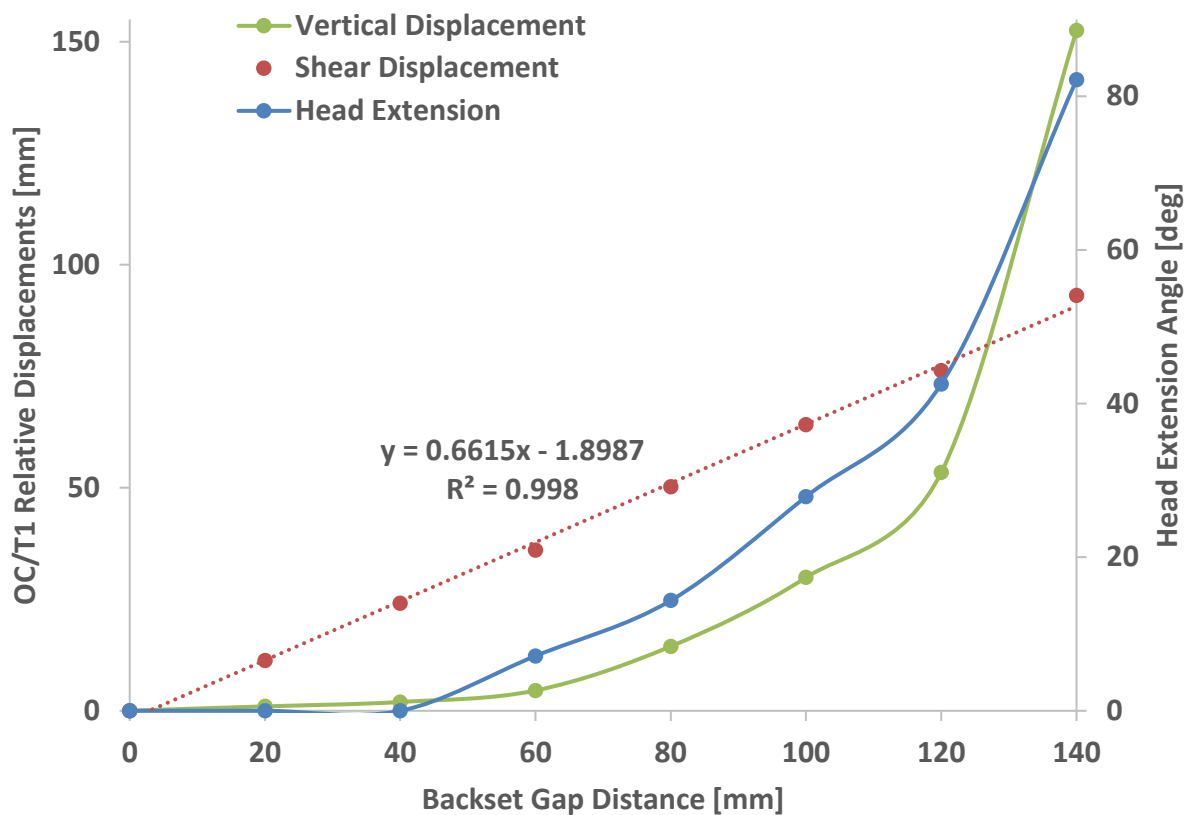


Figure 36. Curves of maximum head extension angle and maximum shear & vertical displacement relative to T1 at different HR positions.

which is very high to the neck which caused whiplash based on Nij and Nkm. This is especially true when the HR becomes closer to the head, which in turn cause sudden deceleration and reverse the rearward/extension movements to forward/flexion motion. At close HR positions, this transition is smoother because the head did not gain high rearward velocity. Figure 35-E shows the axial force, shear force, and extension moment versus time recorded at the occipital condyle for HR positioned at 100 mm gap. The corresponding Nij and Nkm assessments are indicated in Figure 35-F. The head kinematic curves show that the highest Nij and Nkm values occur between

the period of 75 ms to 110 ms. Figure 34 presents this period which includes the event when the HR is at its maximum deflection where the head extension movement is stopped until the head rebounded off the HR.

Lower Neck Load criterion (LNL) injury prediction index was the lowest for HR at 20 mm gap and increases with wider HR gaps as illustrated in Figure 37. This occurs because T1 is experiencing higher extension moments and tension forces. Figure 35-D shows an example of LNL index curve versus time for HR positioned at 100 mm gap. The index begins to increase at 35 ms and reaches a maximum of 5.98 at 69 ms, then drops to zero at 98 ms. It is obvious that LNL index starts to increase when the torso begins to move forward and the head starts to retract backwards as shown in Figure 34. The FEM results also show that the highest LNL index appears just before the HR in a position very close to the head of occupant, which results in the most severe S-shape neck curvature. After the contact is initiated, the HR begins to absorb the head's kinetic energy causing the LNL index to drop until it reaches zero when the head rearward motion is fully reversed to rebound motion.

4.3.2.4 Effect of HR Position on Energy Absorption

Absorbing the head's kinetic energy is a crucial aspect in protecting the neck and the head against injuries. As illustrated in Figure 38, HR energy absorption was low in the small gaps between the head and HR (e.g. 0 mm), then it reaches a maximum at 60 mm gap and starts to decrease to 20.68 J at 120 mm gap. The relation between the energy absorbed and the gap is modeled as:

$$E_n = 16.597 + 0.3586G - 0.0027G^2 \quad (R^2 = 0.9906) \quad (12)$$

where, E_n represents the maximum absorbed energy, and G is the head to head-restraint gap. This trend of energy absorption against HR gap occurs because when the gap is less than 60 mm, the head does not have enough rearward distance to gain much kinetic energy. At HR's gap higher than 60 mm, the neck would have experienced high extension-tension loadings and absorbed some energy causing the head to slow down before it reaches the HR.

4.3.2.1 Intervertebral Neck Injury Criterion (IV-NIC) Assessment

The Intervertebral Neck Injury Criterion (IV-NIC) evaluates whiplash injury based on relative rotations at each vertebral level. IV-NIC suggests that whiplash injury can result during the extension phase or flexion rebound phase due to rotational movements of the cervical vertebrae when they exceeded their physiological range of motion (see section 2.5.4). In addition, no injury

Table 11. Summary of whiplash injury assessments at different backset gap distances.

Gap [mm]	Contact [ms]		Energy [J]	NIC [m ² /s ²]	Nij	Nkm	LNL
	Initial	End					
0	0.00	92.05	16.15	3.90	0.35	0.82	2.87
20	35.07	94.98	23.15	12.54	0.30	0.62	2.09
40	44.04	95.91	27.05	18.04	0.31	0.57	2.80
60	51.06	99.91	28.18	18.04	0.49	0.87	4.25
80	57.00	104.00	27.31	18.22	0.56	1.00	5.60
100	62.12	106.97	25.00	18.05	0.49	0.86	5.98
120	68.07	109.73	20.68	18.16	0.72	1.21	6.00
140	NA	NA	NA	18.07	1.43	2.45	6.64

can occur at C1/C2 and C2/C3 segmental levels, demonstrated in Figure 39. IV-NIC thresholds and maximum values for every intervertebral level at each HR position are listed in Table 12. Figure 35-B shows FEM IV-NIC curves with respect to time for each intervertebral level. The results indicate that if a HR is installed with the seat, no severe injury will occur. Otherwise, severe injury will occur at C3/C4 and C5/C6 segmental levels due to high neck extension movement. C3/C4 and C5/C6 segmental levels are the most vulnerable sites for IV-NIC kind of injury because they are located at the load transition planes [42].

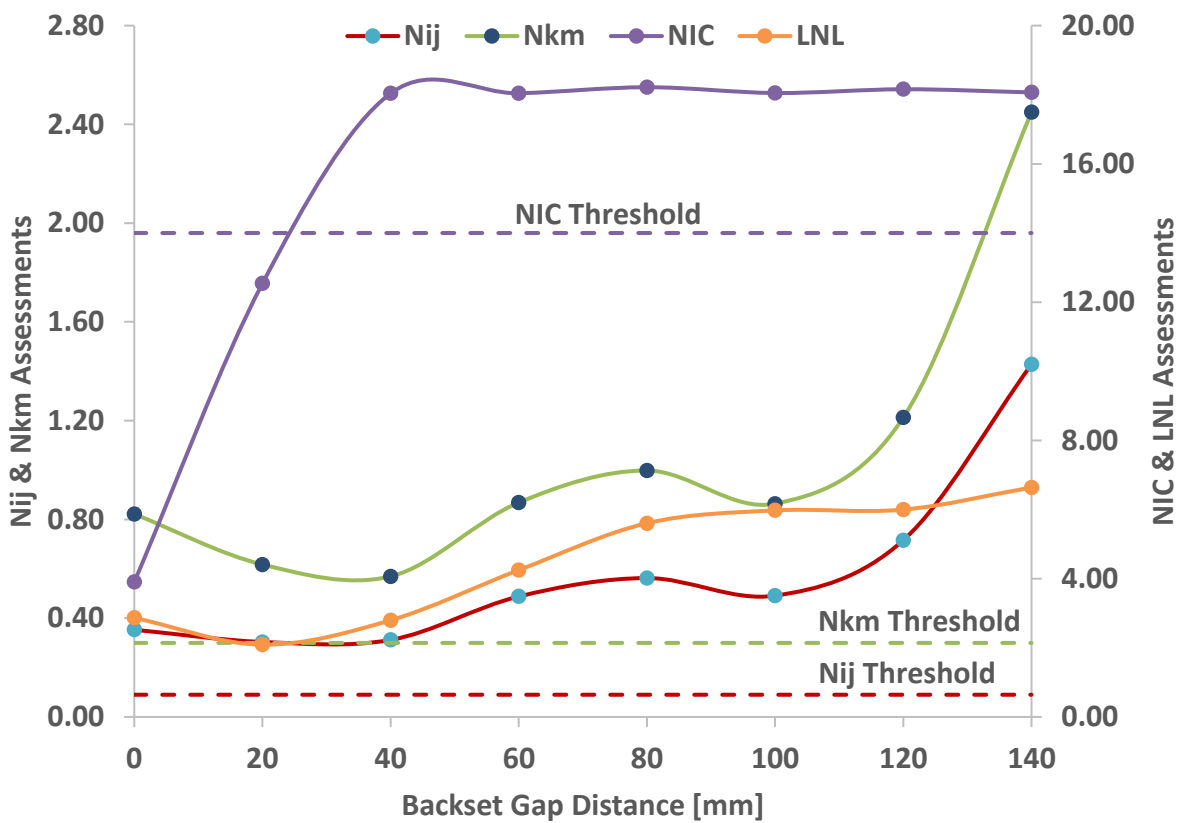


Figure 37. NIC, Nij, Nkm, and LNL injury criteria assessment versus HR gap.

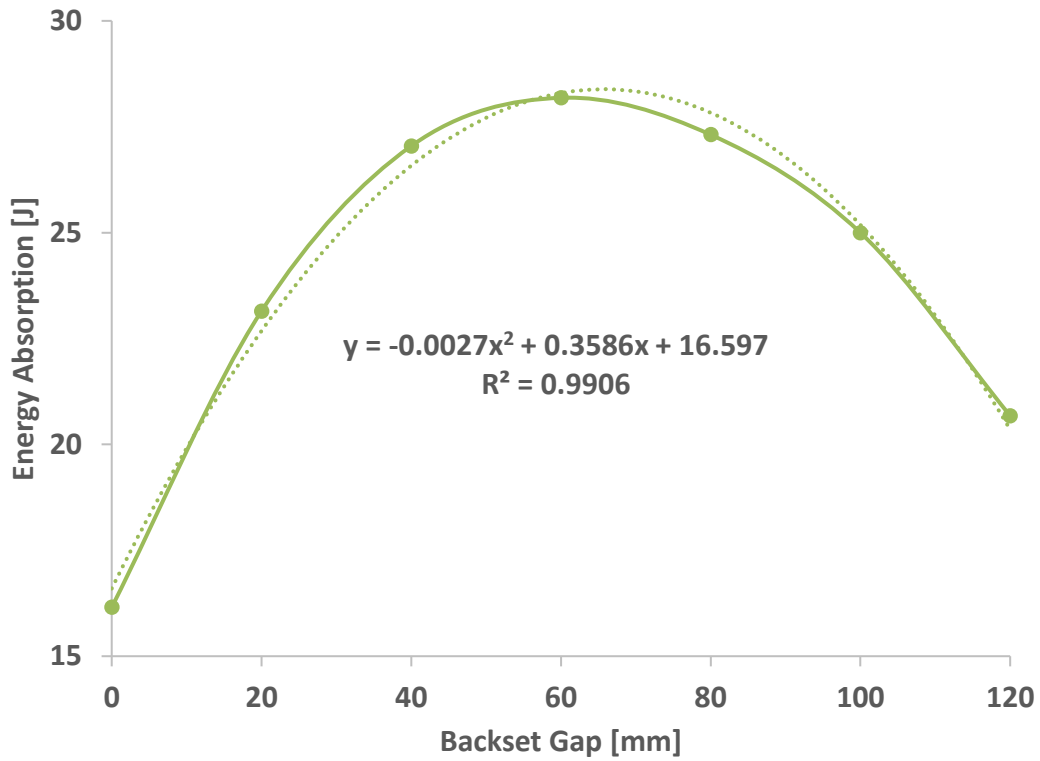


Figure 38. Maximum energy absorbed by the head-restraint position at different gaps during rear-end collision.

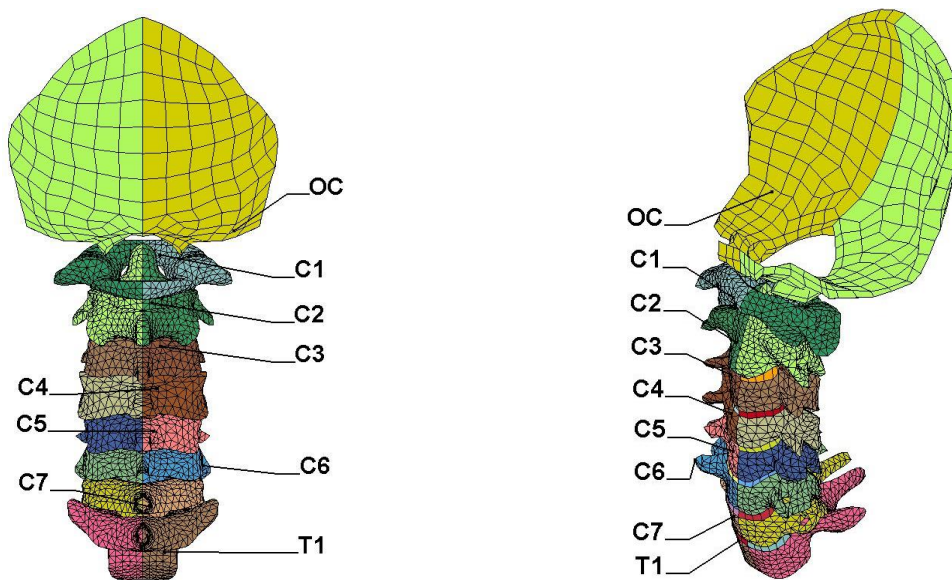


Figure 39. Back (left) and isometric (right) views of the cervical spine (C1-C7) linked with the occipital Condyle (OC) from the top and the first thoracic vertebrae (T1).

Table 12. Maximum IV-NIC values at intervertebral levels for all HR positions from FEM.

Gap [mm]	Head/C1	C1/C2	C2/C3	C3/C4	C4/C5	C5/C6	C6/C7	C7/T1
Threshold	1.60	∞	∞	2.00	2.10	1.50	1.80	3.40
0	1.08	0.80	0.54	0.61	0.42	0.35	0.38	0.44
20	0.91	0.60	0.42	0.50	0.34	0.28	0.30	0.33
40	0.91	0.53	0.33	0.36	0.22	0.28	0.31	0.17
60	1.00	0.70	0.47	0.31	0.22	0.32	0.44	0.25
80	1.08	0.71	0.30	0.41	0.25	0.36	0.48	0.26
100	1.21	0.94	0.89	0.78	0.55	0.43	0.65	0.38
120	1.16	0.95	1.36	1.49	0.95	0.50	0.73	0.56
140	1.16	1.18	4.79	4.46	1.99	1.53	1.21	1.86

4.3.3 Effect of Head-Restraint Material Properties

Material properties is one of the most critical areas in design; it affects the whole performance of any system. Vehicle seat material properties are optimized to provide both seating comfort and safety [10]. However, the most critical selection criterion for head-restraint (HR) material is their performance to arrest the head without any delay or excessive deceleration jerk. HR materials are commonly made of polyurethane (PU) foams and wrapped with a fabric to enhance their appearance and touch. PU foam material behavior is very similar to elastomeric foams [93]. PU foams have a very wide range of material properties and influenced by many factors during manufacturing. Consequently, HR material properties vary among different automobile manufacturers, as shown by the experimental results presented in section 4.2. Table 13 lists HR material properties used by the developed finite element model to investigate their

influence on neck injury and determine the optimum one for protection. Although the optimum HR position was found to be at zero gap, this investigation was conducted while maintain the HR positioned at 20 mm gap for two reasons. The first is essential to choose a wider gap than zero to give the head the chance to gain enough kinetic energy before it strikes the HR. this will allow to compare the HR material's energy absorption capability. The second is that most people do not position the HR to be touching their head while driving because it is uncomfortable. To this end, four materials (JC80, FVLD, FGCM-EF, and FGCM-DE) were added to the list of tested materials (Table 13) to increase the range of the investigated material properties. First material is Johnson Controls 80 (JC80) foam material was adopted from De Vries [93]. This polyurethane foam has an open-cell structure and commonly is used in vehicle seats. It has a lowest Young's modulus (E) compared to the listed materials and second to last in density. Second material is Flexible Very Low Density (FVLD) foam material which has the highest Young's modulus and the lowest density. Its properties were adopted from Jones and Ashby material's book [97]. The third and fourth materials are Functionally graded cellular material (FGCM), which can be defined as a non-homogenous material with properties gradually changing through its depth. In this study, the FGCM is composed of multilayered foam material to achieve the desired neck response. The front face of the HR is designed to be made of soft material to arrest the head and provide slow deceleration. Then a stiffer material is added to restrict the head from further retraction or extension movements. Accordingly, two FGCM configurations were selected; FGCM-EF and FGCM-DE. The front soft portion represents 33.5% of HR depth, and is made of the softest material (E-JC80) for both configurations, as shown in Figure 40. The rest of the HR depth (66.5%) was made of the stiffest material (F-VLDF) for FGCM-EF, whereas FGCM-DE material has a medium stiffness

(D-Mazda M3) compared to others. The equivalent density and the stiffness ratio for both FGCM materials were calculated by;

$$\rho_{FGCM-EF} = 33.5\% \rho_E + 66.5\% \rho_F \quad (13)$$

$$\rho_{FGCM-DE} = 66.5\% \rho_D + 33.5\% \rho_E \quad (14)$$

where, ρ_D , ρ_E and ρ_F are the densities for Mazda M3, JC80 and FVLD materials, respectively.

$$\frac{E_F}{E_E} = 11 \quad \text{and} \quad \frac{E_D}{E_E} = 1.75 \quad (15)$$

where, E_D , E_E and E_F are the stiffness values for Mazda M3, JC80 and FVLD materials, respectively.

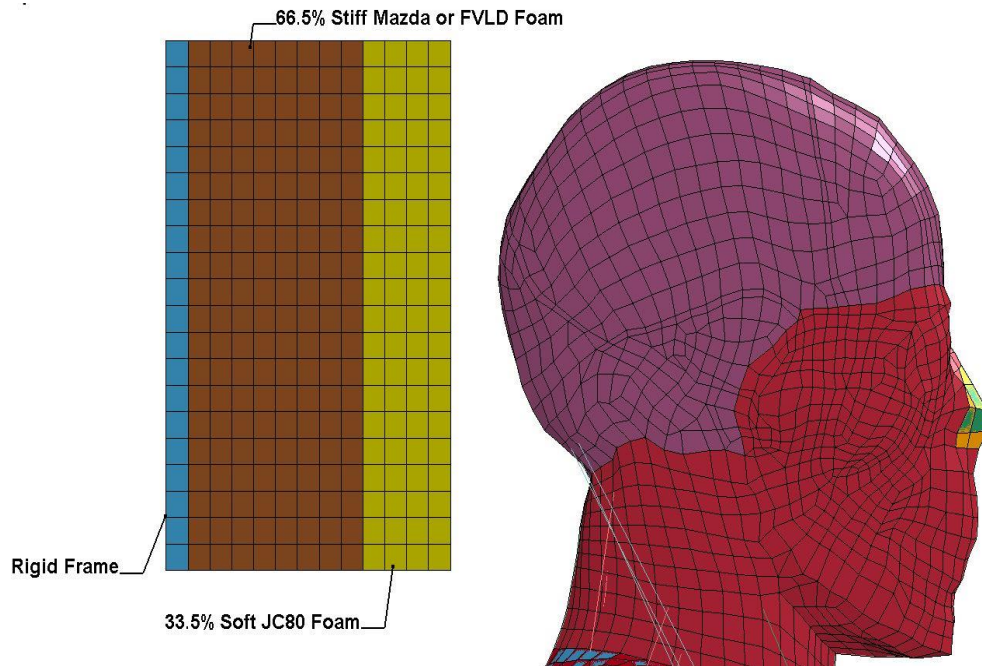


Figure 40. Head-restraint made of FGCM with 33.5% soft JC80 foam and 66.5% stiff Mazda or FVLD foam, positioned at 20 mm gap.

Table 13. Mechanical properties of head-restraint cushion materials.

Label	Material	Density (ρ)	Young's Modulus (E)
		[kg/m ³]	[kPa]
A	Toyota Land Cruiser	386.54	216.25
B	Toyota Camry	170.15	186.67
C	Nissan Tida	189.78	105.37
D	Mazda M3	287.63	158.86
E	Johnson Controls 80 (JC80) [93]	58.08	90.90
F	Flexible Very Low Density (FVLD) [97]	35.00	1000.00
G	FGCM-EF (JC80 with FVLD)	42.73	Ratio 11.00
H	FGCM-DE (Mazda M3 with JC80)	210.73	Ratio 1.75

Table 14 and Figure 41 present the head-to-HR contact period, energy absorbed by the HR material, and neck injury assessment criteria for the selected eight types of foams. Moreover, Figure 42 demonstrates the moment when maximum HR deformation occurs for all the materials to compare their properties effect of head-neck-torso kinematics. VLDF and Land Cruiser foam materials are the stiffest and thus did not experience excessive deformation compared to others which led to early end of contact. Thus, they limited the head's extension, shear, and vertical displacements. Therefore, they exhibited the lowest Nkm and LNL values compared to others. However, as per the NIC assessment, they are the only materials which led to neck injury because they exceeded the threshold of 14 m²/s² due to high head deceleration. Furthermore, VLDF material have absorbed less than half the energy absorbed by the others. This is not the case for Land Cruiser material because during the first contact stages, it acted as a soft material. This was

observed in the indentation force deflection test when it had low force level at 25% deflection like the other materials, but became stiffer afterwards because it had much higher 65% force level as discussed in section 4.2.4. This material behavior is feasible for HR application because the first stage will cause gradual head support and deceleration while the second phase limits the retraction movements of occupant's head. Soft foams exhibit higher energy absorption capabilities compared to stiff foams, due to higher deformation rates. However, head-restraint deformation does not eliminate the relative motion between head-neck-torso. Therefore, if the occupant's head is very close to HR ($G \leq 5$ mm), stiff HR material is highly recommended to limit the head's kinematics without exerting high forces and moments on the neck. However, when the backset gap distance is more than 40 mm, the head will be acting as a projectile object with high velocity due to its relative acceleration to the torso. Thus, there must be a balance between supporting the head quickly or gradually. If the material is too stiff, then it will minimize the relative head-neck-torso kinematics, but it will rapidly increase the deceleration of the head and thus causing excessive loadings and rapid rebound speeds, as indicated by the injury criteria values. JC80 foam had the lowest stiffness, it exhibited the highest performance to absorb the kinetic energy. Consequently, this results in low deceleration and thus low NIC. As Mazda HR material characterized to be in the middle between low and high stiffness, therefore it absorbed considerable impact energy. This found to be sufficient to lower head shear and vertical displacements. On the other hand, Mazda HR material has been assessed by the NIC, Nkm, and LNL as excellent. Therefore, it is the optimum material for HRs because it balances between limiting head kinematics and causing low deceleration to the neck. Using, FGCM EF and FGCM DE materials reducing head displacements, while they are recording the highest Nkm and LNL ratings. This indicates that the neck experienced very high shear forces and moments.

Table 14. Summary of neck injury assessments at different HR materials.

Material	Contact [ms]		Energy [J]	X _{OC-T1} [mm]	Z _{OC-T1} [mm]	NIC [m ² /s ²]	Nkm	LNL
	Initial	End						
Land Cruiser	35.09	91.86	21.30	12.04	1.23	14.94	0.44	1.75
Camry	35.04	99.97	23.56	11.25	0.93	11.14	1.34	2.53
Tida	35.02	100.97	23.84	10.80	0.90	11.34	1.24	2.81
Mazda M3	35.07	94.98	23.15	11.27	0.99	12.54	0.62	2.09
JC80	35.08	100.23	24.03	10.57	0.91	10.56	2.24	2.81
VLDF	35.06	70.95	13.17	10.97	1.37	19.21	0.83	1.85
FGCM EF	35.10	113.63	14.75	6.32	0.85	9.11	3.89	3.53
FGCM DE	35.02	97.41	21.29	9.00	0.91	9.88	2.30	3.28

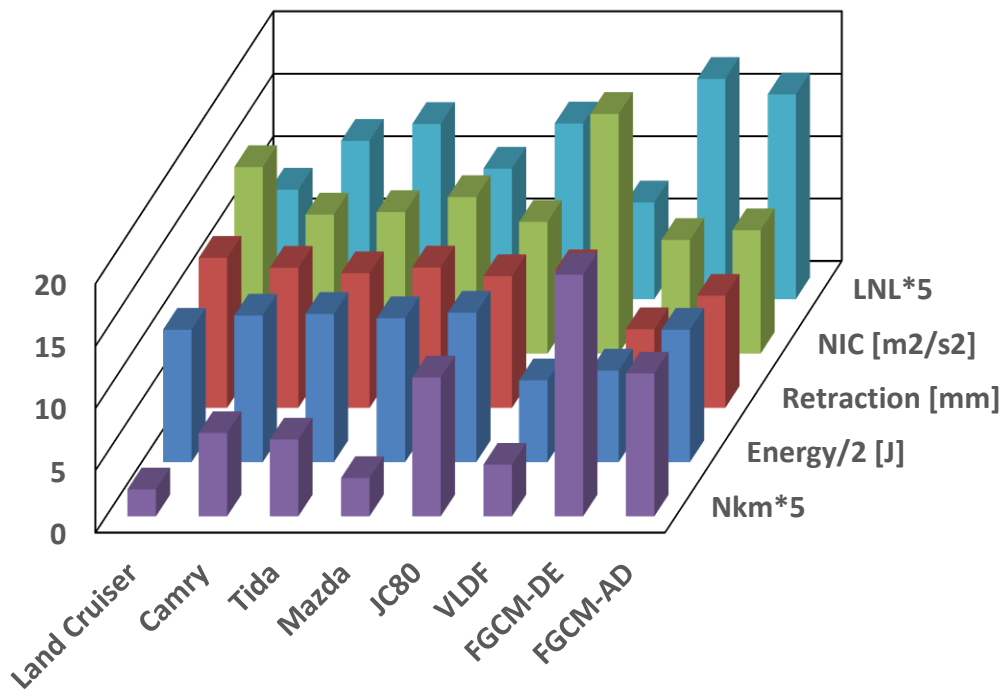


Figure 41. Comparison of HR energy absorption, maximum head retraction, NIC, Nkm, and LNL injury criteria assessments at different HR foam materials.

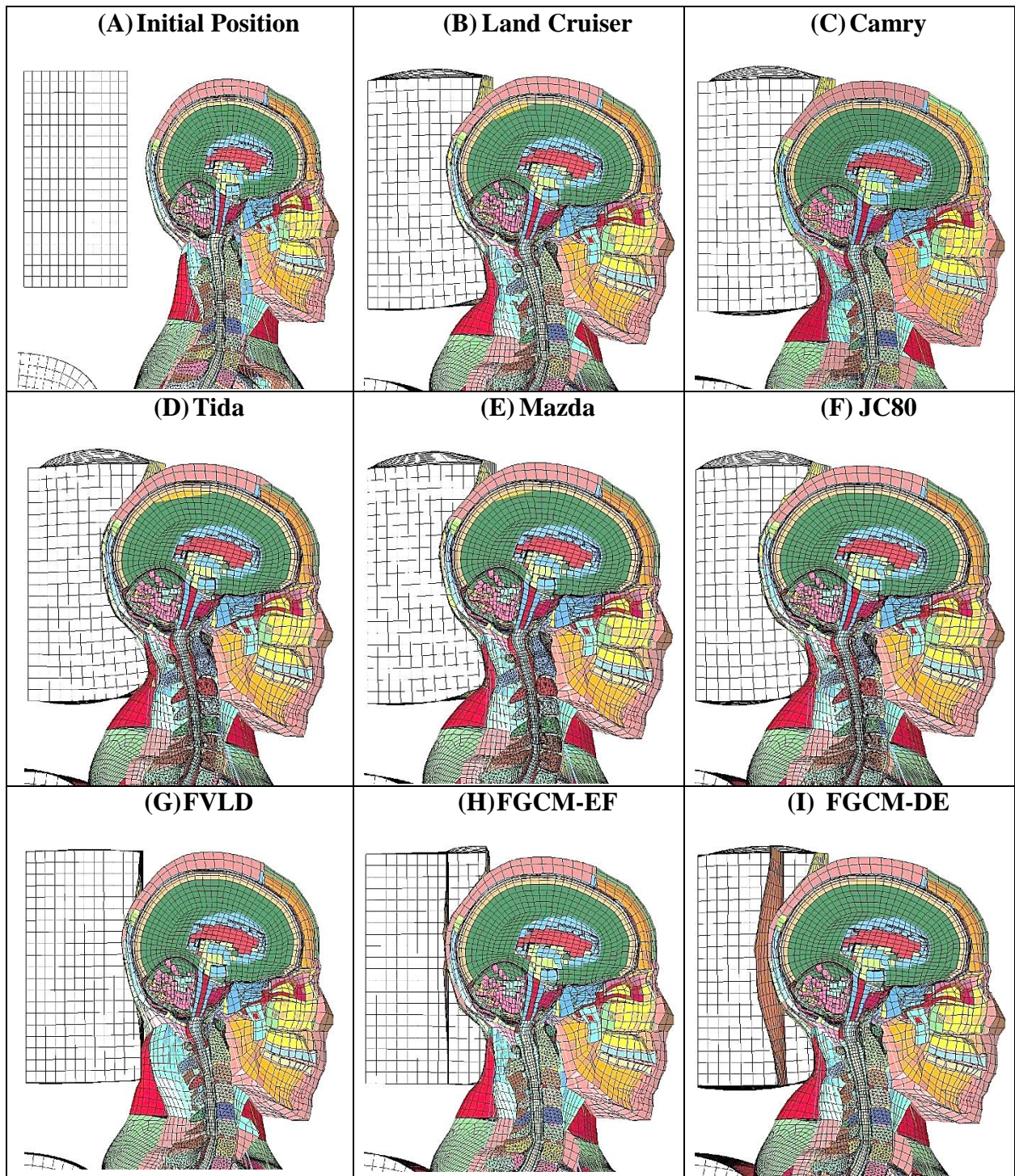


Figure 42. Comparison of HR deflection for different foam materials at maximum head indentation.

4.4 Development of Tracking Head-Restraint (T-HR) System

As proven from the findings of experimental and FEM programs, the HR position relative to the occupant's head has a significant effect on head-neck-torso kinematics and thus neck injuries. Therefore, maintaining the optimum range HR position within 0 mm to 40 mm is crucial to effectively protect the neck against whiplash. Most commercially available Active Head-Restraint (AHR) systems only deploy their mechanism to reduce the gap when the accident occurs. The drawback in these systems are independency of the head's location whether its close or far away from the AHR. When the latter case occurs, the occupant's neck would experience severe extension and retraction before the AHR can reach the head and provide its support. On the other hand, when the head is close to the AHR, the mechanism can impact the head and push it forward rather than supporting it. This can cause an inverse relative head to torso acceleration and excessive neck flexion movement. Therefore, there is a need to develop a Tracking Head-Restraint (T-HR) system which can track the passenger's head while driving and provide the head support effectively when an accident occurs. Because the T-HR will maintain the optimum gap while driving, no mechanism needs to be deployed to reduce the gap to avoid the consequence of pushing the head forward more than the torso.

The designed T-HR system is capable to adapt to the different driver's behavior. Some passengers move their head frequently while driving for different reasons, while others are more calm and relaxed. Consequently, the backset gap varies differently and continuously among drivers. A passive HR or non-tracking AHR would have to be made of soft materials to ensure no brain or head injury will occur in case the gap is big, while allowing relative head-neck-torso motion to occur as discussed in the previous section (4.3.3). However, a relatively stiffer material can be installed to the T-HR to minimize the relative motions without promoting head injuries.

In this study, three T-HR prototypes were developed and operated to compare their effectiveness and robustness during driving. The main difference among them is the mechanism responsible for the translation movements. These prototypes are not only designed to maintain the optimum gap only, but also to adjust their height as per the recommendations of the Insurance Institute for Highway Safety (IIHS), demonstrated in Figure 7.

4.4.1 Tracking Head-Restraint (T-HR) Mechanism Development

The tracking head-restraint (T-HR) system is designed to provide two degrees of freedom to track the head; vertical movement to reach the optimum height at top head level, and horizontal movement to close the backset gap and keep a comfortable distance from the passenger's head. The average variation in human head size between 50th percentile and 95th percentile males is 25 mm and 35 mm in width and length, respectively [98]. This means that if the HR geometry is designed based on the head size for 50th percentile, then the tracking mechanism will be able to move at least 25 mm vertically and 35 mm horizontally.

To generate the required mechanism of the proposed T-HR system, there are three types of motors can be used. These are servo motors, brushed DC motors, and brushless stepper motors. Table 15 compares between the three type of motors based on the response of built T-HR systems. The comparison between these motors has been carried out based on measuring their accuracy, response, torque, and cost. Servo motors are precise, have good position feedback to program, and quick response to actuate [99]. However, servo motors have low to medium torque capability and it is not practical to fit them with a gear box to increase the torque because they already been equipped with internal gear box and their response will be greatly affected. Moreover, its angular displacement is limited to 180 degrees only. Stepper motors are the best in terms of accuracy, response, and torque capacity [100]. They are widely being used in heavy industrial machinery,

such as 3D printers. However, they have very complex internal components which make them less compact in size and heavy to be embedded inside a head-restraint. Brushed motors, on the other hand, have much simpler design compare to the others which makes it very compact in size and cost-effective. Furthermore, it can be fitted with many ranges of gear boxes easily to produce the required torque capacity. Therefore, brushed DC motors are the most commonly used in many fields [100]. However, its angular position cannot be controlled and thus it lacks in precision and movement accuracy. To overcome this issue, movement limit switches are usually used to sense the position of the system.

Table 15. Advantages and drawbacks of servo, brushed and stepper motors.

Motor Type	Accuracy	Response	Torque	Cost	Drawbacks
	[mm]	[sec]	[N.m]	[USD]	
Servo	2 (Low)	<1	1.27	\$48	Limited rotation
Brushed	15 (High)	<1	3.2	\$13	No position control
Stepper	2 (Low)	<1	5.6	\$33	Heavy-less compact

Various mechanisms are used to transform the motors angular motion into translation motion of the system. Rack and pinion linkage system are the most widely used in applications (Figure 43). It offers simple components to maintain and easy to fabricate. Moreover, the motor torque may be adjusted by varying the pinion diameter and number of teeth on the rack. Rack and pinion mechanism is commonly used with stepper motors or brushed motors for their continuous rotations, whereas servo motors are limited in rotation. Other mechanisms have been developed to

be used specifically with servo motors, such as pin-and-slot mechanism (Figure 43). Such mechanism cannot be used with continuously rotating motors.

4.4.2 Sensory System

Properly positioned HR relative to the head is very important prevent whiplash injury. Therefore, it is crucial to detect occupant's head position This can be achieved through different methods and various sensing technology to ensure occupants safety.

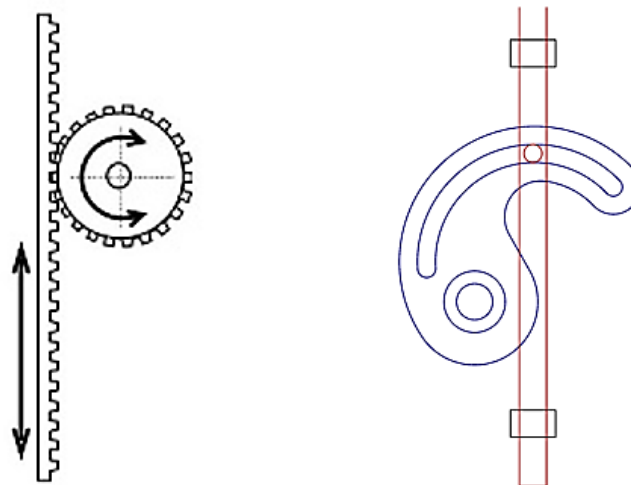


Figure 43. Rack-and-pinion mechanism (left) and pin-and-slot mechanism (right).

Thermal long-wavelength infrared sensors or ultrasonic sensors can be used to detect the head position. Ultrasonic and infrared sensors mounted on the head restraint can detect the presence and height of the passenger. These sensors are cost-effective and high reliable performance for active head restraints. Acar et al. [63] compared the performance of infrared sensors and ultrasonic sensors in a variety of conditions. Figure 44 indicates that ultrasonic sensors

perform more accurately in the presence of different hair colors. Furthermore, Figure 45 shows that ultrasonic sensor also performed better on various interference tests including; light, darkness, loud music, and the use of cell phone. Therefore, ultrasonic sensors are selected to be used in the three prototypes.

Arduino board is used to control the whole T-HR system to track the passenger’s head. It is programmed by using C++ syntax language. The program used to process data input from the equipped ultrasonic sensors and consequently control the movement of the motors. Moreover, an LED screen and emergency stop button are attached to the board to give operation feedbacks to the passenger. The whole system requires a minimum of 5-volts power supply to function and it can withstand up to 12-volts. Thus, the board can be connected easily to the vehicle, for instant connected to cigarettes lighter.

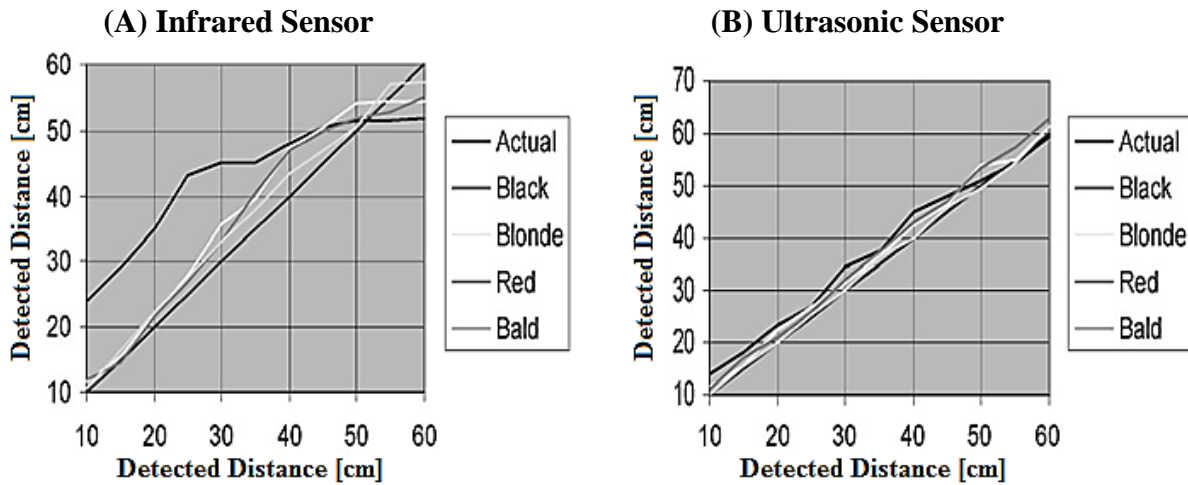


Figure 44. The response of (A) infrared sensor and (B) ultrasonic sensor to four different occupant hair colors [63].

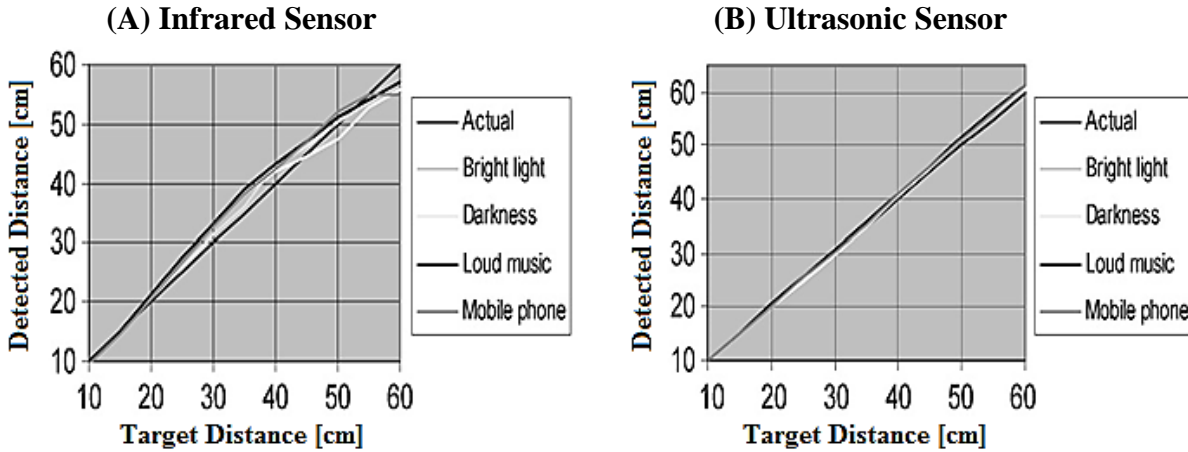


Figure 45. Effects of interference sources on the distance detection performance of (A) infrared sensor and (B) ultrasonic sensor. [63].

4.4.3 1st Tracking Head-Restraint (T-HR) Prototype

The first T-HR prototype is designed to be equipped with HS-5646WP servo motors, as demonstrated in Figure 46. The overall dimension of the prototype is shown in APPENDIX B. Four servo motor are used to achieve the horizontal and vertical movements (two for each). The output torque for one servo motor is 1.27 N.m at 7.4 volts. The rotation angles and direction of the servo motors are controlled via the Arduino board. Their movements can be controlled in a fraction of a second which is very feasible while tracking the head [99]. However, their rotation range is limited to 180 degrees due to the potentiometer embedded inside them. Consequently, the range of motion for the system will be limited, depending on the ratio of gear. Rack and pinion gears were used to transform the servo motors rotational movement into translational displacements. The spur gear was designed to have 18 tooth with pressure angle of 20°, depth of 12.5 mm, and face width of 25 mm. This rack and pinion gears were design to be used in all the prototypes.

The prototype was built by Stratasys uPrint 3D-printer using Acrylonitrile Butadiene Styrene (ABS) material filaments. Two ultrasonic sensors were used to track the head's position; one for detecting the height while the second is for detecting the backset gap distance. The T-HR system was programmed to initially adjust its height until it reaches the top of the occupant's head. After that, the T-HR is designed to move forward until the backset gap is within the range between 5 mm to 40 mm. a minimum distance of 5 mm was set to provide comfort for the driver. During testing of the prototype, it was difficult to synchronize the rotations of the two servo motors due to their quick response. This issue was causing the gears to jam and finally lead to material fracturing in vertical columns.

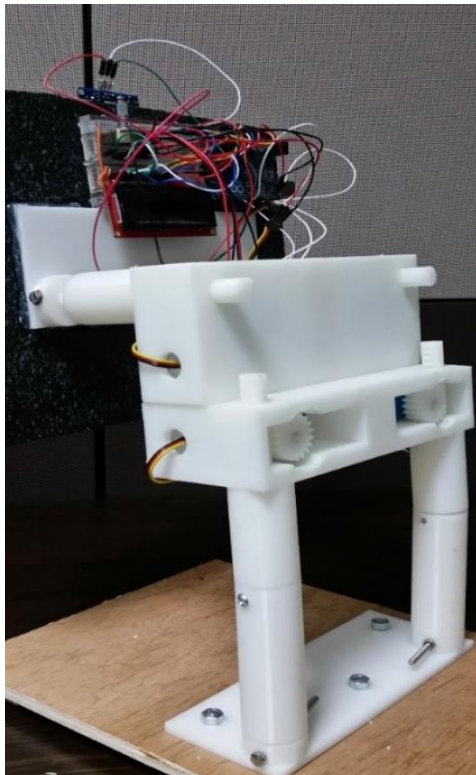


Figure 46. First T-HR prototype built entirely using 3D-printing ABS material.

4.4.4 2nd Tracking Head-Restraint (T-HR) Prototype

The second T-HR prototype was developed to overcome the problem in synchronizing the motion between the servo motors. The mechanism uses two servo motors instead of four, as illustrated in Figure 47. In addition, a third link had to be added, as shown in APPENDIX B, because now the servo motors are positioned in the middle of the T-HR. The prototype was built using 3D-printing technology similar to the previous one. Moreover, it uses the same rack and pinion design and the methodology to track the head using ultrasonic sensors. This prototype showed that the synchronizing problem between the servo motors is eliminated. This because the two servo motors are moving independently. However, the servo motors must produce almost twice their torque output because the overall mass of the T-HR have not change significantly. In addition, there is a limitation for the T-HR motion due to the rotational limit of the servo motors.

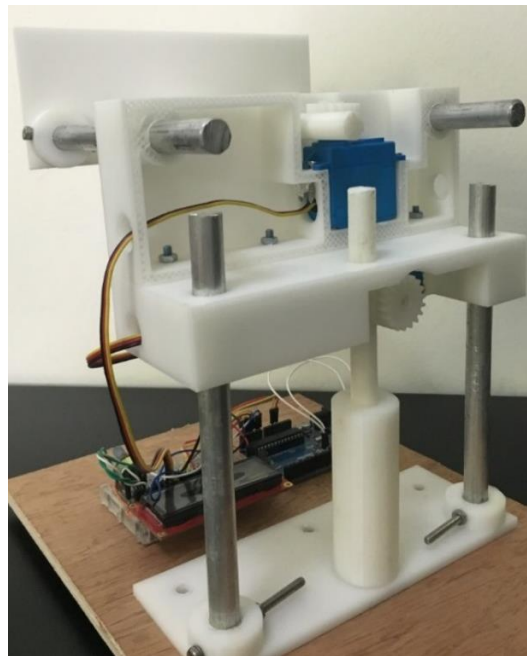


Figure 47. Second T-HR prototype built with 3D-printing ABS material and aluminum rods.

4.4.5 3rd Tracking Head-Restraint (T-HR) Prototype

The third T-HR prototype was developed to overcome the drawback of the previous two prototypes where there was a movement limit for the mechanism. This was achieved by replacing the servo motors with brushed dc motors. Only two motors were used like the second prototype to avoid the synchronization problem appeared in the first prototype. Brushed DC motors have higher torque output and more compact in size compared to servo motors. This is because in addition to the small DC motor, servo motors include a potentiometer and small circuit board with the motor. The disadvantage of using brushed dc motors is that their position cannot be precisely controlled like the servo motors. In addition, the direction of their rotation cannot be reversed unless the power polarity is reversed which cannot be done by the Arduino board itself. An additional H-bridge circuit has been added to reverse the power polarity.

As shown in APPENDIX B, the structure in the third prototype have been redesigned to be more detailed and compacted for two reasons; to be fitted inside the HR limited space without scarifying cushion depth, and to have lighter system to reduce the needed torque output from the motors and thus using smaller motors. The prototype was built from ABS material using 3D-printing technology. Moreover, two ultrasonic sensors were used to track the occupant's head similar to the pervious prototypes.

4.4.5.1 Electrical circuit

The H-bridge is connected to Arduino 8-13 digital pins as shown in Figure 48. The two brushed DC motors are linked with the H-bridge to control their rotation direction. Start/emergency stop button is connected to digital pin 2 to allow the driver to start the T-HR system before starting to drive, or press it while functioning to immediately stop in case of any emergency. An LCD screen is connected to the analog 0-5 pins to provide feedback messages to

the driver or notify him of a limitation in the system, such as “The T-HR system have reached its maximum height”. Two limit switches are connected to the controller via 5 and 6 digital pins. These switches are used to send signals to the controller that the T-HR reach its maximum degrees of freedom.

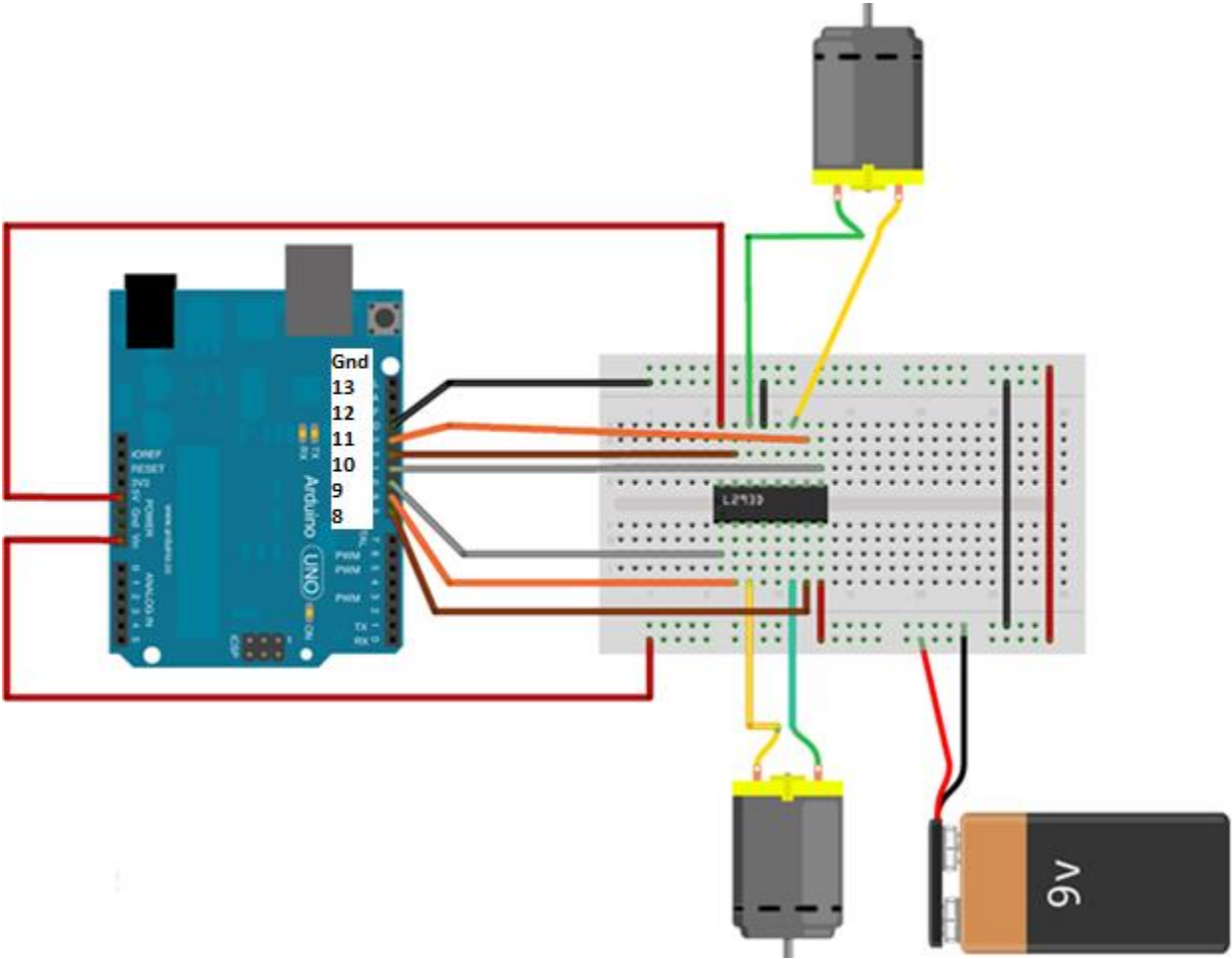


Figure 48. The electrical wiring diagram for controlling the T-HR system using Arduino UNO board and H-bridge.

4.4.5.2 Logical Code

The Arduino program code for controlling the third prototype of the tracking head-restraint systems is presented in APPENDIX C. The logic behind the Arduino code can be explained as follows;

- The system is designed to wait for the driver's input to start functioning by pressing the start button.
- Once the starter button is pressed, the height (top) ultrasonic sensor will start detecting the head's position relative to the system position.
- If the distance is less than 50 cm, then the vertical motor is designed to be actuated to raise the height of the head-restraint to the proper height position.
- After that, the gap sensor (i.e. middle sensor) begins detecting the relative horizontal distance to the middle head.
- If the measured gap is less than 0.5 cm or more than 4 cm, the horizontal motor designed to be actuated to maintain the head-restraint system within the acceptable range.
- Once the middle sensor detects a gap between 0.5 cm to 4 cm, the motor is designed to stop and the system is in standby mode where both sensors keep detecting the head's position of occupant every 100 milliseconds for any change in its height or gap.
- There are two limit switches positioned at the vertical and horizontal movements to detect if the system has reached its movement limits. An emergency button is designed to be controlled by the occupant. Thus, if it is pressed, the whole system stops immediately without returning to its initial position. The system can function again normally once the button is pressed again to start.

4.4.5.3 Ultrasonic sensor performance

The accuracy of the ultrasonic sensor in detecting the target distance was tested by placing a cubical target at a specific distance. The actual distance was measured by using Vernier caliper tool. The accuracy of the sensor was set to read up to one digit after the decimal. The distance reading was recorded after one second and no reading fluctuation was observed. Table 16 lists the actual and the detected target distance by the sensor. The maximum variation in the sensor reading was 0.2 mm which is acceptable. The maximum detecting distance of the ultrasonic sensor was 250 cm.

Table 16. Performance of ultrasonic sensor in detecting target distance.

Target Distance	Detected Distance	S.D.
[mm]	[mm]	[mm]
0	0.1	0.07
5	5.2	0.14
10	10.2	0.14
20	19.7	0.21
30	29.8	0.14
40	40.1	0.07
60	59.9	0.07
80	79.8	0.14
100	99.7	0.21
120	119.8	0.14

4.4.5.4 T-HR system performance

Three passengers with different altitudes volunteered to evaluate the functionality of the T-HR system. Table 17 lists the volunteers' altitude, initial HR position relative to the head, achieved HR position gap, and the system's response time. The HR height in the first volunteer (A) case was initially above the top head level due to the low altitude of the occupant. However, the HR backset gap was more than the acceptable range for safety (50>40 mm). Therefore, the T-HR system has automatically corrected its horizontal position (25 mm) within 64 milliseconds. The HR position for the second volunteer (B) was initially within the desired range and thus the T-HR system did not correct the position. Due to the high altitude of the third volunteer (C), the T-HR was required to correct both the height and backset gap of the HR to be within the desired safe range. Figure 49 illustrates the initial HR position and corrected position for the last volunteer (C). It should be noted that the seatback angle was increased to increase the backset gap in Figure 49 (C & D).

Table 17. The initial and corrected T-HR system vertical (V) and horizontal (H) positions for the three occupants.

No.	Gender	Altitude [cm]	Desired gap [mm]		Initial gap [mm]		Achieved gap [mm]		Response [ms]	
			V	H	V	H	V	H	V	H
A	M	164	>0	<40	20	50	20	25	0	64
B	F	156	>0	<40	40	2	40	2	0	0
C	M	196	>0	<40	75	150	5	10	124	186

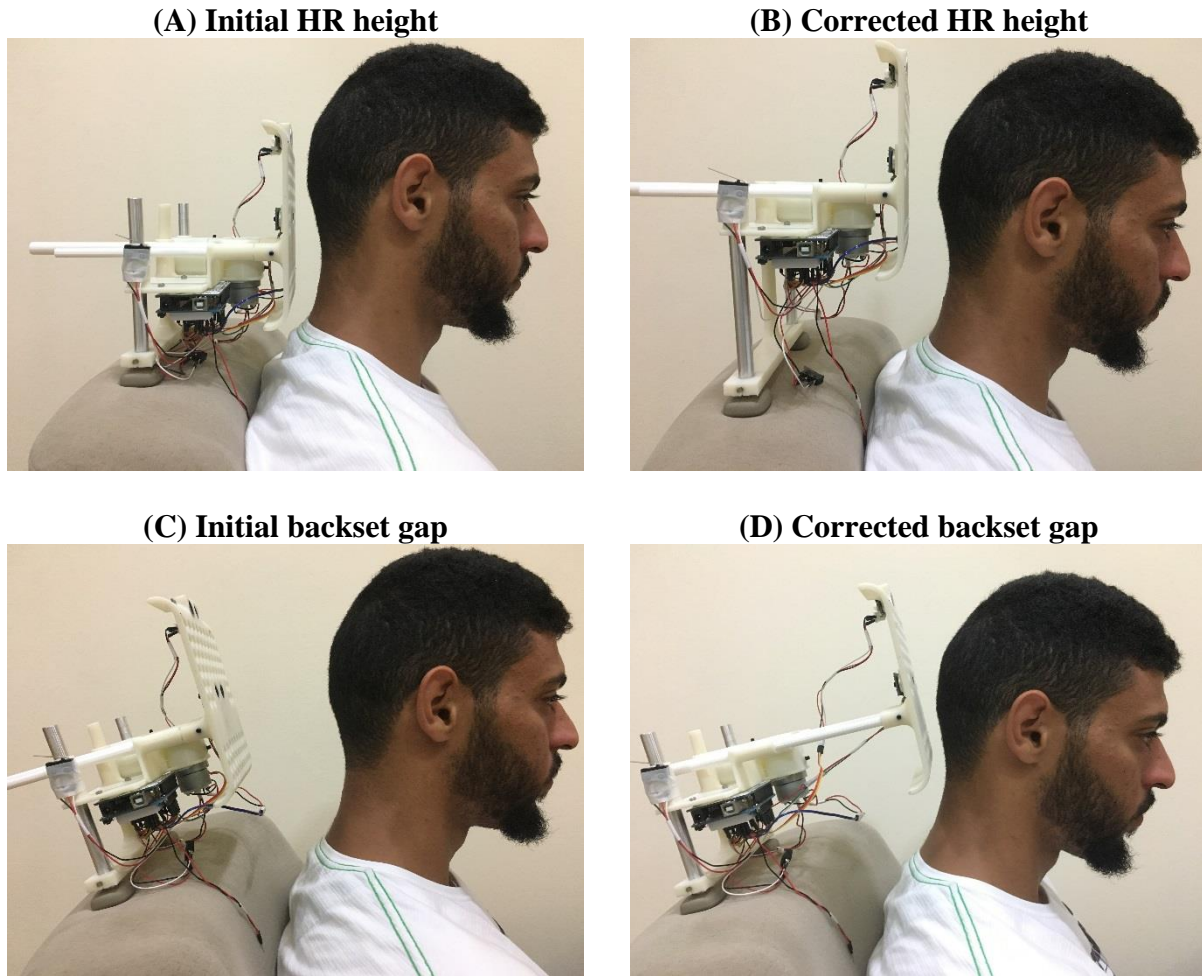


Figure 49. Evaluating the functionality of the T-HR system by the third volunteer; (A) initial HR height position, (B) corrected HR height position, (C) initial HR backset gap, and (D) corrected HR backset gap.

4.5 Overall Discussion

The developed finite element model (FEM) showed an excellent agreement with published works of Stemper et al. [17]. The small discrepancy that has observed is since the developed FEM first thoracic vertebrae (T1) is different from Stemper's model. The developed FEM consists of a complete vertebral spine where T1 is linked from top and bottom by the last cervical vertebrae (C7) and the second thoracic vertebrae (T2), respectively. On the other hand, in Stemper's model is only linked from the top by the cervical vertebrae (C7).

The FEM results indicated that whiplash injury is highly dependent on the Head-Restraint (HR) position relative to the occupant's head. Based on the assessment of various neck injury criteria, neck injury will not result if the gap between occupant's head and HR is less than or equal to 40 mm. Moreover, if the gap between occupant's head and HR is between 40 mm and 100 mm, the results show that tearing of neck muscles due to high neck shear displacement (head retraction) will occur during the S-shape neck curvature. It is also computed and observed that severe neck injuries would result if the gap is more than 100 mm. The observed severe neck injuries include tearing of longitudinal ligament, neck muscles, and fracturing vertebral facet joints at C3/C4 and C5/C6 segmental levels. Here in, it is worth mentioning that if the gap is more than 100 mm and the impact pulse is higher than 10 g, the severity of neck injuries can lead to death [7].

The experimental test conducted on the selected HRs have shown the wide variety of HR material properties. These properties were then proved to have significant influence on whiplash injury. Soft HR materials absorbed high kinetic energies through their deformation, but did not limit the neck's shear and vertical displacements effectively. While, stiff HR materials did not deform nor absorb energy as much, they provided good head support and limited neck motions. However, the neck has experienced high deceleration and thus high forces and moments. In addition, severe head and brain injuries can result due to the high level of contact forces between the head and HR.

CHAPTER 5 CONCLUSIONS

Whiplash injury is a common neck injury which results from excessive relative motions of the head-neck-torso structure. Head-Restraints (HR) are the main protection measure used to limit those motions and provide safe absorption of the impact. This study conducted experimental tests on selected HR materials and developed a Finite Element Model (FEM) to investigate the effects of HR position and material on whiplash injury. Furthermore, a Tracking Head-Restraint (T-HR) system was developed based on the previous findings to improve the function of HRs in protecting the neck against whiplash. In general, the main aims of the current study are:

- The validated FEM showed excellent agreement with the published study. The FEM results showed that HR position have great effect on their performance in limiting whiplash. Assessments of various neck injury criteria showed that maintaining the HR positioned within the optimum range of 0 mm to 40 mm is crucial to effectively protect the neck against whiplash. In addition, gaps 60 mm and 80 mm are marginable causing high neck shear displacement (head retraction). If the gap is more than that, then long term neck injuries will occur due to tearing of the longitudinal ligament and neck muscles during the extension phase.
- Differences in HR material properties have been pointed out by experimental tests, even among the same manufacturer. Moreover, hyper-elastic materials behavior was observed to dominate the response of all HR materials. FEM results showed that HR material properties have a significant effect on whiplash kinematics. Softer HR materials absorbed high energy through deformation, and provided gradual head deceleration which led to low

loading on the neck. On the other hand, stiffer HR materials have limited the relative head-neck-torso kinematics while causing severe deceleration and loadings. Thus, the optimum HR material properties must balance between limiting head-neck-torso kinematics and head deceleration.

- The developed T-HR system allows optimum neck protection performance by maintaining the HR positioned at the optimum gap of 20 mm relative to the head. In addition, its padding is made with the best material properties based on the optimum gap.

CHAPTER 6 FURTHER RECOMMENDATIONS

As has been stated earlier in this study that vehicle accidents can lead to wide range of serious long term injuries to the occupant including; neck, head, back, and internal organs. The current study has focused only on neck injury in rear-end collisions due to the complexity of this field. More work can be achieved using the developed finite element model to investigate the following areas:

- The effect of seatbase inclination angle and seatback angle on whiplash injury. Changing in these angles will produce combined horizontal and vertical torso acceleration. Therefore, the neck will experience axial compression combined with the four whiplash phases presented in this study.
- Various HR geometries are observed among car manufacturers as indicated in this study. Therefore, an investigation on their geometries effects on whiplash injury is very important.
- As well known, presence of jerk can have a significant influence of the relative acceleration of the head-neck-torso complex. This is the real case because the vehicle's structure does not show a uniform energy absorption while crashing. Hence, an investigation on the effect of impact pulse shape and magnitude on whiplash injury is crucial to produce more robust protection system.
- The investigation of neck injuries can be expanded to include different types of impacts. Airbag and seatbelt system have significant influence on the neck flexion phase during a frontal impact.

- The most challenging problem is to study the whiplash during the side impact. This is because side impact can produce fatal neck bending moments and no prevention system is available, except the side airbags, which is only located in one side.
- A third degree of movement can be added to the tacking head-restraint system to correct its position when the occupant's head moves left or right. Moreover, the system can detect the coming collision by mounting ultrasonic sensors around the vehicle to examine the occupant behavior during the collision events.

REFERENCES

1. Staff, T., et al., *A field evaluation of real-life motor vehicle accidents: Presence of unrestrained objects and their association with distribution and severity of patient injuries*. Accident Analysis & Prevention, 2012. **45**: p. 529-538.
2. Ivancic, P.C., *Cervical neural space narrowing during simulated rear crashes with anti-whiplash systems*. European Spine Journal, 2012. **21**(5): p. 879-886.
3. Ivancic, P.C. and M. Xiao, *Cervical spine curvature during simulated rear crashes with energy-absorbing seat*. The Spine Journal, 2011. **11**(3): p. 224-233.
4. Trempe, R.E., D.S. Zuby, and M.A. Edwards, *IHS head restraint ratings and insurance injury claim rates*. Traffic injury prevention, 2016(just-accepted): p. 00-00.
5. Organization, W.H., *Global status report on road safety: time for action*. 2009: World Health Organization.
6. van Ratingen, M., et al., *The European New Car Assessment Programme: a historical review*. Chinese journal of traumatology, 2016. **19**(2): p. 63-69.
7. Bener, A., Y.S.A. Rahman, and B. Mitra, *Incidence and severity of head and neck injuries in victims of road traffic crashes: In an economically developed country*. International Emergency Nursing, 2009. **17**(1): p. 52-59.
8. Ivancic, P.C. and M. Xiao, *Understanding whiplash injury and prevention mechanisms using a human model of the neck*. Accident Analysis & Prevention, 2011. **43**(4): p. 1392-1399.
9. Berglund, A., et al., *Occupant-and crash-related factors associated with the risk of whiplash injury*. Annals of epidemiology, 2003. **13**(1): p. 66-72.
10. Acar, M. and S. Bewsher, *Design concepts for an integrated whiplash mitigating head restraint and seat*. International Journal of Crashworthiness, 2016. **21**(1): p. 79-88.
11. Özdemir, M., S.K. İder, and M.İ. Gökler, *Experimental and numerical investigation of comparability of whiplash sled test results*. Journal of the Brazilian Society of Mechanical Sciences and Engineering, 2016. **38**(2): p. 395-402.
12. Chen, M., et al. *The Effects of Packaging on Collision Energy Absorption of Automotive Seat Headrest*. in *MATEC Web of Conferences*. 2016. EDP Sciences.
13. Yao, H.-D., M.Y. Svensson, and H. Nilsson, *Transient pressure changes in the vertebral canal during whiplash motion—A hydrodynamic modeling approach*. Journal of biomechanics, 2016. **49**(3): p. 416-422.
14. Popa, V., et al., *Studies Regarding Occupant Kinematics in the Vehicle at the Frontal and Rear Impact*. Applied Mechanics & Materials, 2016. **822**.

15. Zhang, X. and Q. Zhou, *An energy-absorbing sliding seat for reducing neck injury risks in rear impact—analysis for prototype built*. Traffic injury prevention, 2016. **17**(3): p. 313-319.
16. Recicar, J., et al., *Does restraint status in motor vehicle crash with rollover predict the need for trauma team presence on arrival? An ATOMAC study*. Journal of pediatric surgery, 2016. **51**(2): p. 319-322.
17. Stemper, B.D., N. Yoganandan, and F.A. Pintar, *Effect of head restraint backset on head–neck kinematics in whiplash*. Accident Analysis & Prevention, 2006. **38**(2): p. 317-323.
18. Nishimura, N., C.K. Simms, and D.P. Wood, *Impact characteristics of a vehicle population in low speed front to rear collisions*. Accident Analysis & Prevention, 2015. **79**: p. 1-12.
19. Ono, K. and K. Kaneoka, *Motion analysis of human cervical vertebrae during low-speed rear impacts by the simulated sled*. Traffic Injury Prevention, 1999. **1**(2): p. 87-99.
20. Siegmund, G.P., et al., *The effect of collision pulse properties on seven proposed whiplash injury criteria*. Accident Analysis & Prevention, 2005. **37**(2): p. 275-285.
21. Ivancic, P., *Cervical spine instability following axial compression injury: a biomechanical study*. Orthopaedics & Traumatology: Surgery & Research, 2014. **100**(1): p. 127-133.
22. Schmitt, K.-U., et al., *Trauma Biomechanics: Accidental injury in traffic and sports*. 2009: Springer Science & Business Media.
23. Sterling, M. and J. Kenardy, *Whiplash: evidence base for clinical practice*. 2011: Elsevier Australia.
24. Forman, J.L., et al., *The tolerance of the human body to automobile collision impact—a systematic review of injury biomechanics research, 1990–2009*. Accident Analysis & Prevention, 2015. **80**: p. 7-17.
25. Kai, W., et al. *Dynamic Response and Injury of Neck Tissues in Low-Speed Rear-Ending*. in *2016 Eighth International Conference on Measuring Technology and Mechatronics Automation (ICMTMA)*. 2016. IEEE.
26. Stokes, I., *Frontiers in whiplash trauma: clinical and biomechanical: Narayan Yoganandan and Frank A. Pintar (Eds.); IOS Press, Inc., Burke, VA, 2000, 590pp., price \$92.00 ISBN 4-274-90354-0 C3047*. Journal of Biomechanics, 2001. **34**(8): p. 1103-1104.
27. Hynes, L.M. and J.P. Dickey, *The rate of change of acceleration: Implications to head kinematics during rear-end impacts*. Accident Analysis & Prevention, 2008. **40**(3): p. 1063-1068.
28. Chen, H.-b., H.Y. King, and Z.-g. Wang, *Biomechanics of whiplash injury*. Chinese Journal of Traumatology (English Edition), 2009. **12**(5): p. 305-314.

29. King, D., et al., *The influence of head impact threshold for reporting data in contact and collision sports: systematic review and original data analysis*. Sports medicine, 2016. **46**(2): p. 151-169.
30. White, A.A. and M.M. Panjabi, *Clinical biomechanics of the spine*. Vol. 2. 1990: Lippincott Philadelphia.
31. Munoz, D., et al. *A study of current neck injury criteria used for whiplash analysis proposal of a new criterion involving upper and lower neck load cells*. in *Proceedings of the 19th Experimental Safety Vehicles Conference*. 2005.
32. Gilchrist, I., et al., *Effects of head flexion posture on the multidirectional static force capacity of the neck*. Clinical Biomechanics, 2016.
33. Yoganandan, N., B.D. Stemper, and R.D. Rao. *Patient mechanisms of injury in whiplash-associated disorders*. in *Seminars in Spine Surgery*. 2013. Elsevier.
34. Galletti, S., et al., *Localized cervical pain: advantages and limits of ultrasound evaluation*. Journal of Ultrasound, 2016: p. 1-7.
35. Arcaute-Velazquez, F.F., et al., *Injury mechanisms in extreme violence settings*. Cirugía y Cirujanos (English Edition), 2016. **84**(3): p. 257-262.
36. Rosenfeld, J., *Practical management of head and neck injury*. 2012: Elsevier Health Sciences.
37. Yoganandan, N., et al., *Cervical spine injuries, mechanisms, stability and AIS scores from vertical loading applied to military environments*. European Spine Journal, 2016: p. 1-9.
38. Heitplatz, F., et al. *An evaluation of existing and proposed injury criteria with various dummies to determine their ability to predict the levels of soft tissue neck injury seen in real world accidents*. in *Proc. 18th ESV Conf*. 2003.
39. Boström, O., et al. *A new neck injury criterion candidate-based on injury findings in the cervical spinal ganglia after experimental neck extension trauma*. in *Proceedings of The 1996 International Ircobi Conference On The Biomechanics Of Impact, September 11-13, Dublin, Ireland*. 1996.
40. Eriksson, L. and A. Kullgren. *Influence of seat geometry and seating posture on NICmax and Nkm AIS 1 neck injury predictability*. in *Proceedings of the International Research Council on the Biomechanics of Injury conference*. 2003. International Research Council on Biomechanics of Injury.
41. Croft, A.C., et al., *The neck injury criterion: future considerations*. Accident Analysis & Prevention, 2002. **34**(2): p. 247-255.
42. Ivancic, P.C. and D. Sha, *Comparison of the whiplash injury criteria*. Accident Analysis & Prevention, 2010. **42**(1): p. 56-63.

43. Panjabi, M.M., et al., *Evaluation of the intervertebral neck injury criterion using simulated rear impacts*. Journal of Biomechanics, 2005. **38**(8): p. 1694-1701.
44. Eppinger, R., et al., *Development of improved injury criteria for the assessment of advanced automotive restraint systems—II*. National Highway Traffic Safety Administration, 1999: p. 1-70.
45. Mertz, H., et al., *An assessment of compressive neck loads under injury-producing conditions*. Physician and Sports medicine, 1978. **6**(11).
46. Nyquist, G.W., et al., *Correlation of field injuries and GM hybrid III dummy responses for lap-shoulder belt restraint*. Journal of biomechanical engineering, 1980. **102**(2): p. 103-109.
47. Mertz, H.J. and L.M. Patrick, *Strength and response of the human neck*. 1971, SAE Technical Paper.
48. Yoganandan, N., et al., *Human head-neck biomechanics under axial tension*. Medical engineering & physics, 1996. **18**(4): p. 289-294.
49. Shea, M., et al., *In vitro hyperextension injuries in the human cadaveric cervical spine*. Journal of orthopaedic research, 1992. **10**(6): p. 911-916.
50. Lenox, J., et al. *Development of Neck Injury Tolerance Criteria in Human Surrogates. I. Static Tensile Loading in the Baboon Neck: Preliminary Observations*. in *Proceedings of the Ninth International Technical Conference on the Enhanced Safety of Vehicles*. 1982.
51. Schmitt, K.-U., et al., *N km --A Proposal for a Neck Protection Criterion for Low-Speed Rear-End Impacts*. Traffic Injury Prevention, 2002. **3**(2): p. 117-126.
52. Krafft, M., et al., *Assessment of Whiplash Protection in Rear Impacts*. Stockholm, Sweden, 2005.
53. Viano, D.C. and J. Davidsson, *Neck Displacements of Volunteers, BioRID P3 and Hybrid III in Rear Impacts: Implications to Whiplash Assessment by a Neck Displacement Criterion (NDC)*. Traffic Injury Prevention, 2002. **3**(2): p. 105-116.
54. Hwang, S.H., et al. *Seat Headrest Development to Detect the Head Position of Passenger*. in *22nd International Technical Conference on the Enhanced Safety of Vehicles (ESV)*. 2011.
55. Wiklund, K. and H. Larsson, *Saab active head restraint (SAHR)-seat design to reduce the risk of neck injuries in rear impacts*. 1998, SAE Technical Paper.
56. Jakobsson, L., et al., *WHIPS—Volvo’s whiplash protection study*. Accident Analysis & Prevention, 2000. **32**(2): p. 307-319.

57. Lundell, B., et al. *The WHIPS seat-a car seat for improved protection against neck injuries in rear end impacts*. in *Proc. 16th ESV Conference, Paper*. 1998.
58. Sekizuka, M. *Seat designs for whiplash injury lessening*. in *Proc. 16th Int. Techn. Conf. on ESV, Windsor, Canada*. 1998.
59. Bloecher, H., J. Dickmann, and M. Andres. *Automotive active safety & comfort functions using radar*. in *2009 IEEE International Conference on Ultra-Wideband*. 2009. IEEE.
60. Maher, J., *Report investigating the importance of head restraint positioning in reducing neck injury in rear impact*. Accident Analysis & Prevention, 2000. **32**(2): p. 299-305.
61. Linder, A., et al., *ADSEAT-Adaptive seat to reduce neck injuries for female and male occupants*. Accident Analysis & Prevention, 2013. **60**: p. 334-343.
62. Ivancic, P.C., D. Sha, and M.M. Panjabi, *Whiplash injury prevention with active head restraint*. Clinical Biomechanics, 2009. **24**(9): p. 699-707.
63. Acar, M., S. Clark, and R. Crouch, *Smart head restraint system*. International Journal of Crashworthiness, 2007. **12**(4): p. 429-435.
64. Latchford, J. and E. Chirwa, *Airbag head restraint system*. Proceedings of the Institution of Mechanical Engineers, Part D: Journal of Automobile Engineering, 2000. **214**(3): p. 229-241.
65. Bunketorp, O.B. and L.K. Elisson, *Cervical status after neck sprains in frontal and rear-end car impacts*. Injury, 2012. **43**(4): p. 423-430.
66. Gu, X. and J. Lu, *Reliability-based robust assessment for multiobjective optimization design of improving occupant restraint system performance*. Computers in Industry, 2014. **65**(8): p. 1169-1180.
67. Nilson, G., et al., *Rear-End Collisions-The Effect of Recliner Stiffness and Energy Absorption on Occupant Motion*. Effects of Seat-Belt Design on Car Occupant Response in Frontal and Rear Impacts, Ph. D. Thesis, Chalmers Univ. of Technology, Göteborg, 1994.
68. Boström, O., et al. *Prediction of neck injuries in rear impacts based on accident data and simulations*. in *Proceedings of the 1997 International IRCOBI Conference on the Biomechanics of Impact*. 1997.
69. Morris, A.P. and P. Thomas, *Neck injuries in the UK co-operative crash injury study*. 1996, SAE Technical Paper.
70. Olsson, I. *An in-depth study of neck injuries in rear end collisions*. in *1990 International Ircobi Conference on The Biomechanics Of Impacts: Proceedings, September 12-13-14, Bron-Lyon (France)/International Research Council On Biokinetics Of Impacts*. 1990.

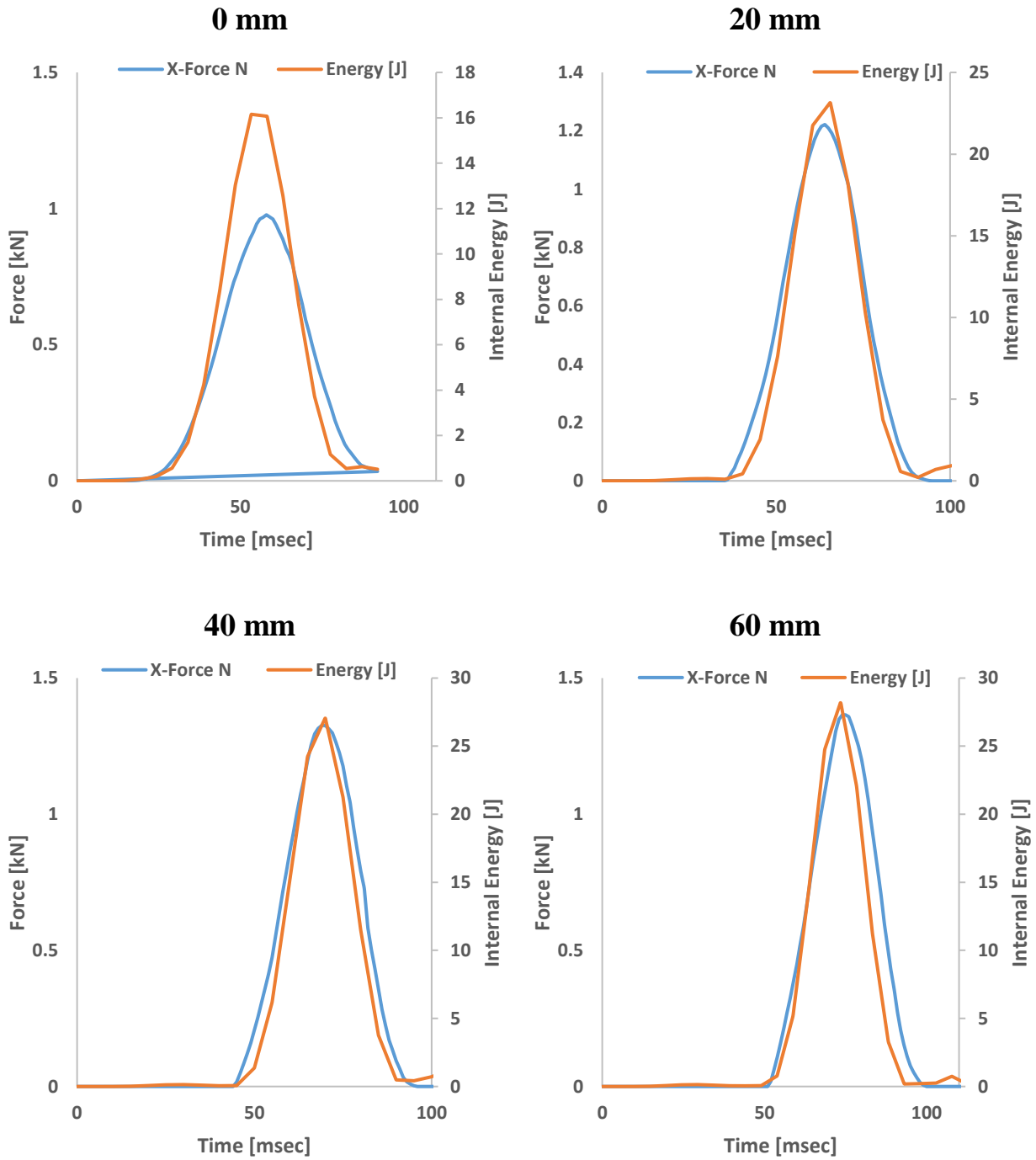
71. Schmitt, K.-U., M.H. Muser, and P. Niederer, *Evaluation of a new visco-elastic foam for automotive applications*. International journal of crashworthiness, 2003. **8**(2): p. 169-177.
72. Özdemir, M., S.K. İder, and M.İ. Gökler, *Parametric analysis of an anti-whiplash system composed of a seat suspension arrangement*. Journal of the Brazilian Society of Mechanical Sciences and Engineering, 2015. **37**(2): p. 777-784.
73. Kitagawa, Y., T. Yasuki, and J. Hasegawa. *Consideration of possible indicators for whiplash injury assessment and examination of seat design parameters using human FE model*. in *20th International Conference of the Enhanced Safety of Vehicles (ESV)*, Lyon, France. 2007.
74. Carter, P.R. and V.K. Maker, *Changing paradigms of seat belt and air bag injuries: what we have learned in the past 3 decades*. Journal of the American College of Surgeons, 2010. **210**(2): p. 240-252.
75. Kumar, S., et al., *The effect of seat belt use on the cervical electromyogram response to whiplash-type impacts*. Journal of manipulative and physiological therapeutics, 2006. **29**(2): p. 115-125.
76. Claytor, B., et al., *Cervical spine injury and restraint system use in motor vehicle collisions*. Spine, 2004. **29**(4): p. 386-389.
77. Kuska, T.C., *Air Bag Safety: An Update*. Journal of Emergency Nursing, 2016.
78. Potula, S., et al., *Investigating occupant safety through simulating the interaction between side curtain airbag deployment and an out-of-position occupant*. Accident Analysis & Prevention, 2012. **49**: p. 392-403.
79. Yang, H.-I., Y.-W. Yun, and G.-J. Park, *Design of a pedestrian protection airbag system using experiments*. Proceedings of the Institution of Mechanical Engineers, Part D: Journal of Automobile Engineering, 2015: p. 0954407015603854.
80. Anderson, R. and M. Baldock, *Vehicle improvements to reduce the number and severity of rear end crashes*. 2008: Centre for Automotive Safety Research.
81. Bener, A., et al., *Obesity index that better predict metabolic syndrome: body mass index, waist circumference, waist hip ratio, or waist height ratio*. Journal of obesity, 2013. **2013**.
82. Manna, D.R., et al., *Sustainable Markets: Case Study Of Toyota Motor Sales, USA, Inc*. Journal of Business Case Studies, 2011. **7**(3): p. 63.
83. Shimizu, K., *A maverick in the age of mega-mergers? Toyota's global strategies, in Globalization or Regionalization of the American and Asian Car Industry?* 2003, Springer. p. 119-143.

84. Yasuki, T. and Y. Yamamae, *Validation of kinematics and lower extremity injuries estimated by total human model for safety in SUV to pedestrian impact test*. Journal of Biomechanical Science and Engineering, 2010. **5**(4): p. 340-356.
85. Hallquist, J.O., *LS-DYNA theory manual*. Livermore software Technology corporation, 2006. **3**: p. 25-31.
86. LS-DYNA, L.-D., *LS-DYNA keyword User's Manual Version 971*. Lawrence Livermore Software Technology Corporation (CA), USA, 2014.
87. Iwamoto, M., et al. *Development of a finite element model of the total human model for safety (THUMS) and application to injury reconstruction*. in *Proceedings of the International Research Council on the Biomechanics of Injury conference*. 2002. International Research Council on Biomechanics of Injury.
88. Chawla, A., et al. *Validation of the cervical spine model in THUMS*. in *Proceedings of the 19th International Technical Conference on the Enhanced Safety of Vehicles Washington DC USA*. 2005.
89. CHAWLS, A., et al. *Validation of lower extremity model in THUMS*. in *Proceedings of The Ircobi-International Research Council On The Biomechanics Of Impact Conference Held September 2004, Graz, Austria*. 2004.
90. Segura, R., et al., *Real World Accident Reconstruction with the Total Human Model for Safety (THUMS) in Pam-Crash*. Berichte der Bundesanstalt fuer Strassenwesen. Unterreihe Fahrzeugtechnik, 2013(87).
91. Schinkel-Ivy, A., W.J. Altenhof, and D.M. Andrews, *Validation of a full body finite element model (THUMS) for running-type impacts to the lower extremity*. Computer methods in biomechanics and biomedical engineering, 2014. **17**(2): p. 137-148.
92. Poston, A., *Human engineering design data digest*. Washington, DC: Department of Defense Human Factors Engineering Technical Advisory Group, 2000.
93. De Vries, D., *Characterization of polymeric foams*. Eindhoven University of Technology, Eindhoven, 2009.
94. Ouellet, S., D. Cronin, and M. Worswick, *Compressive response of polymeric foams under quasi-static, medium and high strain rate conditions*. Polymer testing, 2006. **25**(6): p. 731-743.
95. Khaleghi, B., et al., *Multisensor data fusion: A review of the state-of-the-art*. Information Fusion, 2013. **14**(1): p. 28-44.
96. Kalawy, H., et al., *New objective findings after whiplash injuries: high blood flow in painful cervical soft tissue: an ultrasound pilot study*. Scandinavian Journal of Pain, 2013. **4**(4): p. 173-179.

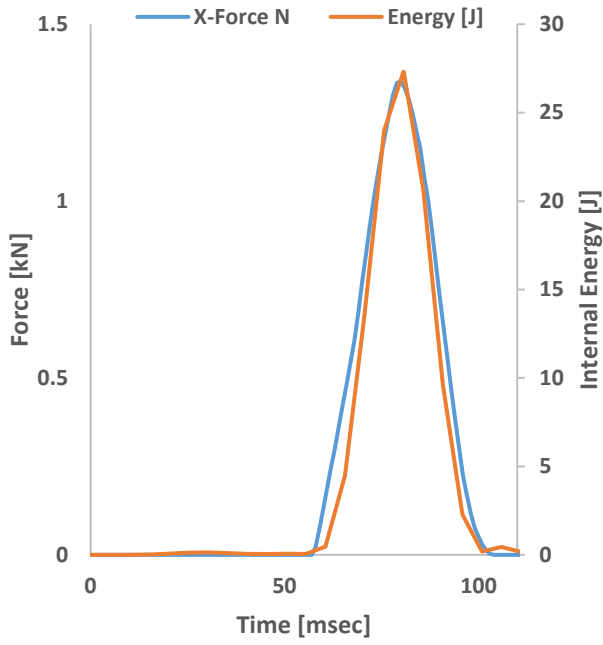
97. Jones, D.R. and M.F. Ashby, *Engineering materials 2: an introduction to microstructures, processing and design*. 2005: Butterworth-Heinemann.
98. Kleiven, S. and H. von Holst, *Consequences of head size following trauma to the human head*. *Journal of Biomechanics*, 2002. **35**(2): p. 153-160.
99. Qureshi, M.S., P. Swarnkar, and S. Gupta. *Assessment of DC servo motor with sliding mode control approach*. in *2016 IEEE First International Conference on Control, Measurement and Instrumentation (CMI)*. 2016. IEEE.
100. Fujita, Y., S. Sakurazawa, and K. Ito. *Response in Delayed Human Control System*. in *Studies in Perception and Action XIII: Eighteenth International Conference on Perception and Action*. 2015. Psychology Press.

APPENDIX A FINITE ELEMENT RESULTS DATA

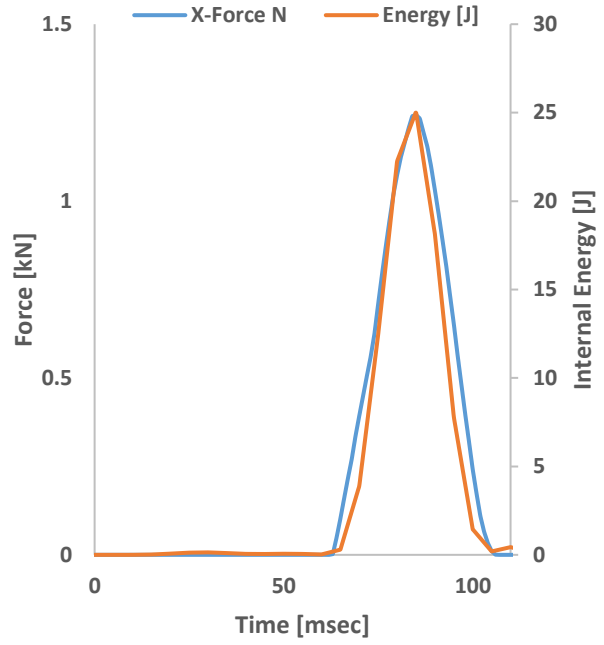
Energy Absorption and Applied Force on Head-Restraint



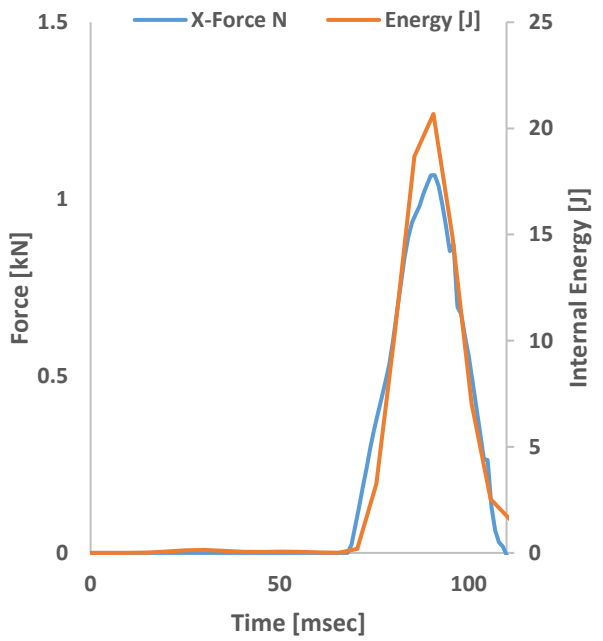
80 mm



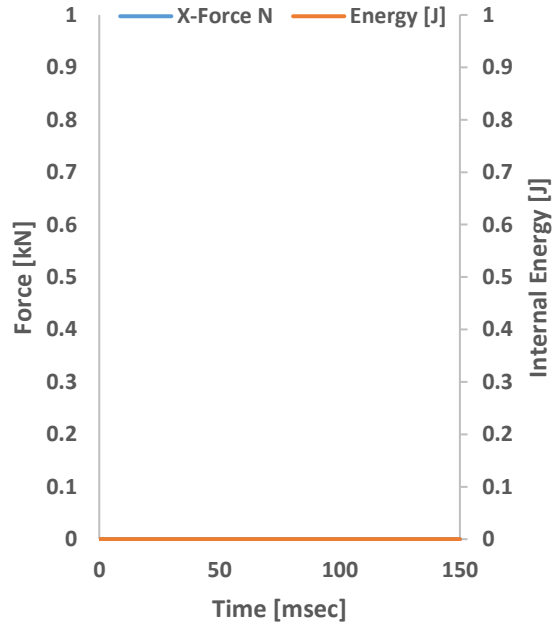
100 mm



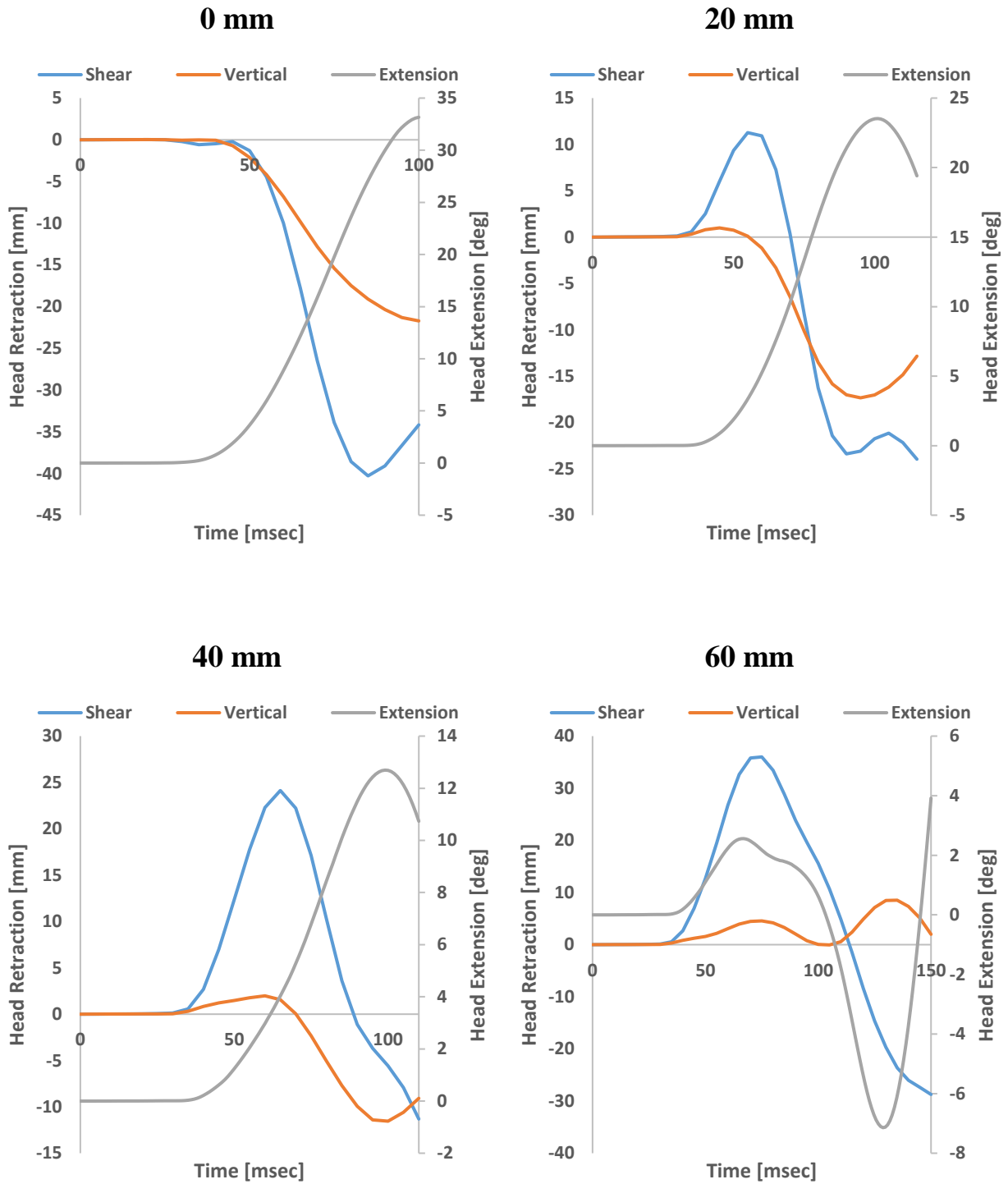
120 mm



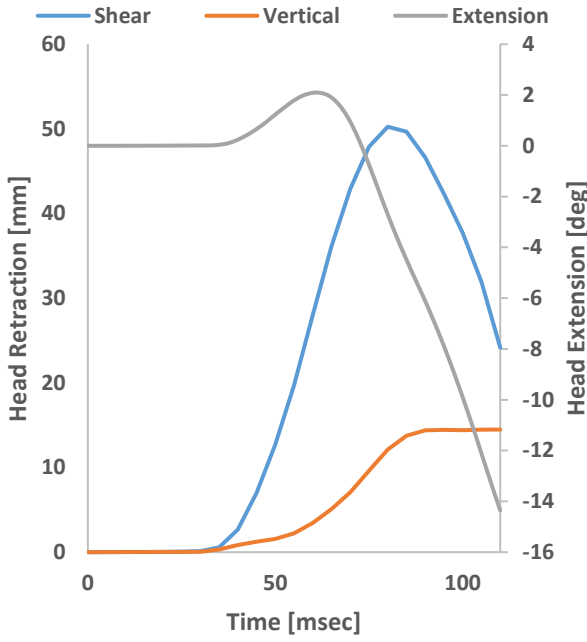
140 mm



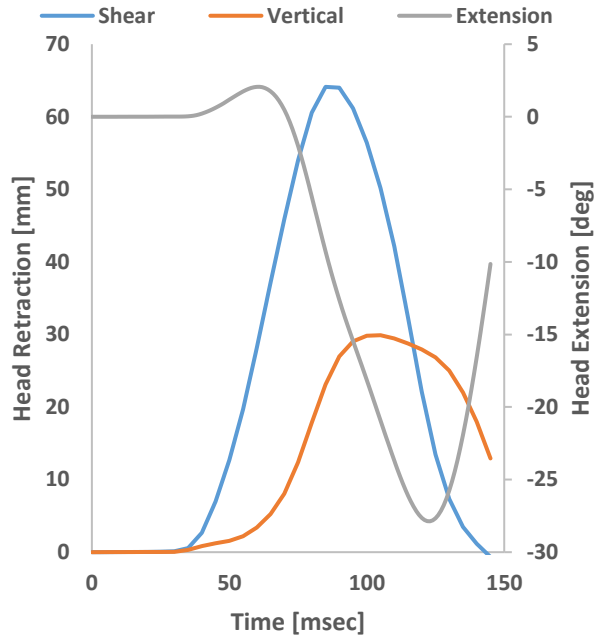
Head Extension, Shear Displacement, and Vertical Displacement



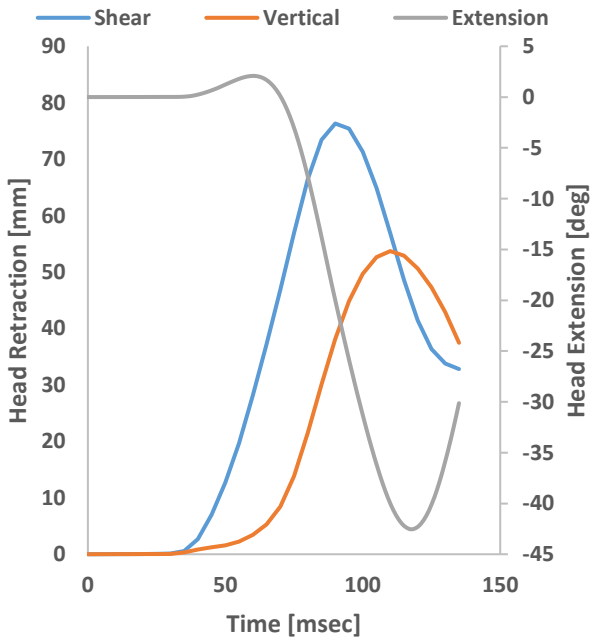
80 mm



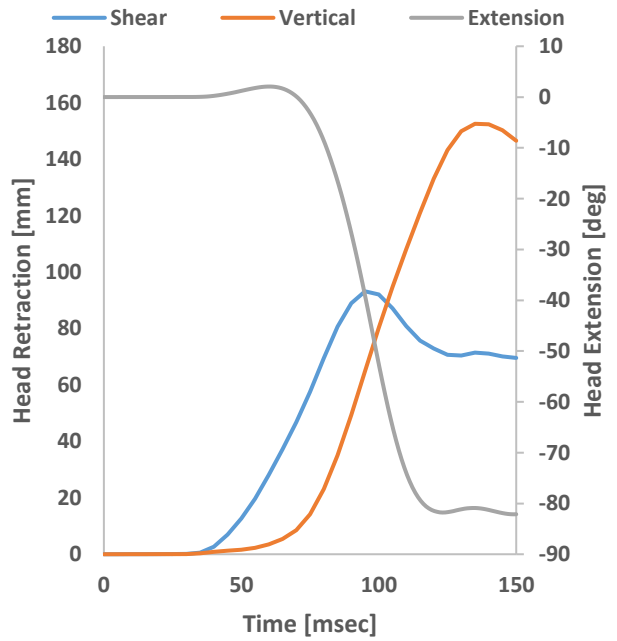
100 mm



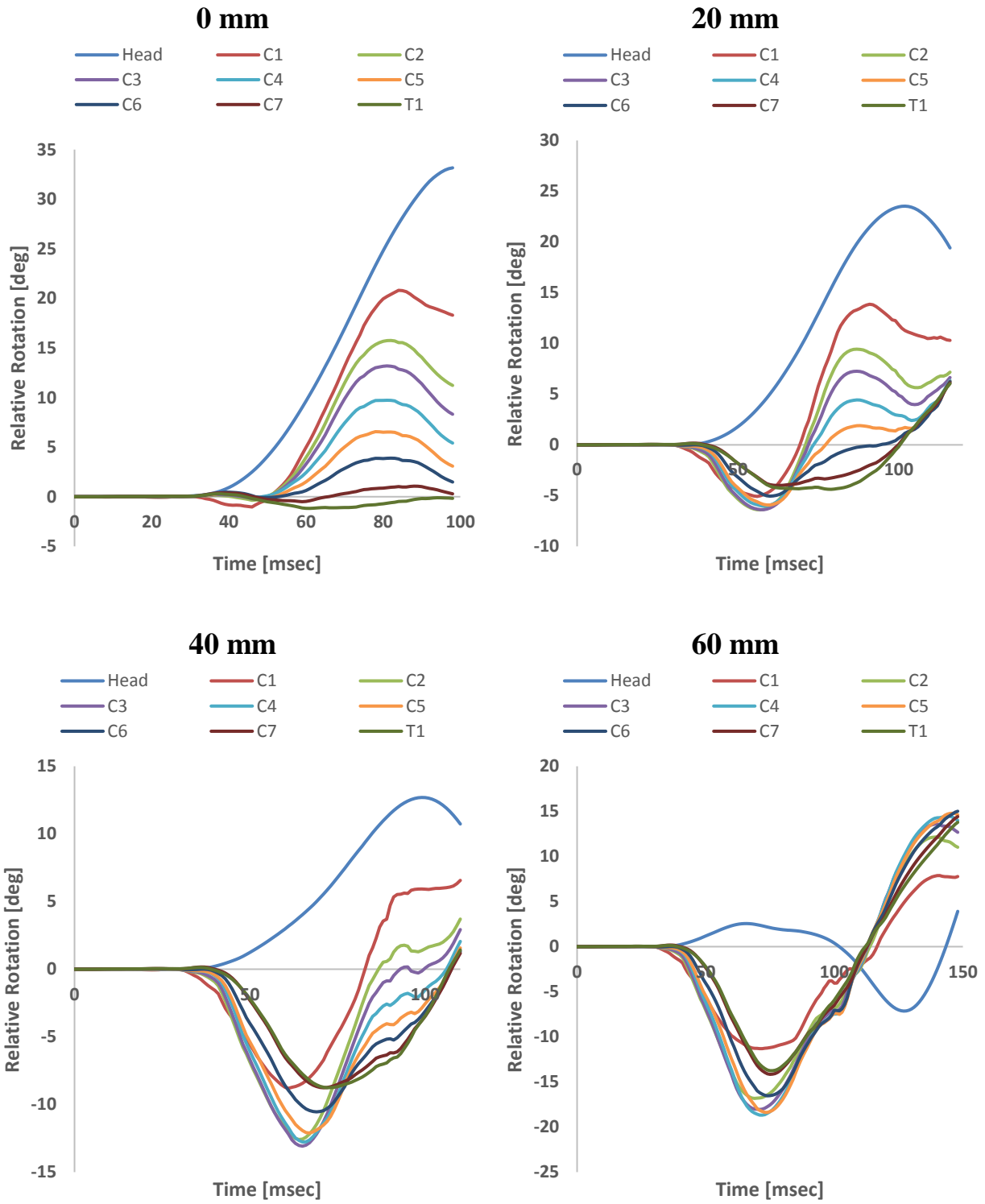
120 mm

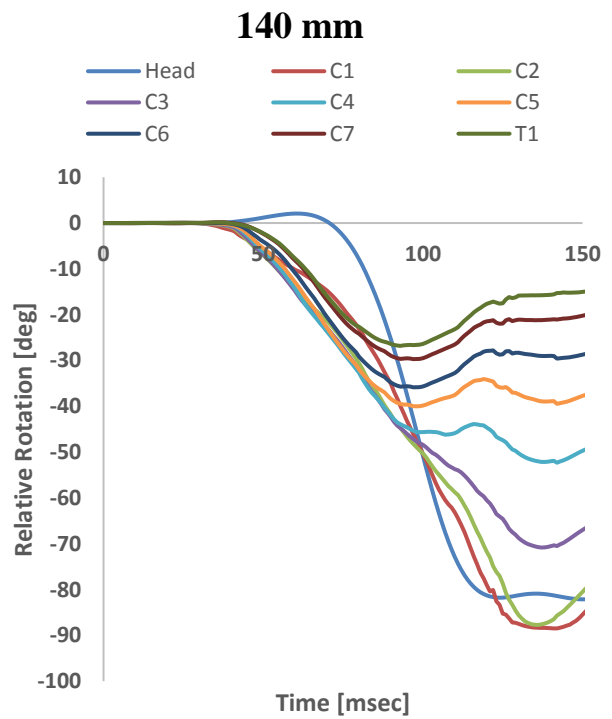
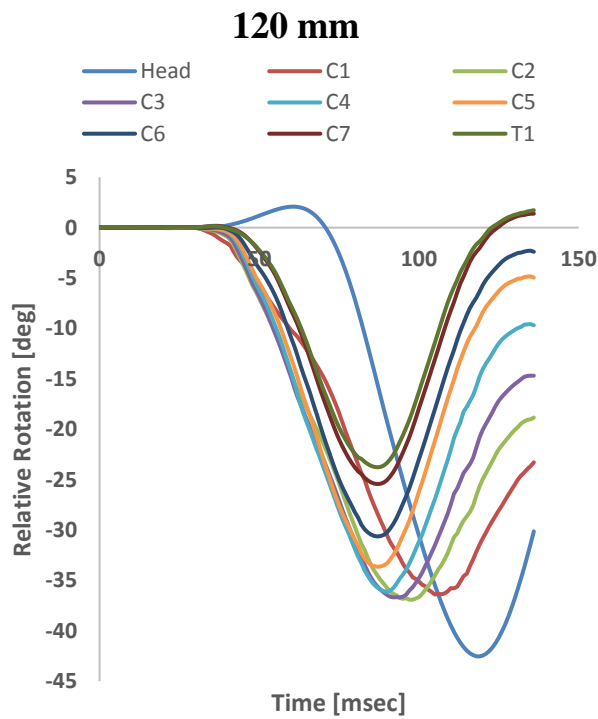
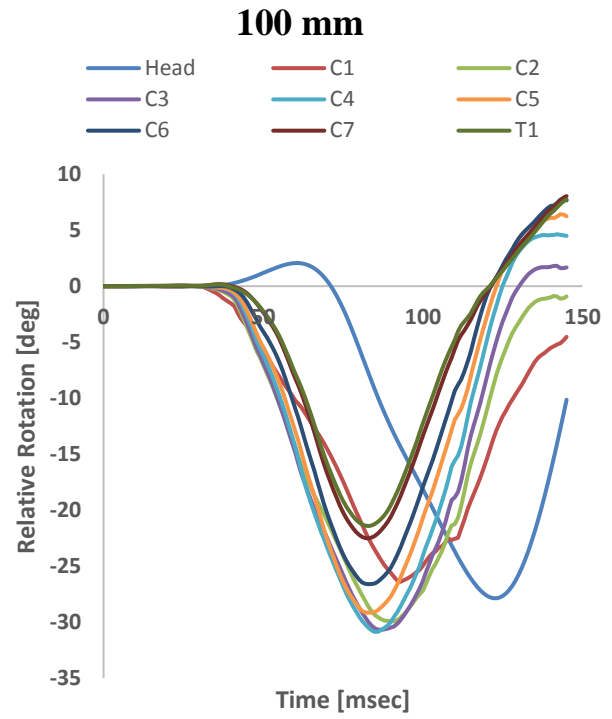
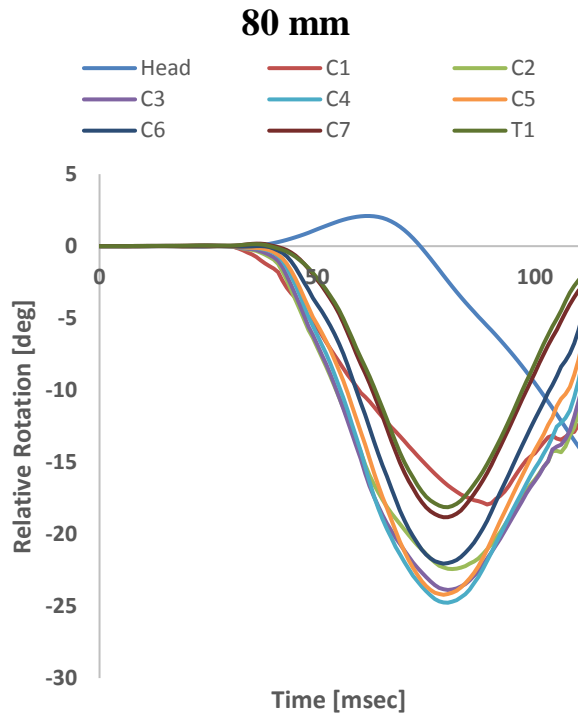


140 mm

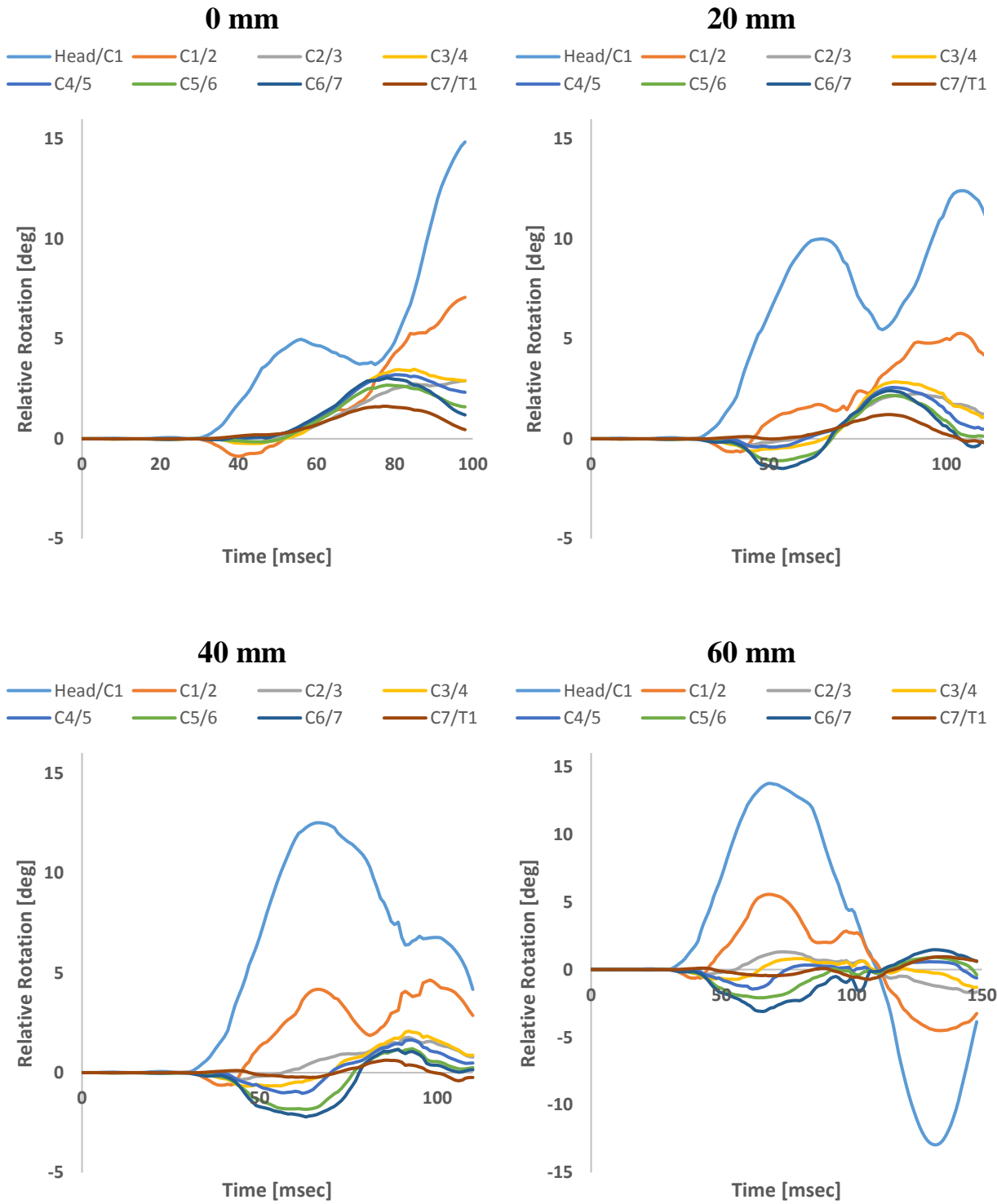


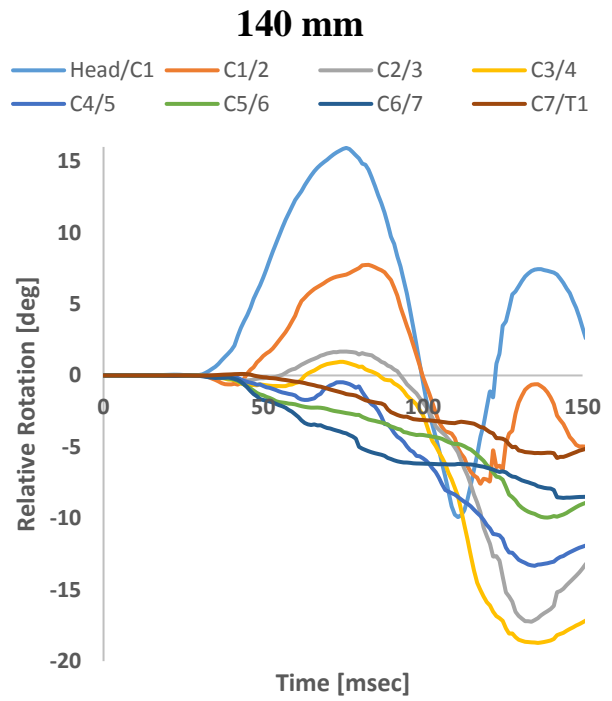
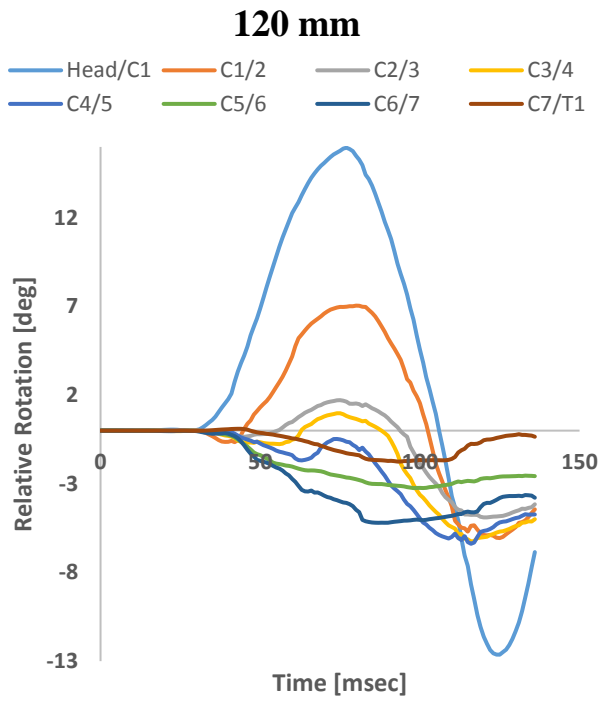
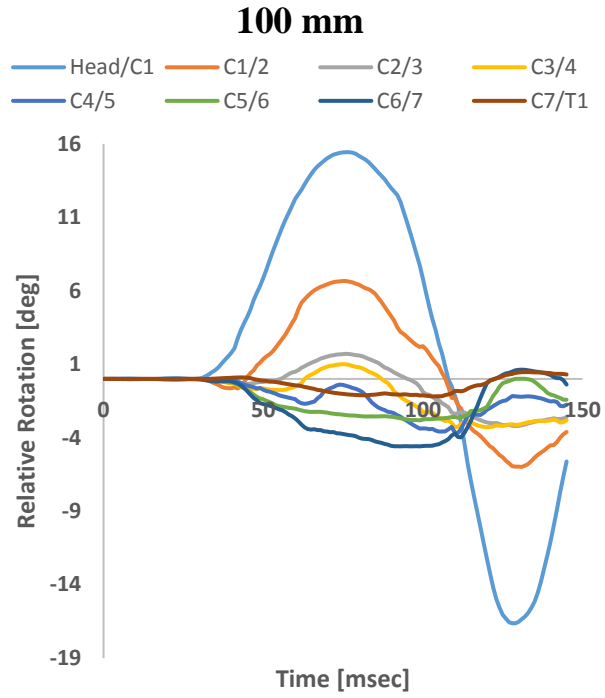
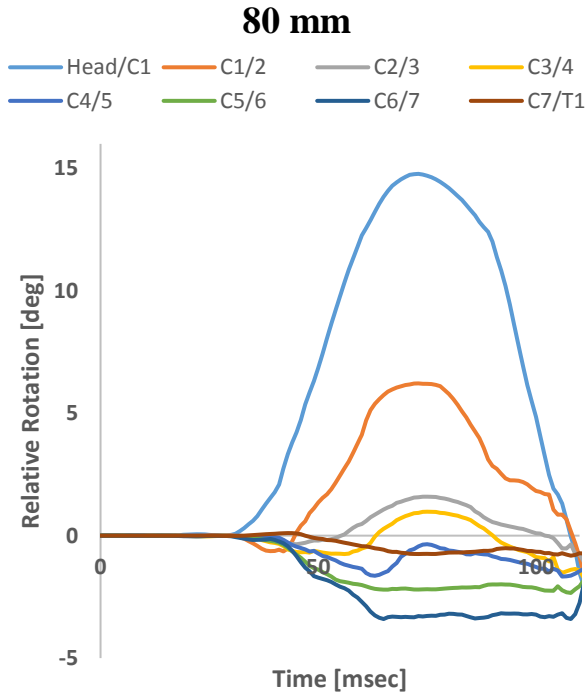
Vertebrae Rotational Displacements



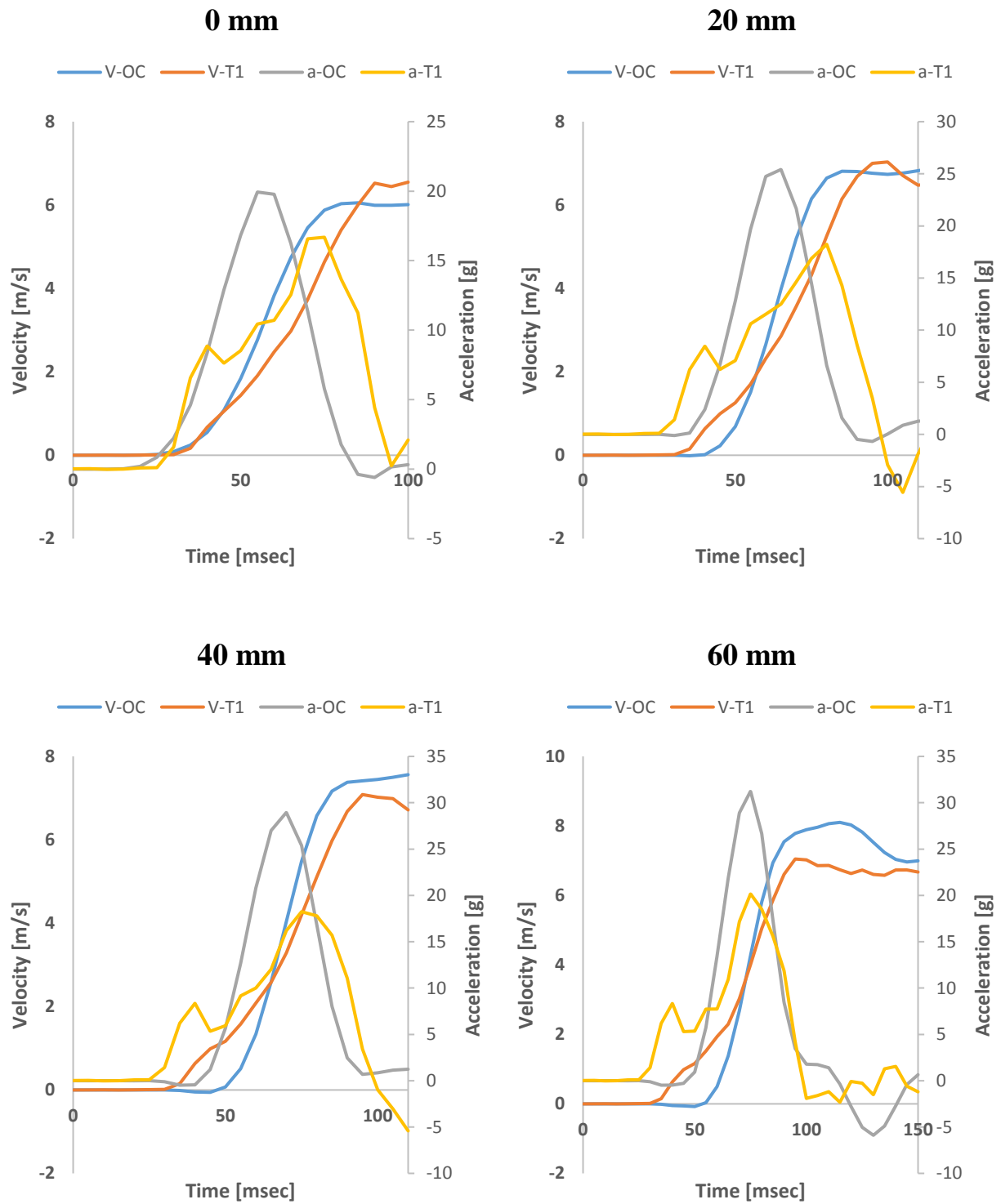


Relative Segmental Angular Displacements

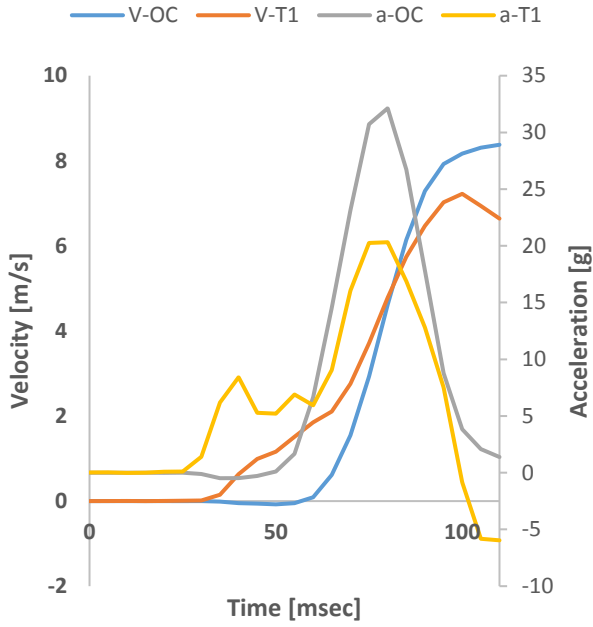




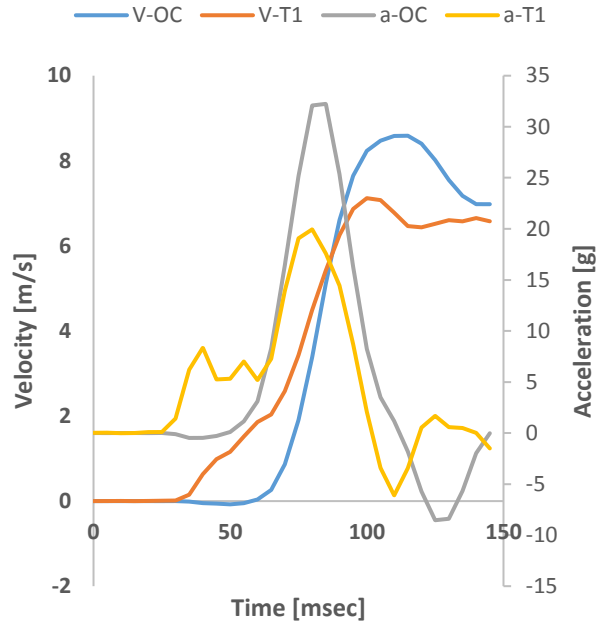
Velocity and Acceleration of the Occipital Condyle (OC) and First Thoracic Vertebrae (T1)



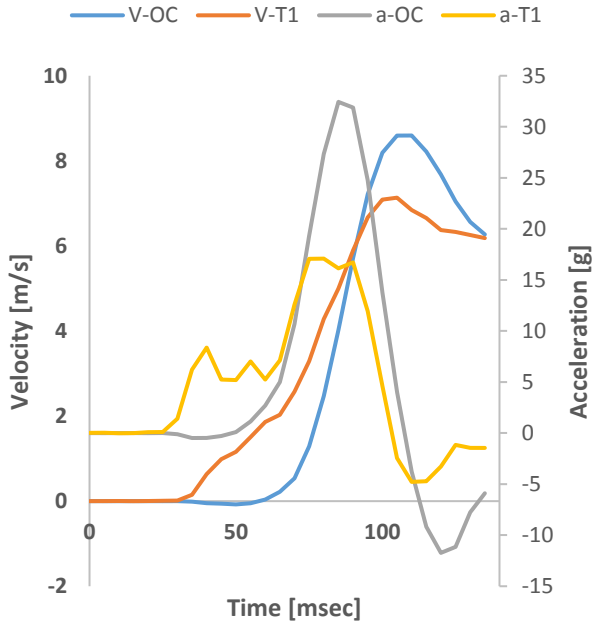
80 mm



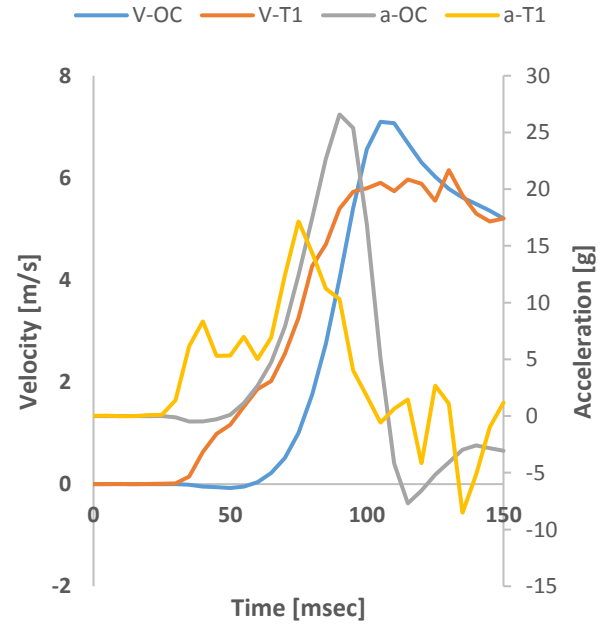
100 mm



120 mm

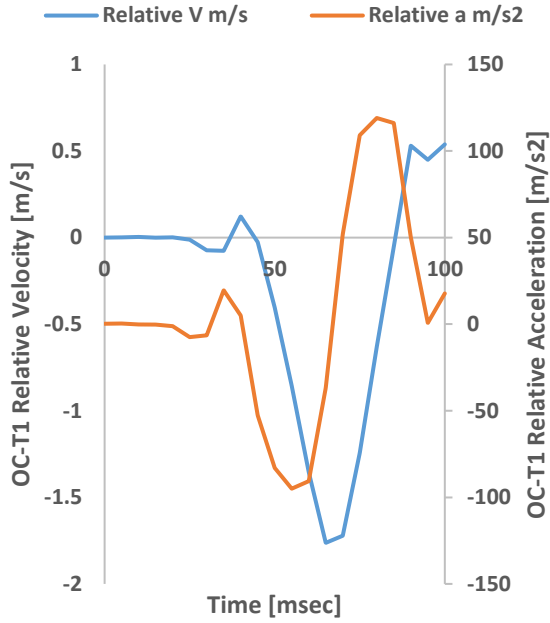


140 mm

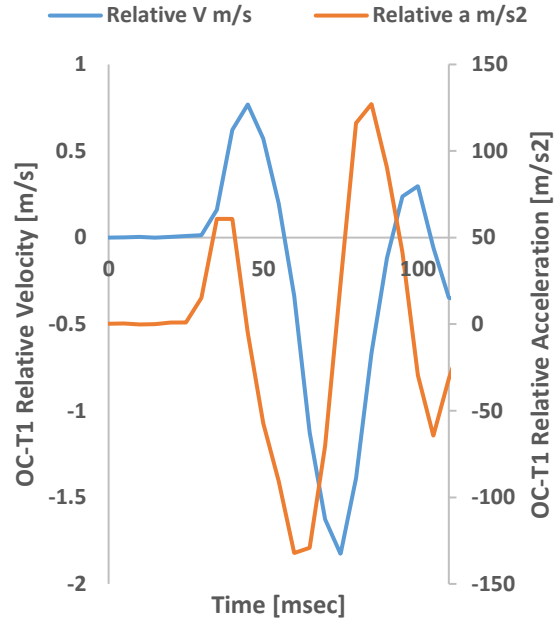


Relative Velocity and Acceleration Between OC and T1

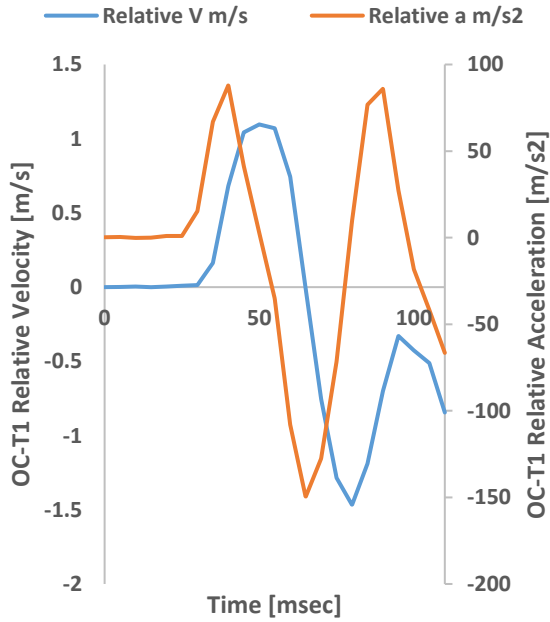
0 mm



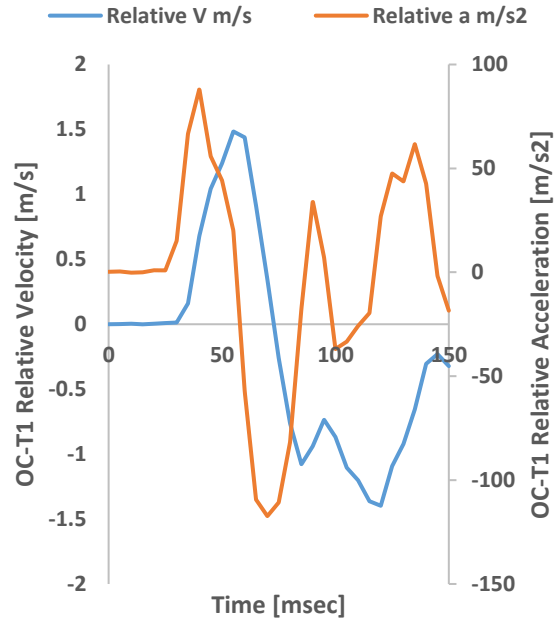
20 mm



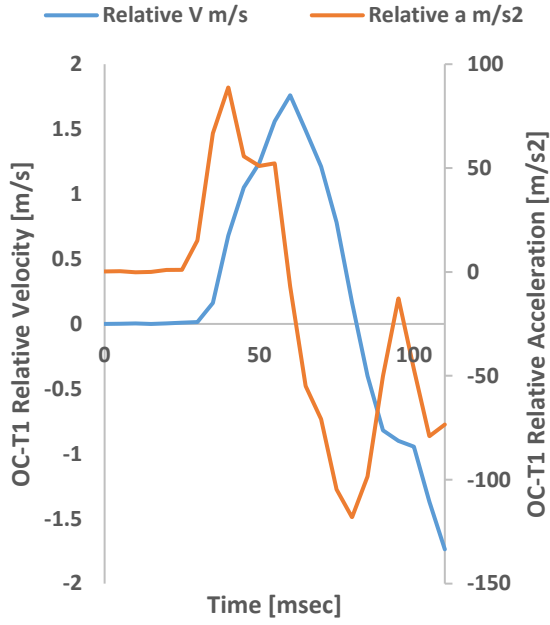
40 mm



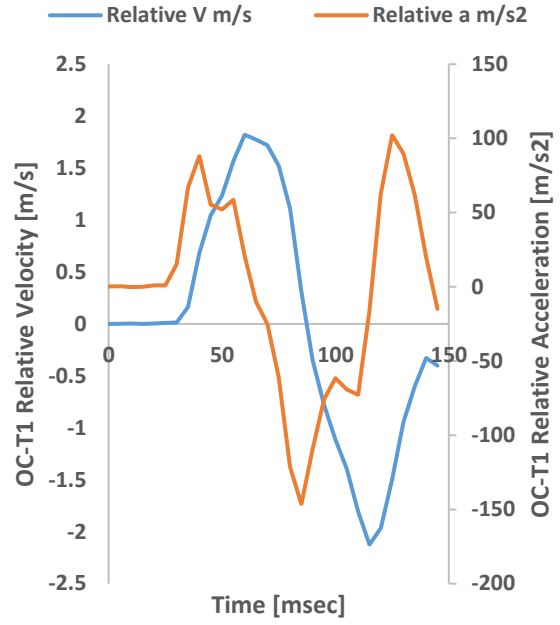
60 mm



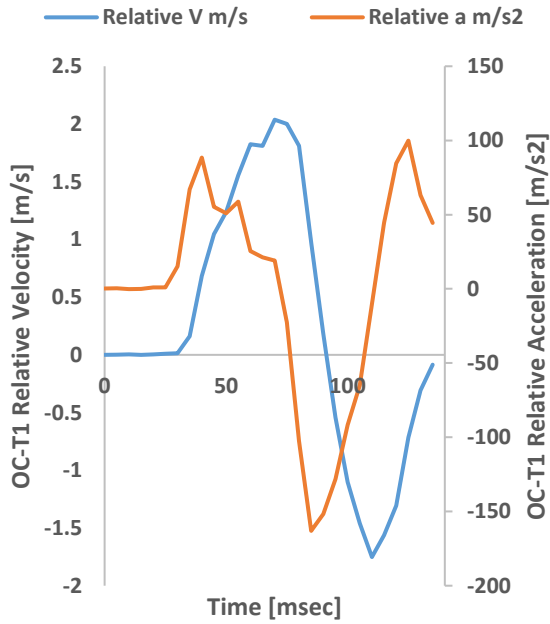
80 mm



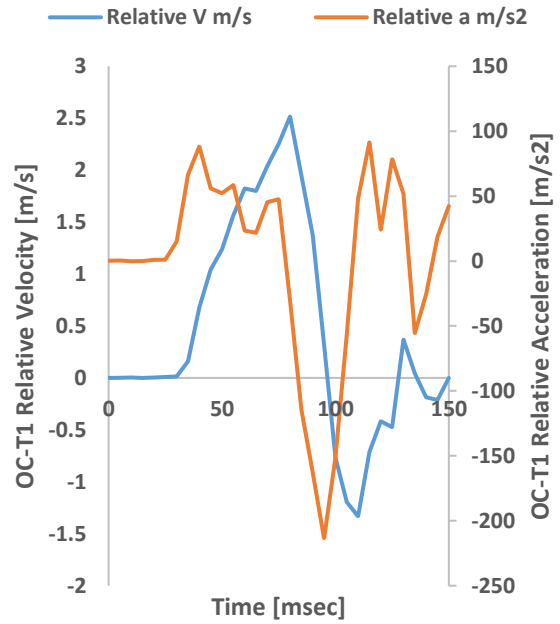
100 mm



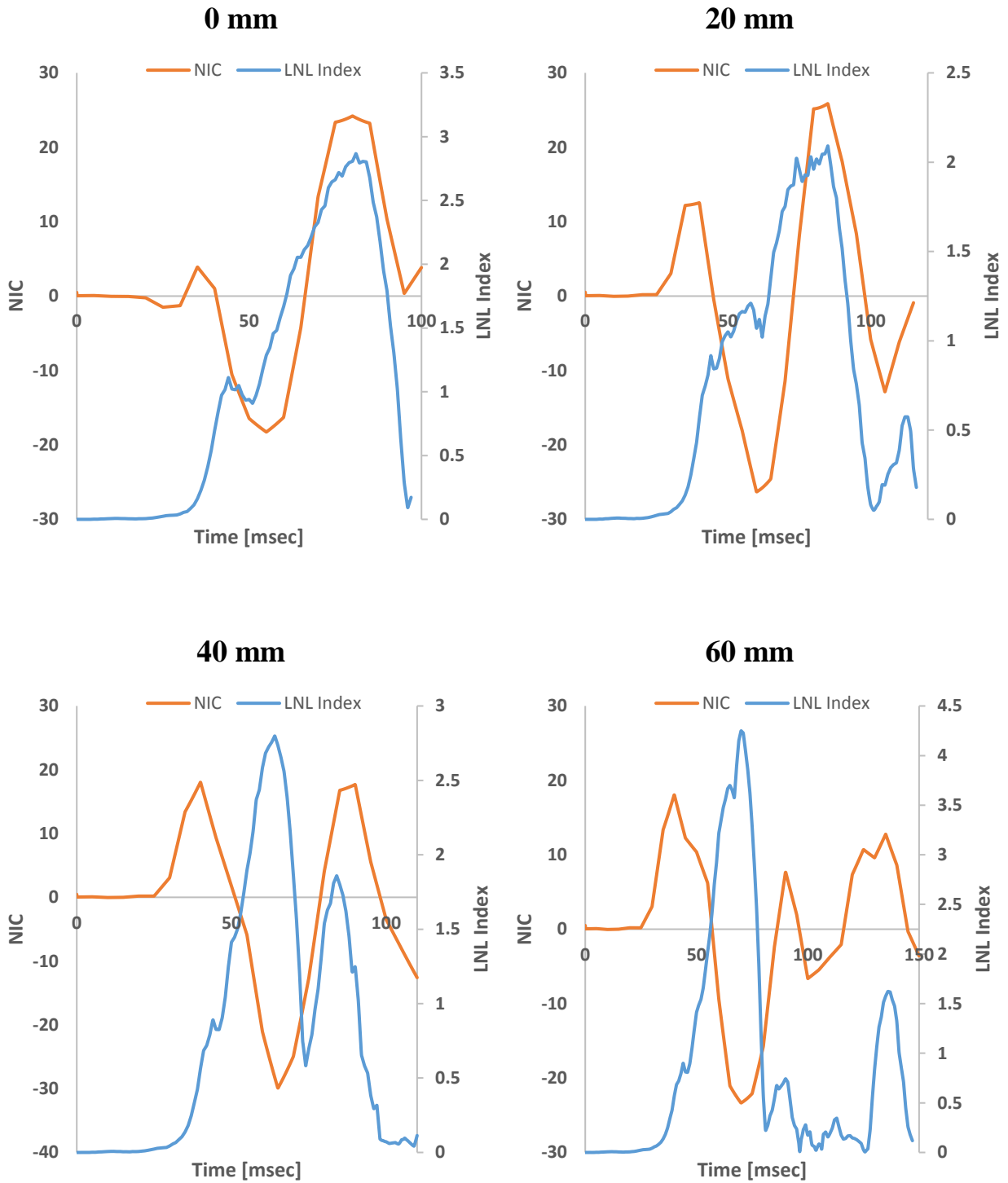
120 mm



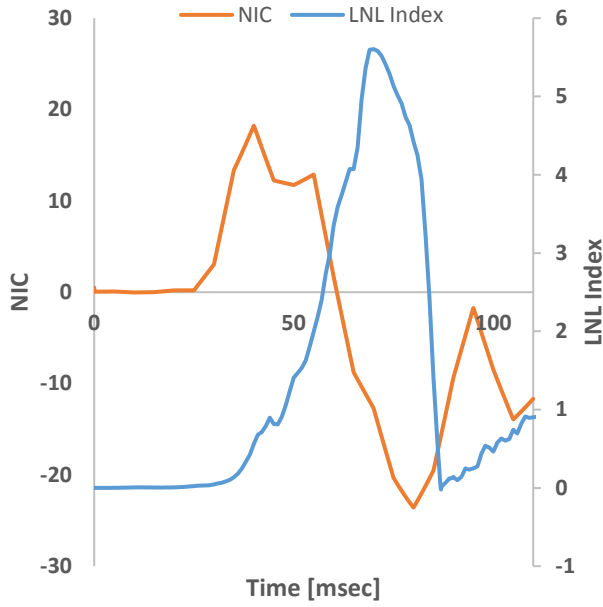
140 mm



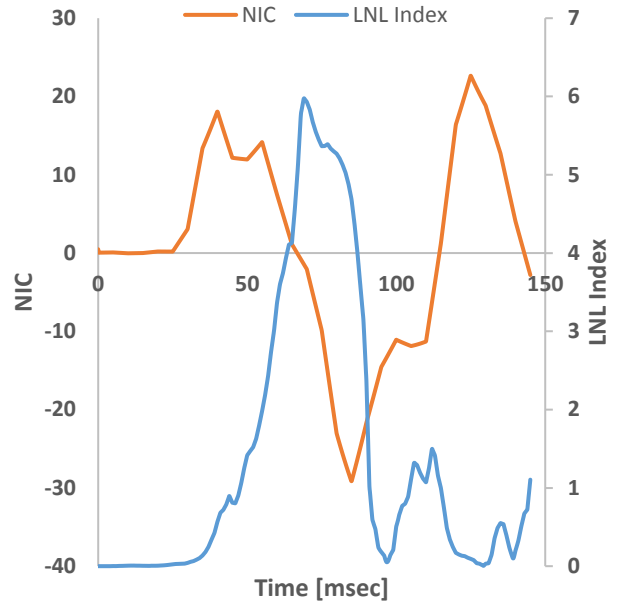
NIC and LNL Injury Assessments



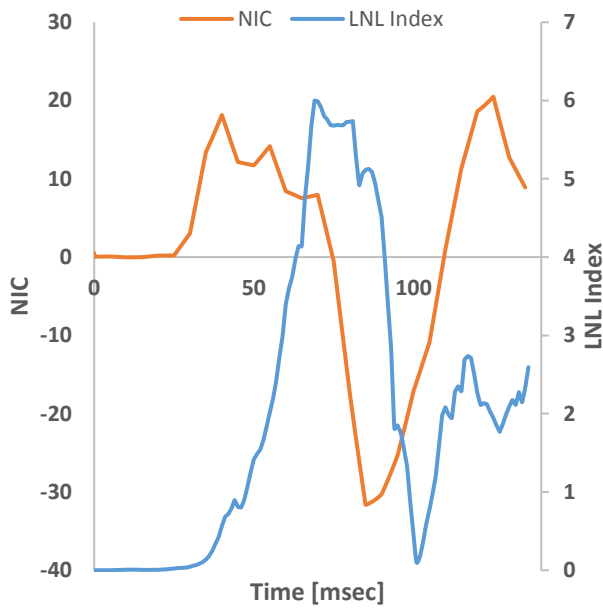
80 mm



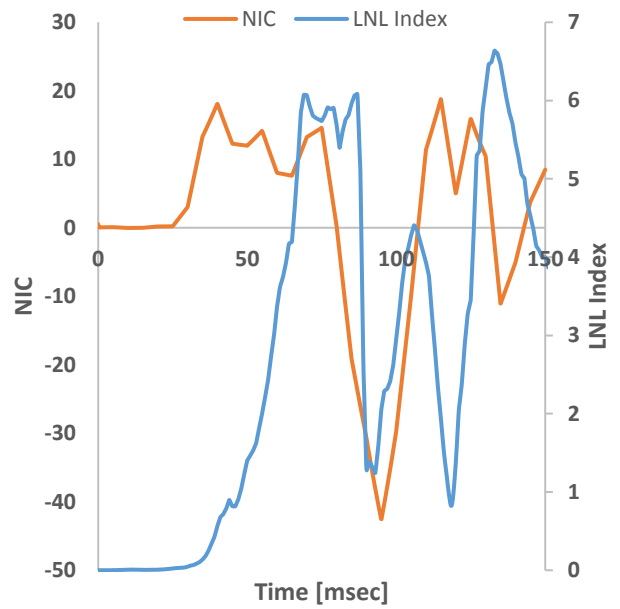
100 mm



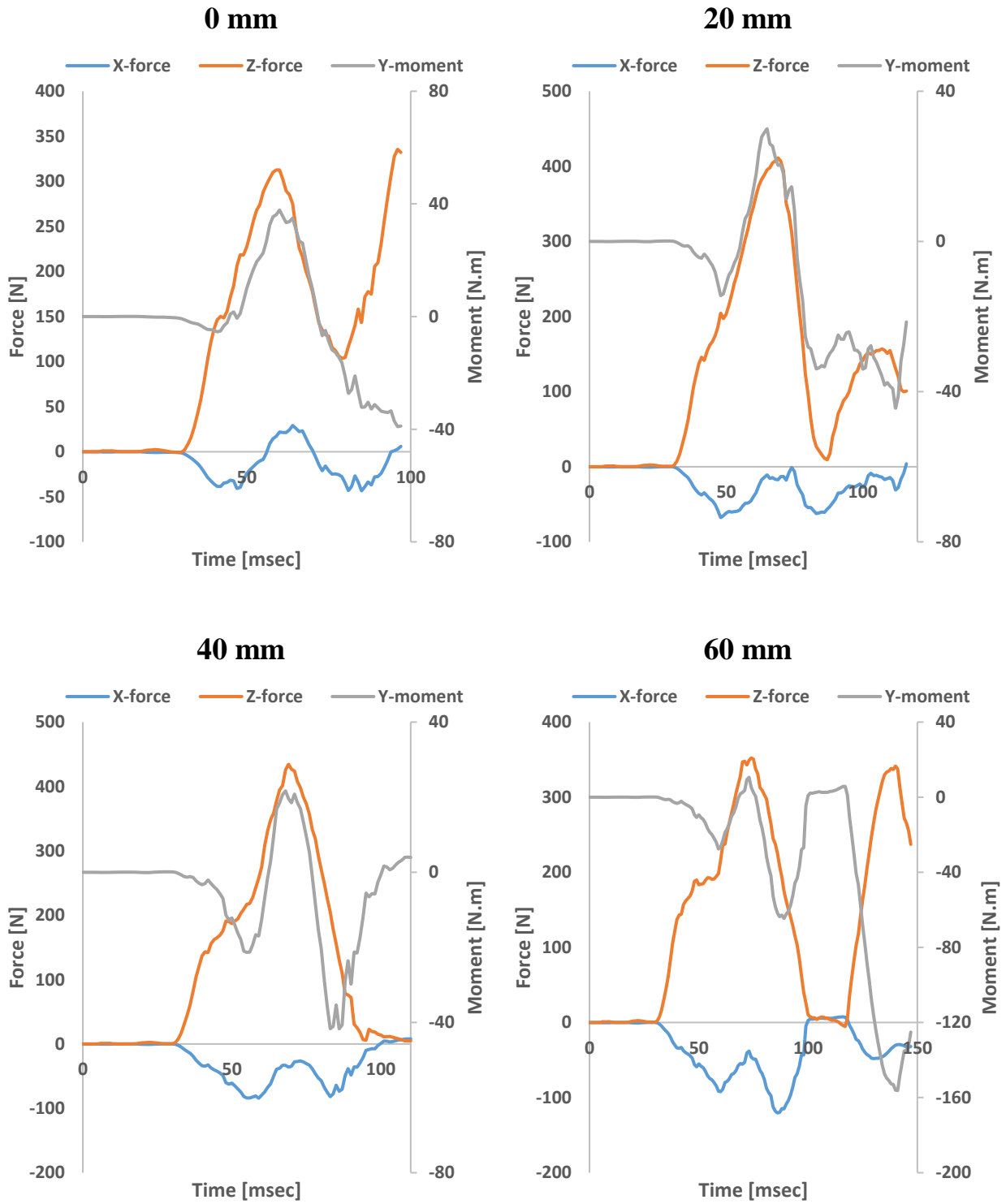
120 mm



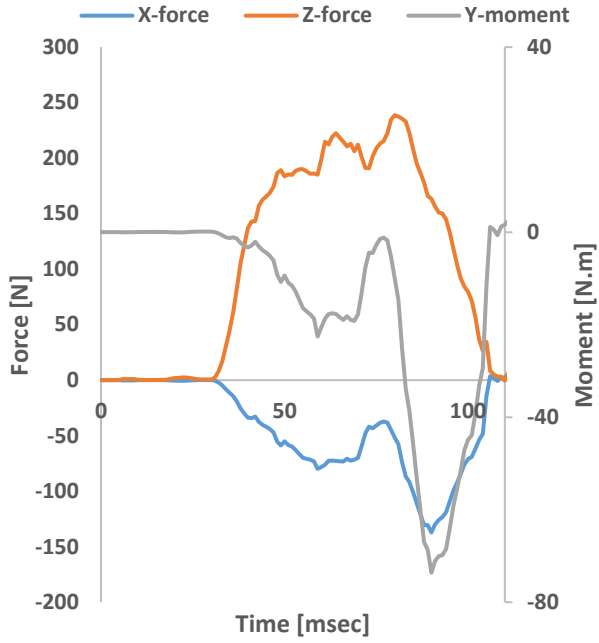
140 mm



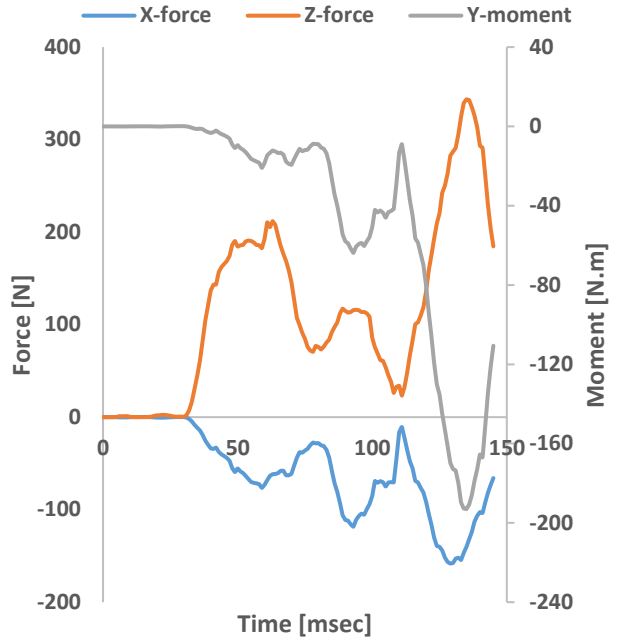
Loadings and Moments at the Occipital Condyle (OC)



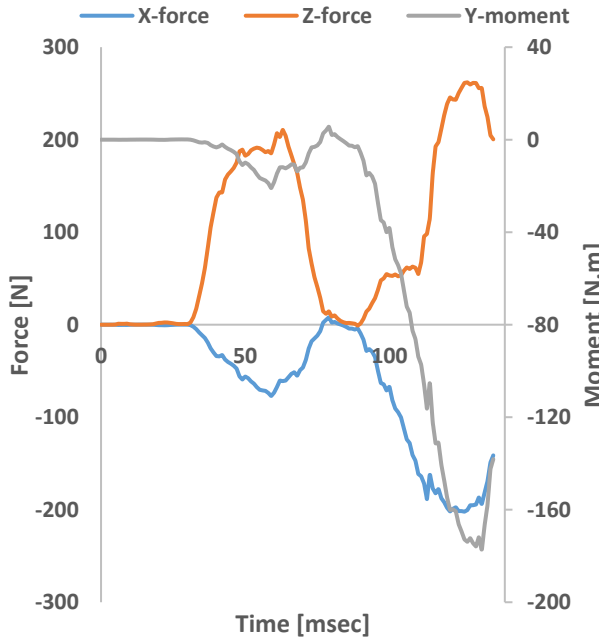
80 mm



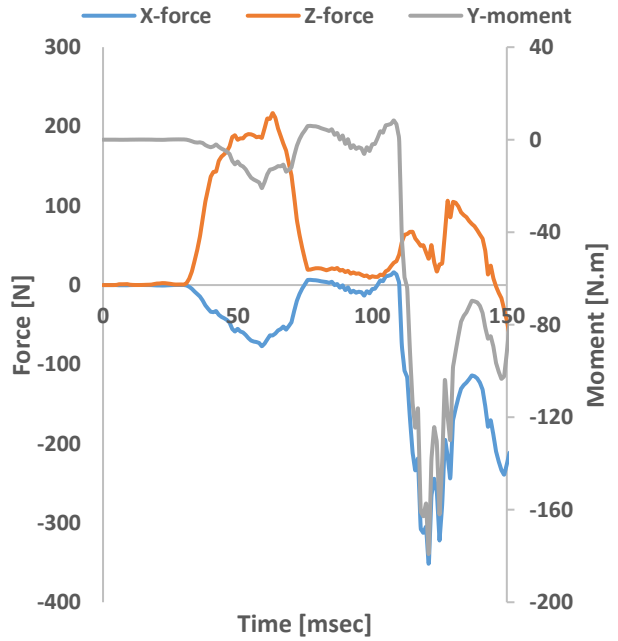
100 mm



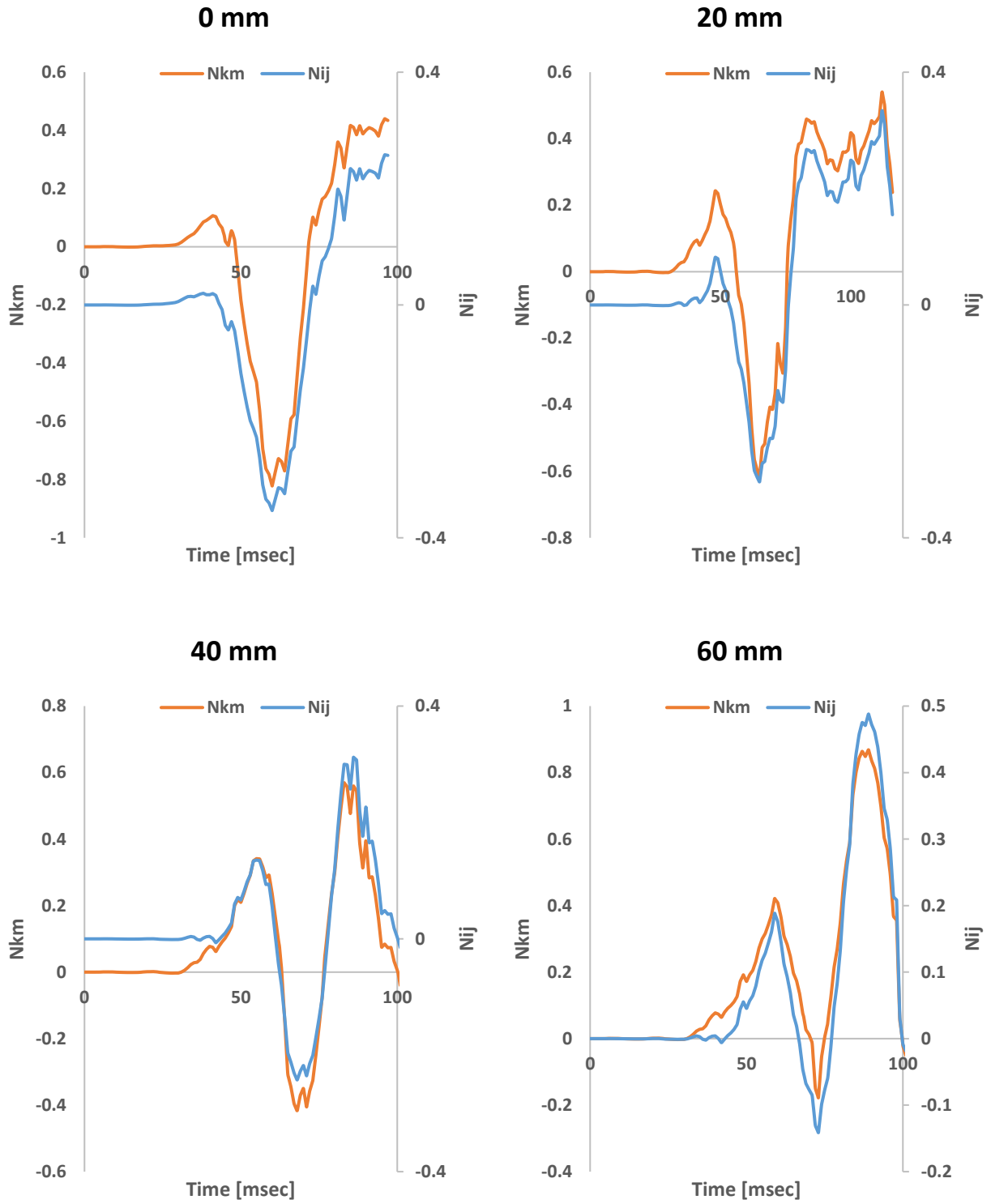
120 mm



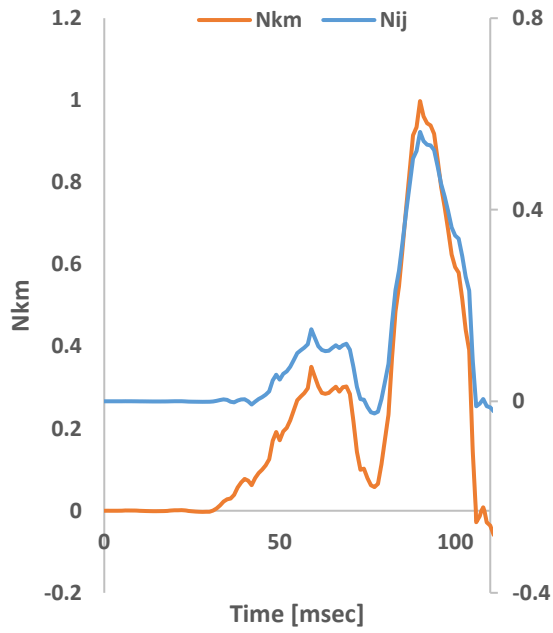
140 mm



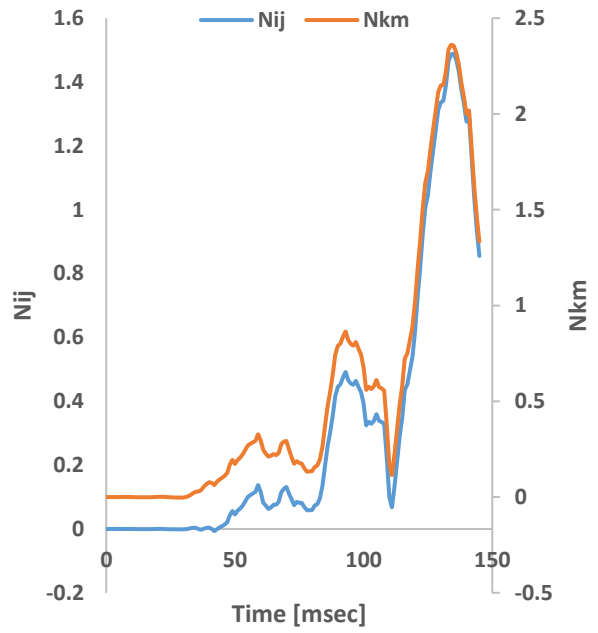
Nij and Nkm Injury Assessments



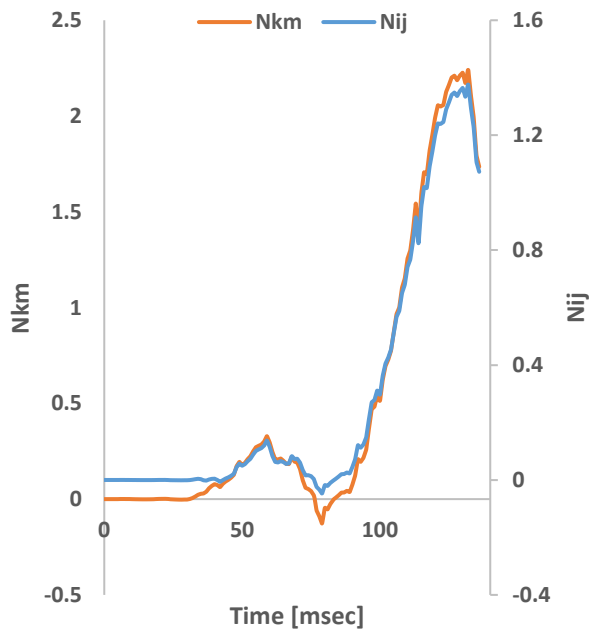
80 mm



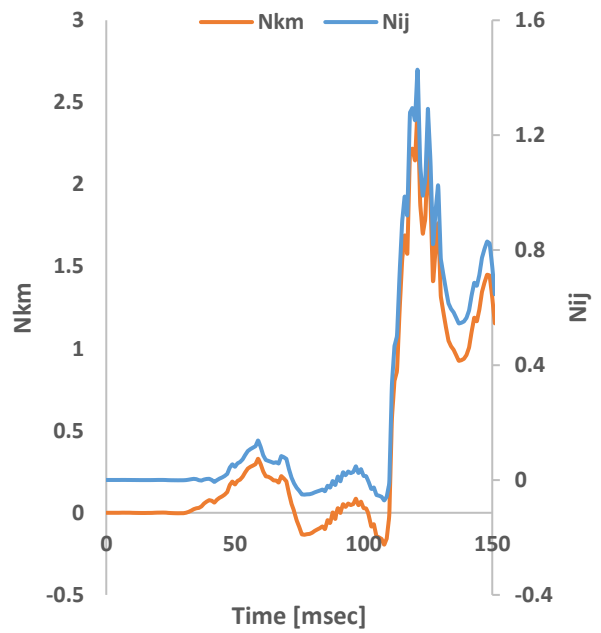
100 mm



120 mm

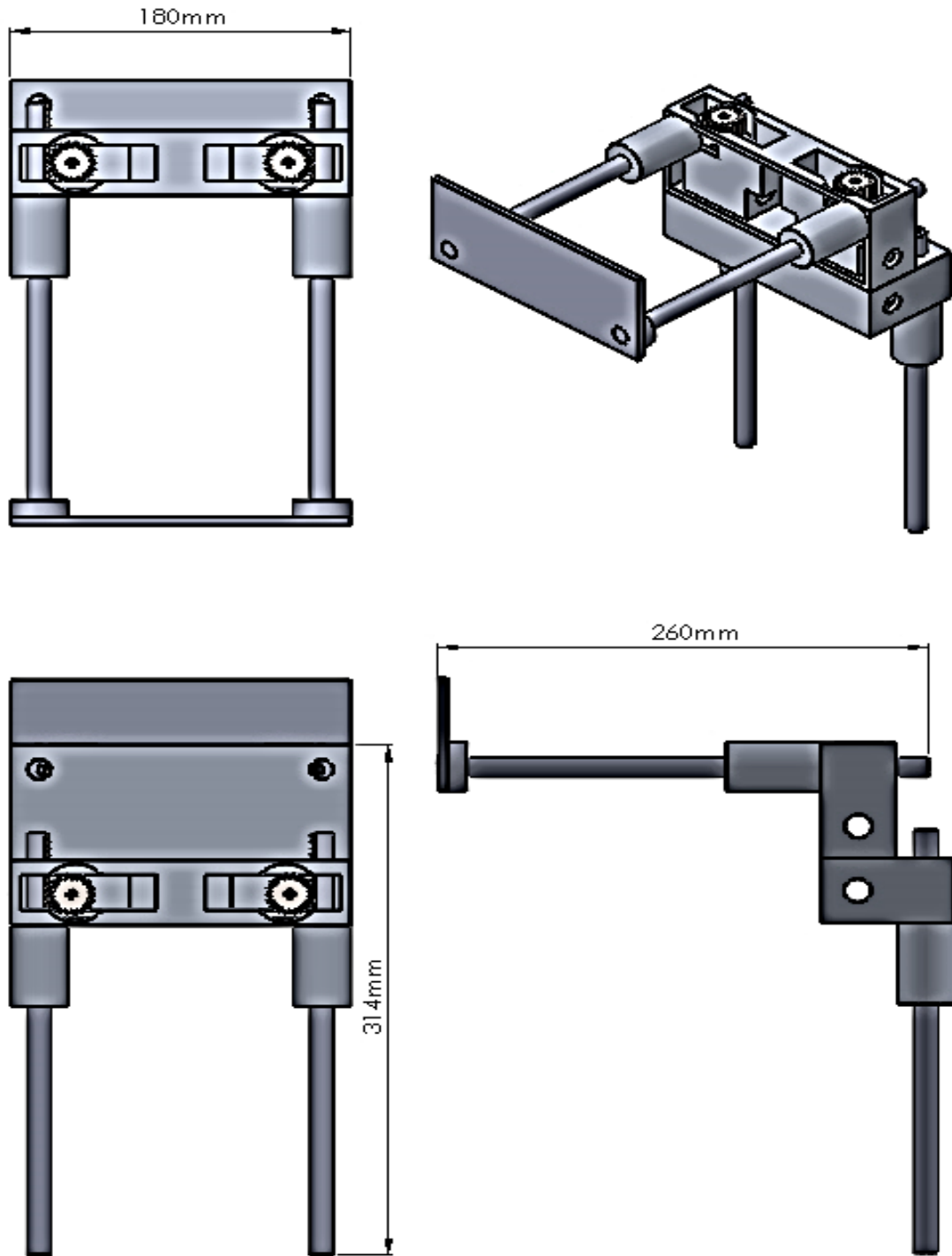


140 mm

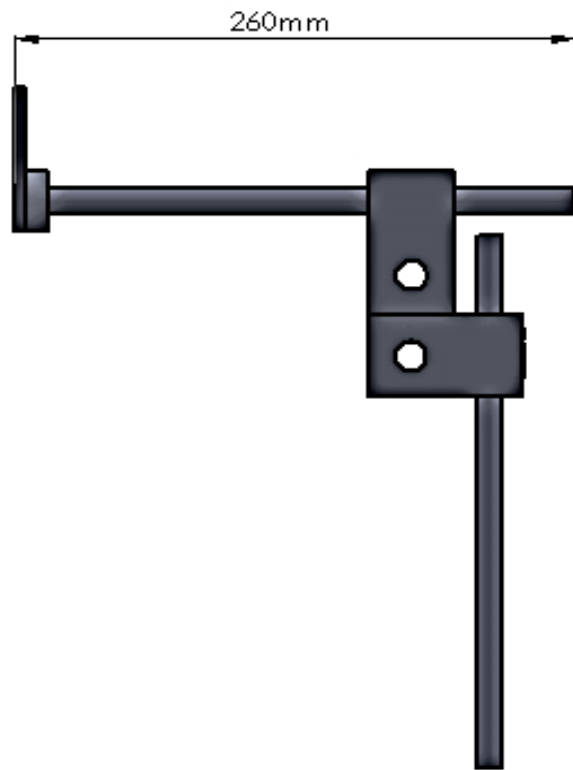
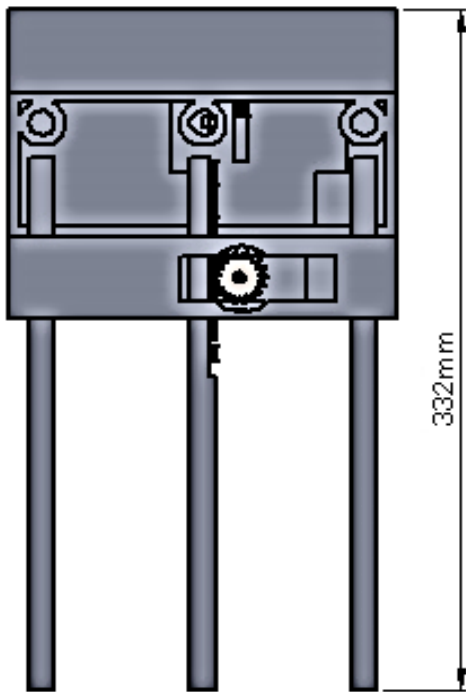
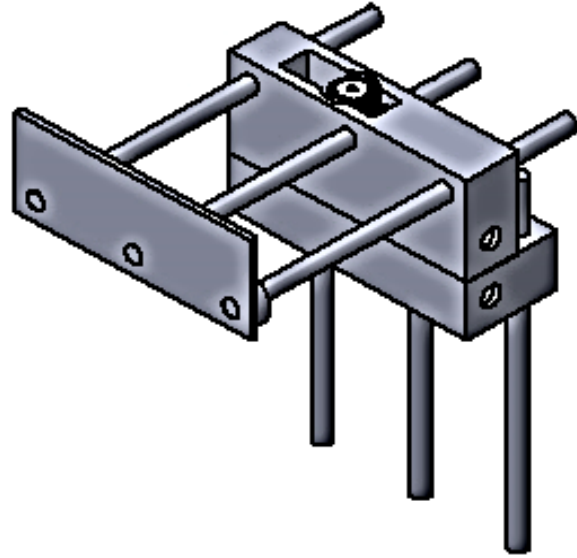
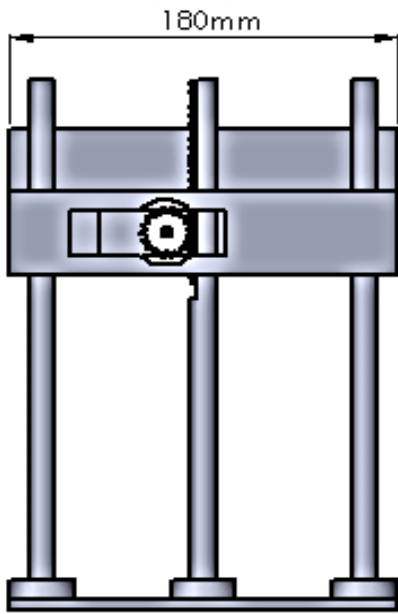


APPENDIX B T-HR PROTOTYPE VIEWS

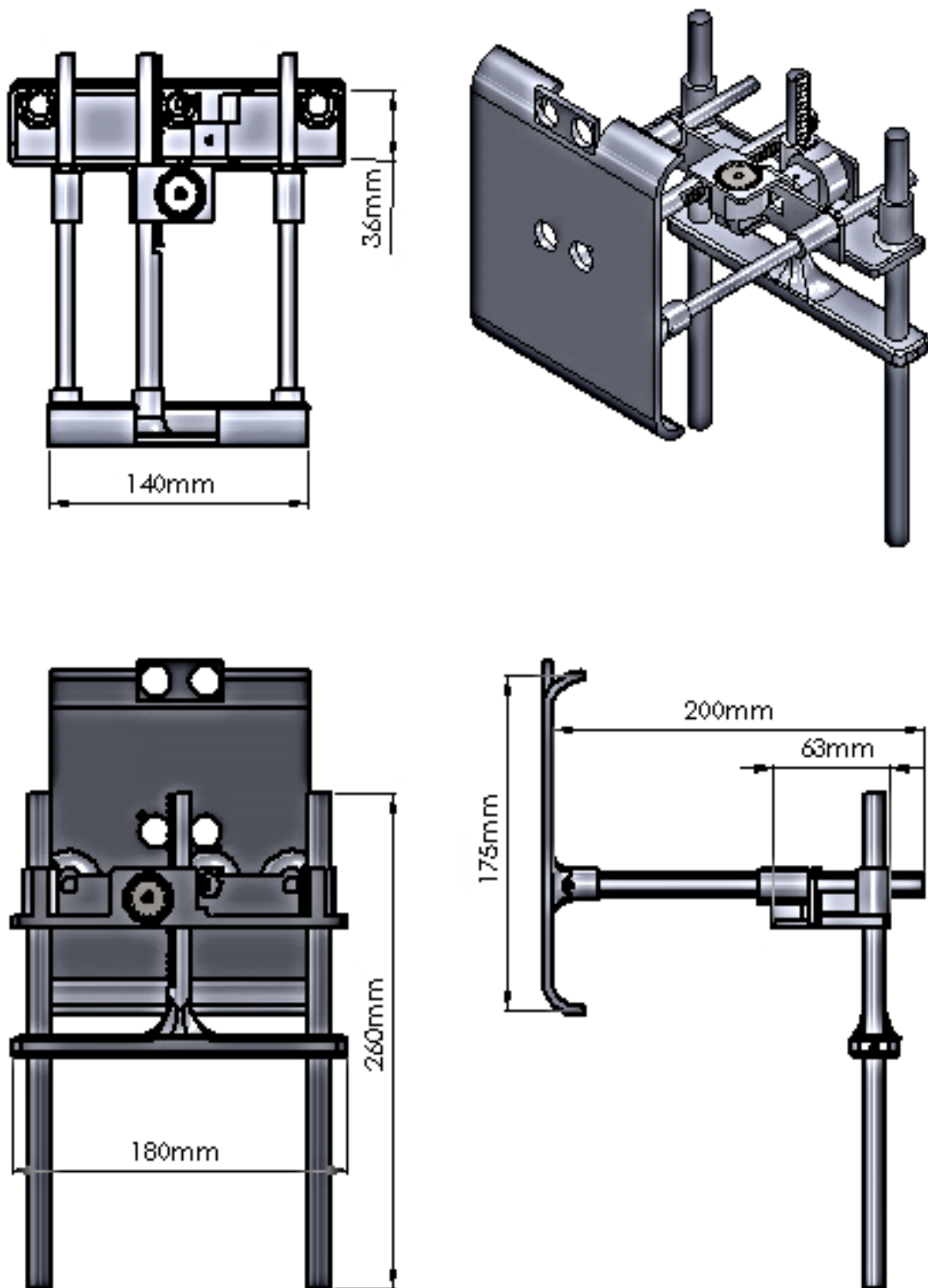
Isometric, Front, Side, and Top Views of the First T-HR Prototype



Isometric, Front, Side, and Top Views of The Second T-HR Prototype



Isometric, Front, Side, and Top Views of The Third T-HR Prototype



APPENDIX C ARDUINO PROGRAM CODE

```
/*******
```

```
*/
```

```
* Master of Science, Mechanical Engineering  
* Tracking Head-Restraint System  
* Othman Abu Laban - 200909341  
* January 2017
```

```
*/
```

```
/* List of Abbreviations:
```

```
* Vertical stands for Hight adjustment and given a sympol (V)  
* Horizontal stands for backset gap adjustment and given a sympol (H)  
* Vping is the pin for height adjusting Ping sensor  
* Hping is the pin for backset gap adjusting Ping sensor  
* H is the backset gap distance  
* V is the height  
* S is the status  
* E1 is the height adjusting motor  
* E2 is the backset gap adjusting motor  
* I1, I2, I3, I4 are used for controlling motor directions through H-bridge ship
```

```
*/
```

```
/* Distance detecting circuit :
```

```
* pin 2 is connected to start & end button  
* pin 3 is connected to Vping  
* pin 4 is connected to Hping  
* pin 5 is connected to vertical limit switch  
* pin 6 is connected to horizontal limit switch  
* pin 8-10 is connected Vmotor  
* pin 11-13 is connected Hmotor  
* The Top level of the headrest must be above occupant's head  
* The Backset gap distance must be maintained within 40 mm
```

```
*/
```

```
/* LCD circuit:
```

```
* LCD RS pin to digital pin A0  
* LCD Enable pin to digital pin A1  
* LCD D4 pin to digital pin A2  
* LCD D5 pin to digital pin A3  
* LCD D6 pin to digital pin A4  
* LCD D7 pin to digital pin A5  
* LCD R/W pin to ground
```

```
*/
```

```

/* List of functions:
 * Hscan() function for measuring H
 * Vscan() function for measuring V
 */

//*****
#include <LiquidCrystal.h>
LiquidCrystal lcd(A0,A1,A2,A3,A4,A5);           // Define pins for LCD screen

double V, H;                                  // Define Hight and backset gap, and status
int state=0, H_limit=0;                       // Process status and horizontal limit switch status
long duration;

#define buttonPin 2
#define Vping 3
#define Hping 4
#define E1 11 // Enable Pin for motor 1
#define E2 10 // Enable Pin for motor 2
#define I1 13 // Control pin 1 for motor 1
#define I2 12 // Control pin 2 for motor 1
#define I3 9 // Control pin 1 for motor 2
#define I4 8 // Control pin 2 for motor 2

void setup() {
  Serial.begin(9600);                          // initialize serial communication
  lcd.begin(16, 2);                             // set up the LCD's number of columns and rows
  lcd.print("Welcome");
  Serial.print("Welcome");
  pinMode(buttonPin, INPUT);
  pinMode(5, INPUT);
  pinMode(6, INPUT);
  pinMode(E1, OUTPUT);
  pinMode(E2, OUTPUT);
  pinMode(I1, OUTPUT);
  pinMode(I2, OUTPUT);
  pinMode(I3, OUTPUT);
  pinMode(I4, OUTPUT);
  delay(2000);
  Serial.print("Press Button to Start");
}

void loop(){
  lcd.clear();
  lcd.print("Press Button");
  lcd.setCursor(0, 1);

```

```

    lcd.print("to Start");
    if (digitalRead(buttonPin) == HIGH) state = 1;

    while (state>0){
        Vscan(V);
        delay(100);
        Serial.print(V);
        while (V<50 && state==1){
            digitalWrite(E1, HIGH);           // Start vertical motor
            digitalWrite(I1, HIGH);
            digitalWrite(I2, LOW);
            Vscan(V);
            delay(100);
            lcd.clear();
            lcd.print("Adjusting hight");
            lcd.setCursor(0, 1);
            lcd.print(V);
            Serial.print("Adjusting hight  ");
            Serial.print(V);
            lcd.print(" cm");
            if (digitalRead(buttonPin) == HIGH) state = 0;
            if (digitalRead(5) == HIGH) state = 2;           // Vertical Limit switch stop
        }
        digitalWrite(E1, LOW);           // Stop vertical motor
        if (V>50) state = 2;
        Hscan(H);
        delay(100);
        Serial.print(H);
        if (digitalRead(6) == LOW) H_limit = 0;           // Horizontal Limit switch disengaged
        while (state==2 && H>4 && H_limit==0){
            digitalWrite(E2, HIGH);           // Start horizontal motor
            digitalWrite(I3, LOW);
            digitalWrite(I4, HIGH);
            Hscan(H);
            delay(100);
            lcd.clear();
            lcd.print("Adjusting Backset");
            lcd.setCursor(0, 1);
            lcd.print(H);
            lcd.print(" cm");
            Serial.print("Adjusting Backset  ");
            Serial.print(H);
            if (digitalRead(buttonPin) == HIGH) state = 0;
            if (digitalRead(6) == HIGH) H_limit = 1;           // Horizontal Limit switch stop
        }
        digitalWrite(E2, LOW);           // Stop horizontal motor

```

```

Hscan(H);
delay(100);

while (state==2 && H<0.5){
digitalWrite(E2, HIGH);           // reverse horizontal motor
digitalWrite(I3, HIGH);
digitalWrite(I4, LOW);
Hscan(H);
delay(100);
  lcd.clear();
  lcd.print("Adjusting Backset");
  lcd.setCursor(0, 1);
  lcd.print(H);
  lcd.print(" cm");
if (digitalRead(buttonPin) == HIGH) state = 0;
}
digitalWrite(E2, LOW);           // Stop horizontal motor
if (digitalRead(6) == LOW) H_limit = 0; // Horizontal Limit switch disengaged

if (state == 0){
  lcd.clear();
  lcd.print("* Emergency *");
  lcd.setCursor(0, 1);
  lcd.print("Button pressed");
digitalWrite(E1, HIGH);           // return vertical motor to initial position
digitalWrite(I1, LOW);
digitalWrite(I2, HIGH);
digitalWrite(E2, HIGH);           // return horizontal motor to initial position
digitalWrite(I3, HIGH);
digitalWrite(I4, LOW);
delay(10000);
digitalWrite(E1, LOW);
digitalWrite(E2, LOW);
}

if (state==2 && H<=4 && H>=0.5){
  lcd.clear();
  lcd.print("Good position");
  lcd.setCursor(0, 1);
  lcd.print(V);
  lcd.print(" cm, ");
  lcd.print(H);
  lcd.print(" cm");
}
}
}
}

```

```

double Hscan(double &H){
    pinMode(Hping, OUTPUT);
    digitalWrite(Hping, LOW);
    delayMicroseconds(2);
    digitalWrite(Hping, HIGH);
    delayMicroseconds(5);
    digitalWrite(Hping, LOW);
    pinMode(Hping, INPUT);
    double duration = pulseIn(Hping, HIGH);
    H = duration/29/2; // convert the time into a distance
    delay(100);
}

double Vscan(double &V){
    pinMode(Vping, OUTPUT);
    digitalWrite(Vping, LOW);
    delayMicroseconds(2);
    digitalWrite(Vping, HIGH);
    delayMicroseconds(5);
    digitalWrite(Vping, LOW);
    pinMode(Vping, INPUT);
    double duration = pulseIn(Vping, HIGH);
    V = duration/29/2; // convert the time into a distance
    delay(100);
}

// The End
//***** Aug 22, 2016

```